UTILIZATION OF 3D CELL CULTURE METHODOLOGIES TO MODEL ALZHEIMER'S DISEASE

A Thesis Submitted to
the Graduate School of Engineering and Sciences of
İzmir Institute of Technology
in Partial Fulfillment of the Requirement for the Degree of

DOCTOR OF PHILOSOPHY

in Bioengineering

by
Rümeysa BİLGİNER KARTAL

January 2025
İZMİR

We approve the thesis of **Rümeysa BİLGİNER KARTAL**

Examining Committee Members:

Assoc. Prof. Dr. Ahu ARSLAN YILDIZ
Department of Bioengineering, İzmir Institute of Technology

Prof. Dr. Pınar AKAN
Department of Medical Biochemistry, Dokuz Eylül University

Prof. Dr. Sacide ALSOY ALTINKAYA
Department of Chemical Engineering, İzmir Institute of Technology

Prof. Dr. Erdal BEDİR
Department of Bioengineering, İzmir Institute of Technology

Prof. Dr. Özlem YEŞİL ÇELİKTAŞ
Department of Bioengineering, Ege University

08 January 2025

Assoc. Prof. Dr. Ahu ARSLAN YILDIZ
Supervisor, Department of Bioengineering, İzmir Institute of Technology

Assoc. Prof. Dr. Sinan GÜVEN
Co-Supervisor, Department of Health Sciences, Dokuz Eylül University

Dr. Öğr. Üyesi Arzu UYAR
Head of the Biotechnology Department, İzmir Institute of Technology

Prof. Dr. Mehtap EANES,
Dean of the Graduate School of Engineering and Sciences

ACKNOWLEDGMENTS

Completing this PhD thesis has been a long journey, and it would not have been possible without the support and guidance of many individuals. I would like to take this opportunity to express my gratitude to those who have made this work possible.

First and foremost, I would like to thank my advisor, Assoc. Prof. Dr. Ahu ARSLAN YILDIZ, for her unwavering support, invaluable guidance, and continuous encouragement throughout my research. Their insightful feedback and persistent confidence in my work have been instrumental in shaping this thesis.

I am also profoundly grateful to the members of my dissertation committee, Prof. Dr. Pınar AKAN and Prof. Dr. Sacide ALSOY ALTINKAYA for their time, advice, and constructive critiques, which significantly contributed to the quality and comprehensiveness of this research.

I want to thank my colleagues and fellows in the Biomimetics Lab/Research Group at Izmir Institute of Technology. I sincerely thank my friends Başak ÇOBAN, Özüm YILDIRIM SEMERCİ, Ece ÖZMEN, Arda PİŞİRİCİ, Zeynep ALTAN, Duygu ARSLANTAŞ, Hilal Deniz YILMAZ DAĞDEVİREN, Ezgi BAYRAKTAR, Elif GÜNER, Rukiye Bilge ŞANLI, Alper Baran SÖZMEN and Özgür ÜLKER for supporting me throughout this thesis journey, providing both motivation and making the process a little more enjoyable. I will remember most are our coffee breaks within sleepless nights, endless analyses, and countless revisions.

I sincerely thank my husband, Anıl KARTAL, and BİLGİNER family for their unconditional love and support. My husband has been my strength, always standing by my side with patience and encouragement. His belief in me has been a constant source of motivation, pushing me forward even in the most challenging moments. I would also like to express my heartfelt gratitude to my beloved sisters for always being by my side, offering their love, patience, and uplifting words. Their understanding and support during difficult times have made this journey easier and more meaningful for me. Their presence has always been a great source of strength in my life.

I would like to thank the support from the Scientific and Technological Research Council of Turkey (TÜBİTAK) through the 2211-A National PhD Scholarship and 2250 Performance-Based Scholarships Program. Additionally, I would like to express my

gratitude to the Council of Higher Education (YÖK) PhD Scholarship for the 100/2000 program in Biomaterials and Tissue Engineering. Furthermore, I would like to acknowledge the financial support for this thesis provided by the IZTECH-Scientific Research Project (2022IYTE) and 1002 program TÜBİTAK under project number of 223M335.

This journey has been a collective effort, and I am sincerely thankful to everyone who has contributed to it.

ABSTRACT

UTILIZATION OF 3D CELL CULTURE METHODOLOGIES TO MODEL ALZHEIMER'S DISEASE

This thesis introduces modeling Alzheimer's disease within a three-dimensional (3D) *in-vitro* platform by employing Magnetic Levitation (MagLev) technology. Alzheimer's disease is characterized by amyloid beta (Aβ) accumulation, leading to cognitive decline and neuronal degeneration. Alzheimer's disease has been modeled using conventional two-dimensional (2D) cell cultures and animal models. Despite experimental models having provided valuable insights, these models fail to recapitulate the human brain's physiology. Therefore, there is a need for more realistic experimental platforms.

This study involved the fabrication of 3D Alzheimer's disease models from two different cell lines. SH-SY5Y and PC-12 cells were cultured to form 3D cellular structures using MagLev technology. Then, 3D Alzheimer's disease models were established by the incorporation of Aβ1-42 aggregates, which are known to drive neurotoxicity and disease progression in Alzheimer's pathology.

Another aspect of this study is utilizing the 3D disease model as a drug screening platform by evaluating the neuroprotective potential of Curcumin, which is known for the disassociation of Aβ aggregates. The findings revealed that Curcumin, at optimal concentrations, significantly reduced Aβ-induced neurotoxicity, underscoring its potential as a therapeutic agent.

This study demonstrated that Aβ-induced three-dimensional models of Alzheimer's disease were successfully developed through the MagLev technique and applied as a drug screening platform. This model represents a valuable alternative to traditional approaches in neurodegenerative disease research. This model can provide an understanding of the underlying mechanisms of Alzheimer's disease and facilitate the exploration of novel therapeutic strategies.

ÖZET

ALZAYMIR HASTALIĞINI MODELLEMEK İÇİN 3B HÜCRE KÜLTÜRÜ METODOLOJİLERİNİN KULLANILMASI

Bu tez, Manyetik Levitasyon (MagLev) teknolojisini kullanarak Alzaymır hastalığının üç boyutlu (3B) bir *in-vitro* platformda modellenmesini tanıtmaktadır. Alzaymır hastalığı, bilişsel gerileme ve nöronal dejenerasyona yol açan amiloid beta (Aβ) birikimi ile karakterize edilir. Alzaymır hastalığı, geleneksel iki boyutlu (2B) hücre kültürleri ve hayvan modelleri kullanılarak modellenmiştir. Deneysel modeller değerli bilgiler sağlamış olsa da bu modeller insan beyninin fizyolojisini yansıtmakta başarısız olmaktadır. Bu nedenle, daha gerçekçi deneysel platformlara ihtiyaç vardır.

Bu çalışmada, iki farklı hücre hattı kullanılarak 3B Alzaymır hastalığı modelleri oluşturulmuştur. SH-SY5Y ve PC-12 hücreleri, MagLev teknolojisi kullanılarak 3B hücresel yapılar oluşturacak şekilde kültürlenmiştir. Daha sonra, Alzaymır hastalığının patolojisinde nörotoksisiteyi artıran ve hastalığın ilerlemesine neden olan Aβ1-42 agregatları modele eklenerek 3B Alzaymır hastalık modelleri oluşturulmuştur.

Bu çalışmanın bir diğer yönü, Aβ agregatlarını disosiye ettiği bilinen Kurkumin'in nöroprotektif potansiyelini değerlendirerek 3B hastalık modelini bir ilaç tarama platformu olarak kullanmaktır. Elde edilen bulgular, optimal konsantrasyonlarda Kurkumin'in, Aβ kaynaklı nörotoksisiteyi önemli ölçüde azalttığını göstererek terapötik bir ajan olarak potansiyelini vurgulamaktadır.

Bu çalışma, Aβ ile indüklenen 3B Alzaymır hastalığı modellerinin MagLev tekniği kullanılarak başarıyla geliştirildiğini ve bir ilaç tarama platformu olarak uygulandığını göstermektedir. Bu model, nörodejeneratif hastalık araştırmalarında geleneksel yaklaşımlara değerli bir alternatif sunmaktadır. Ayrıca, Alzaymır hastalığının altında yatan mekanizmaların anlaşılmasına katkıda bulunarak yeni terapötik stratejilerin keşfini kolaylaştırabilir.

TABLE OF CONTENTS

LIST OF FIGURES x
LIST OF TABLES xviii
CHAPTER 1. INTRODUCTION 1
1.1. Neurodegenerative Diseases 1
1.2. Alzheimer's Disease and its Pathology 2
1.3. Diagnosis of Alzheimer’s Disease 6
1.3.1. PET Scanning for Aβ and Tau Detection 7
1.3.2. CSF for Aβ Detection 8
1.3.3. MRI for Brain Volume 9
1.4. Alzheimer's Disease Models 9
1.4.1. Animal Models of Alzheimer's Disease 10
1.4.2. 2D In-vitro Models of Alzheimer's Disease 11
1.4.3. 3D In-vitro Models of Alzheimer's Disease 12
1.5. 3D Cell Culture by MagLev 20
1.6. Current Therapeutics for the Treatment of Alzheimer's Disease 25
1.7. Scope of the Thesis 28
CHAPTER 2. MATERIALS & METHODS 31
2.1. Standard 2D Cell Culture 31
2.2. MagLev Setup for 3D Cell Culture 32
2.3. Differentiation of SH-SY5Y Spheroids in MagLev Setup 33
2.4. 3D Alzheimer's Disease Modeling through Aβ 1-42 Induction 34
2.5. Curcumin Treatment on 3D Cell Culture 35
2.6. Statistical Analysis 36
CHAPTER 3. RESULT & DISCUSSION 37
3.1. Formation of SH-SY5Y Spheroids *via* MagLev 37

3.1.1. Optimization of Gx Concentration for 3D Cell Culture Formation of SH-SY5Y in MagLev Setup 37
3.1.2. Optimization SH-SY5Y Cell Number for 3D Cell Culture Formation in MagLev Setup 39
3.1.3. Differentiation of SH-SY5Y Cells Using RA-BDNF 41
3.1.3.1. Optimization and Characterization of Differentiation Protocol for SH-SY5Y on 2D Cell Culture 42
3.1.3.2. 3D Cell Culture in MagLev Setup while Maintaining Optimized Differentiation Protocol 51
3.2. Utilizing SH-SY5Y Spheroids to Model Alzheimer's Disease in 3D ...58
3.2.1. Formation and Characterization of Aβ 1-42 Aggregates 58
3.2.2. Optimization of Aβ 1-42 Aggregate Concentration on 2D Cell Culture of SH-SY5Y Cells 60
3.2.3. Alzheimer’s Disease Modeling via Aβ Induction Using SH-SY5Y Spheroids 65
3.2.4. Characterization of 3D Alzheimer's Disease Modeling of SH-SY5Y Using Immunostaining 69
3.3. Investigating the Neuroprotective Effect of Curcumin on 3D Alzheimer's Disease Model of SH-SY5Y 70
3.3.1. Evaluating the Disassociation Ability of Curcumin Against Aβ 1-42 Aggregates 70
3.3.2. Optimization of Curcumin Concentration on 2D Cell Culture of SH-SY5Y 75
3.3.3. Investigating Curcumin Cytotoxicity on 3D SH-SY5Y Spheroids 76
3.3.4. Evaluation of the Neuroprotective Effect of Curcumin on 3D Alzheimer’s Disease Model of SH-SY5Y 78
CHAPTER 4 81
4.1. Formation 3D cell culture of PC-12 via MagLev 81
4.1.1. Optimization of Gx Concentration for 3D Cell Culture Formation of PC-12 in MagLev Setup 81

4.1.2. Optimization of PC-12 Cell Number for 3D Cell Culture Formation in MagLev Setup 83
4.1.3. 3D Cell Culture of PC-12 Cells in MagLev Setup for Long Term Culture 86
4.2. Utilizing 3D Cultured PC-12 Cells to Model Alzheimer's Disease in 3D 88
4.2.1. Optimization of Aβ 1-42 Aggregate Concentration on 2D Cell Culture of PC-12 Cells 88
4.2.2. Alzheimer's Disease Modeling via Aβ Induction Using 3D Cultured PC-12 Cells 90
4.2.3. Characterization of 3D Alzheimer's Disease Modeling of PC-12 Using Immunostaining 93
4.3. Investigating the Neuroprotective Effect of Curcumin on 3D Alzheimer's Disease Modeling of PC-12 95
4.3.1. Optimization of Curcumin Concentration on 2D Cell Culture of PC-12 95
4.3.2. Investigating Curcumin Cytotoxicity on 3D Cultured PC-12 Cells 96
4.3.3. Evaluation of the Neuroprotective Effect of Curcumin on 3D Alzheimer's Disease Model of PC-12 98
CHAPTER 5. CONCLUSION 103
REFERENCES 105

LIST OF FIGURES

Figure **Page**

Figure 1. The hallmarks of neurodegenerative diseases (Wilson et al., 2023). 2
Figure 2. A) Aβ plaques and neurofibrillary tangles B) Brain atrophy, which correlates with a reduction in both synapses and neurons at an anatomical scale (Masters et al., 2015). 4
Figure 3. The schematic shows proteolytic pathways of human amyloid precursor protein (APP): non-amyloidogenic and amyloidogenic pathways (Chen et al., 2017). 5
Figure 4. The aggregation mechanism of Aβ plaques (Jokar et al., 2020). 6
Figure 5. A visual representation illustrating the critical phases of the diagnostic process, in addition to the suggested tests to reinforce each phase (Porsteinsson et al., 2021).....7
Figure 6. The advantages and disadvantages of *in-vivo* and *in-vitro* models in the diagram, showing the disadvantages and advantages of employing animal models, 2D or 3D, and organ-on-a-chip platforms (Balestri et al., 2024). 17
Figure 7. The setup and testing of a magnetic levitation system for 3D culture of adipocyte cells (Daquinag et al., 2013).....22
Figure 8. The illustration depicts A) MagLev technology and the formation of 3D cell cultures B) MagLev systems utilizing a four-mirror configuration are presented in 2D and 3D drawings. C) A frontal and 3D perspective of the MagLev components: mirrors, a capillary glass channel, and NdFeB magnets and transparent PMMA holders (Türker et al., 2018). 23
Figure 9. Illustration of the MagLev setup. A) 32T bitter magnet installation B) Image of the bitter magnet C) Cuvette with paramagnetic agent and medium, placed in the custom-designed setup (Parfenov et al., 2020).....24
Figure 10. The illustration of the developed MagLev setup and formation of 3D cellular structures (Onbas and Arslan Yildiz, 2021).....25

Figure **Page**

Figure 11. Curcumin's chemical structure: a beta-diketone compound containing two substituted aromatic rings linked by a seven-carbon chain and an aromatic ring with one hydroxy and one methoxy group (Zhai et al., 2020). 28
Figure 12. Depiction of the 3D Alzheimer's disease model formation (A) 3D cell culture formation via MagLev (B) Aβ 1-42 aggregates induction to 3D cell culture (C) Curcumin treatment and Aβ 1-42 aggregates disassociation (*The illustration was created by BioRender.com*). 29
Figure 13. MagLev setup components: NdFeB N35 disc magnets, PMMA holders, and petri dish....32
Figure 14. Depiction of 3D Alzheimer's disease protocol: SH-SY5Y cells formed spheroid and differentiated via RA-BDNF sequentially in MagLev, then induced by Aβ aggregates. PC-12 cells formed 3D cell culture and were induced by Aβ aggregates. 35
Figure 15. Bright-field and fluorescence microscopy images for SH-SY5Y spheroid formation at $25x10^3$ cell number between 10-100 mM Gx with for 24h (Scale bar: 200 μm, Green: Live, Red: Dead). 38
Figure 16. Cell viability results of SH-SY5Y spheroids between 10-100 mM Gx at $25x10^3$ cell number for 24h (n=6, there is no significant difference between groups, one-way ANOVA followed by Tukey's test). 39
Figure 17. Bright-field and fluorescence microscopy images for SH-SY5Y spheroid formation between $5x10^3$-$100x10^3$ cell number at 10 mM Gx cells for 24h (Scale bar: 200 μm, Green: Live, Red: Dead). 40
Figure 18. Cell viability results of SH-SY5Y spheroids between $5x10^3$-$100x10^3$ cell number at 10 mM Gx for 24h (n=6, there is no significant difference (ns) between groups, one-way ANOVA followed by Tukey's test). 41
Figure 19. Differentiation of SH-SY5Y cells via 10 μM RA with high cell density ($50x10^3$) for 10 days (Scale bar: 100 μm). 43
Figure 20. Differentiation of SH-SY5Y cells via 10 μM RA with low cell density ($25x10^3$) for 10 days (Scale bar: 100 μm). 45

Figure **Page**

Figure 21. Neurite extension analysis of A) high ($50x10^3$) and B) low cell density ($25x\ 10^3$) for SH-SY5Y after differentiation via 10 μM RA for 10 days (n=10, ns:not significant, ***p <0 .001, ****p<0.0001 compared to the control of each group, two-way ANOVA followed by Tukey's test).....46

Figure 22. Morphology of un-/differentiated SH-SY5Y after sequential treatment with RA and RA-BDNF for 9 days (Scale bar: 50 μm).....48

Figure 23. Neurite extension analysis of un-/differentiated SH-SY5Y cells after sequential treatment by RA and RA-BDNF for 9 days (n = 10, ns: not significant, ****p < 0.0001, two-way ANOVA followed by Tukey's test). 49

Figure 24. Immunostaining of β-III tubulin and NeuN for un-/differentiated SH-SY5Y cells on A) day 5, B) day 7, and C) day 9 (Scale bar: 50 μm, Blue: DAPI, Green: β-III tubulin and NeuN).....50

Figure 25. Relative fluorescence intensity (F.I.) of A) β-III tubulin and B) NeuN for un-/differentiated SH-SY5Y cells (n = 6, ns: not significant ***p < 0.001, ****p < 0.0001, two-way ANOVA followed by Tukey's test).....51

Figure 26. Bright-field and fluorescence microscopy images for un-/differentiated 3D SH-SY5Y spheroids analyzed by Live-Dead assay on day 5, 7, and 9 (Scale bar: 200 μm, Green: Live, Red: Dead). 52

Figure 27. Cell viability results of A) undifferentiated and B) differentiated SH-SY5Y spheroids for days 5, 7, and 9 (n=3, there is no significant difference between groups, one-way ANOVA followed by Tukey's test). 53

Figure 28. Circularity and area analysis of A) undifferentiated and B) differentiated SH-SY5Y spheroids on days 5, 7, and 9.....54

Figure 29. Bright-field and fluorescence microscopy images of SH-SY5Y cells differentiated in 2D and cultured in MagLev (Scale bar: 200 μm, Green: Live, Red: Dead).....55

Figure 30. Fluorescence microscopy images of β-III tubulin and NeuN for un-/differentiated SH-SY5Y spheroids on A) day 5, B) day 7, and C) day 9 (Scale bar: 100 μm, Blue: DAPI, Green: β-III tubulin and NeuN).....56

Figure **Page**

Figure 31. Relative fluorescence intensity (F.I.) of A) β-III tubulin and B) NeuN for un-/differentiated SH-SY5Y spheroids (n = 3, *p <0 .05, **p < 0.01, two-way ANOVA followed by Tukey's test).....57
Figure 32. Monitoring Aβ 1-42 A) monomer and B) aggregates by light microscopy after applying Congo red (Scale bar 50 μm) C) Morphology of Aβ 1-42 aggregates monitoring by SEM (Scale bar: 500 nm).....58
Figure 33. Spectrophotometric analysis of Aβ 1-42 aggregates formation through Congo red assay. 59
Figure 34. Size distribution profile of Aβ 1-42 aggregates by histogram graph (n=100).....60
Figure 35. Bright-field and fluorescence microscopy images of SH-SY5Y cells after 0-15 μM Aβ 1-42 exposure for A) 24h, B) 48h, and C) 72h (Scale bar: 50 μm, Green: Live, Red: Dead).....61
Figure 36. Cell viability measurement of SH-SY5Y cells after 0-15 μM Aβ 1-42 exposure for 24h, 48h, and 72h, analyzed by MTT (n=5, *p <0 .05, **p <0 .01, ***p <0 .001, ****p<0.0001 compared to the control of each group, two-way ANOVA followed by Tukey's test).....62
Figure 37. Bright-field and fluorescence microscopy images of differentiated SH-SY5Y cells after 0-15 μM Aβ 1-42 exposure for A) 24h, B) 48h, and C) 72h, analyzed by Live-dead assay (Scale bar: 50 μm, Green: Live, Red: Dead).....63
Figure 38. Cell viability measurement of differentiated SH-SY5Y cells after 0-15 μM Aβ 1-42 exposure for 24h, 48h, and 72h, analyzed by MTT (n=5, *p <0 .05, **p <0 .01, ***p <0 .001, ****p<0.0001 compared to the control of each group, two-way ANOVA followed by Tukey's test).....64
Figure 39. Aβ 1-42 aggregate staining in cell culture environment via A) Congo red and B) Thioflavin T assays (Scale bar: 50 μm).....65
Figure 40. A) Bright-field and fluorescence microscopy images of un-/differentiated SH-SY5Y spheroids after 10-50 μM Aβ 1-42 aggregate exposure for 72h, analyzed by Live-dead assay (Scale bar: 200 μm, Green: Live, Red: Dead). 66

Figure **Page**

Figure 41. Cell viability of un-/differentiated SH-SY5Y spheroids after 10-50 µM Aβ 1-42 exposure for 72h (n=5, *p <0 .05, ***p <0 .001, ****p<0.0001 compared to the DMSO control of each group, two-way ANOVA followed by Tukey's test).....67
Figure 42. Bright-field and fluorescence microscopy images of un-/differentiated SH-SY5Y spheroids after 3-7 days of 50 µM Aβ 1-42 exposure, analyzed by Live-dead assay (Scale bar:200 µm, Green: Live, Red: Dead). 68
Figure 43. Cell viability of un-/differentiated SH-SY5Y spheroids after 3-7 days of 50 µM Aβ 1-42 exposure (n=5, *p <0 .05, ***p <0 .001, ***p<0.0001 compared to DMSO control of each group, two-way ANOVA followed by Tukey's test).....69
Figure 44. A) Fluorescence microscopy images of ChAT marker for 3D Alzheimer's disease model of SH-SY5Y spheroids B) Calculated fluorescence intensity (F.I.) of ChAT for Control and AD (Alzheimer's disease) model (Scale bar:200 µm) (Blue: DAPI, Green: ChAT) (n=4, **p <0 .0, t-test analysis). 70
Figure 45. A) Monitoring Aβ 1-42 aggregates by bright-field microscopy following 0-100 µM Curcumin treatment for 72h (Scale bar: 200 µm).....71
Figure 46. Size distribution profile of Aβ 1-42 aggregates after Curcumin treatment with varied concentrations A) 0 µM B) 25 µM C) 50 µM D) 75 µM and E) 100 µM.....72
Figure 47. Relative absorbance (Abs.) values of Congo red staining following 0-100 µM Curcumin treatment for 72h (n=6, **p<0.01 ***p <0 .001, compared 0 µM (Aβ), one-way ANOVA followed by Tukey's test). 73
Figure 48. Relative fluorescence intensity (F.I.) of Thioflavin T assay following 0-100 µM Curcumin treatment for 72h (n=6, **p<0.01 ***p <0 .001, compared 0 µM (Aβ), one-way ANOVA followed by Tukey's test). 74
Figure 49. Bright-field and fluorescence microscopy images of SH-SY5Y after 0-100 µM Curcumin screening for 72h (Scale bar: 50 µm, Green: Live, Red: Dead). 75

Figure **Page**

Figure 50. Evaluation of cell viability of SH-SY5Y after 0-100 μM Curcumin screening for 72h by MTT (n=6, **p<0.01, ***p <0 .001, ****p <0 .0001 compared 0 μM, one-way ANOVA followed by Tukey's test).....76
Figure 51. Bright-field and fluorescence microscopy images of SH-SY5Y spheroids after Curcumin cytotoxicity assessment by Live-Dead assay (Scale bar: 200 μm, Green: Live, Red: Dead).....77
Figure 52. Cell viability measurement of SH-SY5Y spheroids after Curcumin cytotoxicity assessment by Live-Dead assay (n=6, *p <0 .05, **p <0 .01, ****p<0.0001 compared to the control of each group, one-way ANOVA followed by Tukey's test).....77
Figure 53. Investigating neuroprotective effect of Curcumin on Aβ 1-42 aggregates in 3D spheroids; Bright-field and fluorescence images of spheroids before and after 0-100 μM Curcumin treatment for 72h on Aβ–induced 3D Alzheimer's disease model (Scale bar: 200 μm, Green: Live, Red: Dead).....78
Figure 54. Cell viability after 0-100 μM Curcumin treatment for 72h in Aβ–induced 3D Alzheimer's disease model of SH-SY5Y (n=5, *p <0 .05, **p <0 .01, compared Aβ-treated group (0 μM), one-way ANOVA followed by Tukey's test).....79
Figure 55. Fluorescence microscopy images of Aβ 1-42 aggregates in 3D Alzheimer's disease model before and after Curcumin treatment at 25 μM (Scale bar: 100 μm).....80
Figure 56. Bright-field and fluorescence microscopy images of 3D cell culture of PC-12 at $25x10^3$ cell number between 10-100 mM Gx for 24h (Scale bar:200 μm, Green:Live, Red:Dead). 82
Figure 57. Cell viability results of 3D cultured PC-12 at 10-100 mM Gx with $25x10^3$ cell number for 24h (n=6, there is no significant difference between groups). 83
Figure 58. Bright-field and fluorescence microscopy images for 3D cell culture formation of PC-12 cells between $5x10^3$-$100x10^3$ cell number at 30 mM Gx cells for 24h (Scale bar:200 μm, Green: Live, Red: Dead). 84

Figure **Page**

Figure 59. Cell viability measurement for 3D cellular structure of PC-12 between $5x10^3$-$100x10^3$ cell number at 30 mM Gx for 24h (n=6, ***p <0 .001, ****p<0.0001, two-way ANOVA followed by Tukey's test). 85
Figure 60. Area analysis of 3D cultured PC-12 cells based on A) Gx concentration and B) cell number for 24h. 86
Figure 61. Bright-field and fluorescence microscopy images of 3D cell culture of PC-12 at $25x10^3$ and 30 mM Gx for long term culture (Scale bar:200 µm, Green: Live, Red: Dead). 87
Figure 62. Cell viability measurement for 3D cellular structure of PC-12 12 at $25x10^3$ and 30 mM Gx for long term culture (n=6, there is no significant difference between groups). 87
Figure 63. Bright-field and fluorescence microscopy images of PC-12 cells after 0-15 µM Aβ 1-42 exposure for A) 24h, B) 48h, and C) 72h (Scale bar: 50 µm, Green: Live, Red: Dead). 89
Figure 64. Cell viability measurement of PC-12 cells after 0-15 µM Aβ 1-42 exposure for 24h, 48h, and 72h, analyzed by MTT (n=6, *p<0.005, **p<0.01, ***p <0 .001, ****p<0.0001 compared to 0 µM, one-way ANOVA followed by Tukey's test). 90
Figure 65. Bright-field and fluorescence microscopy images of 3D cultured PC-12 after 10-50 µM Aβ 1-42 exposure for 72h (Scale bar:200 µm, Green: Live, Red: Dead). 91
Figure 66. Cell viability measurement of 3D cultured PC-12 after 10-50 µM Aβ 1-42 exposure for 72h (n=6, *p<0.005, **p<0.01, one-way ANOVA analysis). 91
Figure 67. Bright-field and fluorescence microscopy images of 3D cultured PC-12 after 50 µM Aβ 1-42 exposure for 3-21 days (Scale bar:200 µm, Green: Live, Red: Dead). 92
Figure 68. Cell viability measurement of 3D cultured PC-12 after 50 µM Aβ 1-42 exposure for 3–21 days (n=6, *p<0.005, **p<0.01, ****p<0.0001 compared to 0 µM, one-way ANOVA followed by Tukey's test). 93

Figure **Page**

Figure 69. A) Fluorescence microscopy images of ChAT marker B) Calculated fluorescence intensity (F.I.) of ChAT based on the area (%) for Control and AD (Alzheimer's disease) model (Scale bar:100 μm) (Blue: DAPI, Green: ChAT) (n=4, **p <0 .01, t-test analysis). 94
Figure 70. Bright-field and fluorescence microscopy images of PC-12 after 0-100 μM Curcumin screening for 72h (Scale bar: 50 μm, Green: Live, Red: Dead).....95
Figure 71. Cell viability measurement of PC-12 cells after 0-100 μM Curcumin screening for 72h (n=6, ***p <0 .001, ****p<0.0001 compared to the control of each group, one-way ANOVA followed by Tukey's test). 96
Figure 72. Bright-field and fluorescence microscopy images of 3D culture of PC-12 after Curcumin cytotoxicity assessment by Live-Dead assay (Scale bar: 200 μm, Green: Live, Red: Dead). 97
Figure 73. Cell viability measurement of 3D cultured PC-12 after Curcumin cytotoxicity assessment by Live-Dead assay (n=6, there is no significant difference between groups).....97
Figure 74. Bright-field and fluorescence images of 3D cultured PC-12 before and after 0-100 μM Curcumin treatment for 72h in Aβ–induced 3D Alzheimer's disease model (Scale bar: 200 μm, Green: Live, Red: Dead). 98
Figure 75. Cell viability measurement after 0-100 μM Curcumin treatment for 72h in Aβ–induced 3D Alzheimer's disease model of PC-12 (n=6, there is no significant difference between groups).....99
Figure 76. Bright-field and fluorescence images of 3D culture of PC-12 before and after Curcumin treatment at 25 μM for 21 days in Aβ–induced 3D Alzheimer's disease model (Scale bar: 200 μm, Green: Live, Red: Dead). 99
Figure 77. Cell viability after Curcumin treatment at 25 μM for 21 days in Aβ–induced 3D Alzheimer's disease model of PC-12 (n=6, *p <0 .05, **p <0 .01, ***p <0 .001, ****p<0.0001 compared to the control of each group, two-way ANOVA followed by Tukey's test).....100

Figure **Page**

Figure 78. Fluorescence microscopy images of Aβ 1-42 aggregates in 3D Alzheimer's disease model before and after Curcumin treatment at 25 μM (Scale bar: 100 μm).....101

LIST OF TABLES

Table **Page**

Table 1. Studies of Alzheimer's disease modeling utilizing 3D cell culture methodologies. 18

CHAPTER 1

INTRODUCTION

1.1. Neurodegenerative Diseases

Neurodegenerative disorders are age-related diseases that involve the uncontrolled death of neurons, resulting in a progressive decline in the cognitive function of the brain. These diseases show a wide range of clinical symptoms, such as cognitive decline and the loss of motor functions. The prevalence of these conditions is increasing due to the aging global population, and their detrimental impact on quality of life has burdened healthcare systems worldwide (Heemels, 2016). Among age-related neurodegenerative diseases, dementias pose the most significant challenge. This term encompasses various conditions characterized by cognitive impairments, including Alzheimer's disease, vascular dementia, frontotemporal dementia, mixed dementia, and dementia with Lewy bodies. Additionally, other neurodegenerative diseases primarily affect the motor system, such as amyotrophic lateral sclerosis, Huntington's disease, Parkinson's disease, multiple sclerosis, and spinocerebellar ataxias. Key features of neurodegenerative diseases include the death of neuronal cells, the accumulation of abnormal proteins, and defects in synaptic function (Figure 1). Each feature corresponds to a specific mechanism, such as inflammatory processes, disturbances in energy homeostasis, and damage to DNA and RNA that play a significant role in the progression of diseases like Alzheimer’s and Parkinson’s. The resulting clinical syndromes differ based on the specific protein(s) and brain region(s) implicated (Wray, 2021). Key indicators of these disorders include the existence of Amyloid β (Aβ) plaques and phosphorylated Tau (pTau)-containing tangles in Alzheimer's disease (Masters et al., 2015), α-synuclein-associated Lewy bodies in Parkinson's disease (Dettmer et al., 2015), and mutant huntingtin (Htt)-containing inclusion bodies in Huntington's disease (Jeon et

al., 2012). The aggregation of these proteins can lead to neuronal axon damage through loss-of-function or gain-of-toxicity mechanisms.

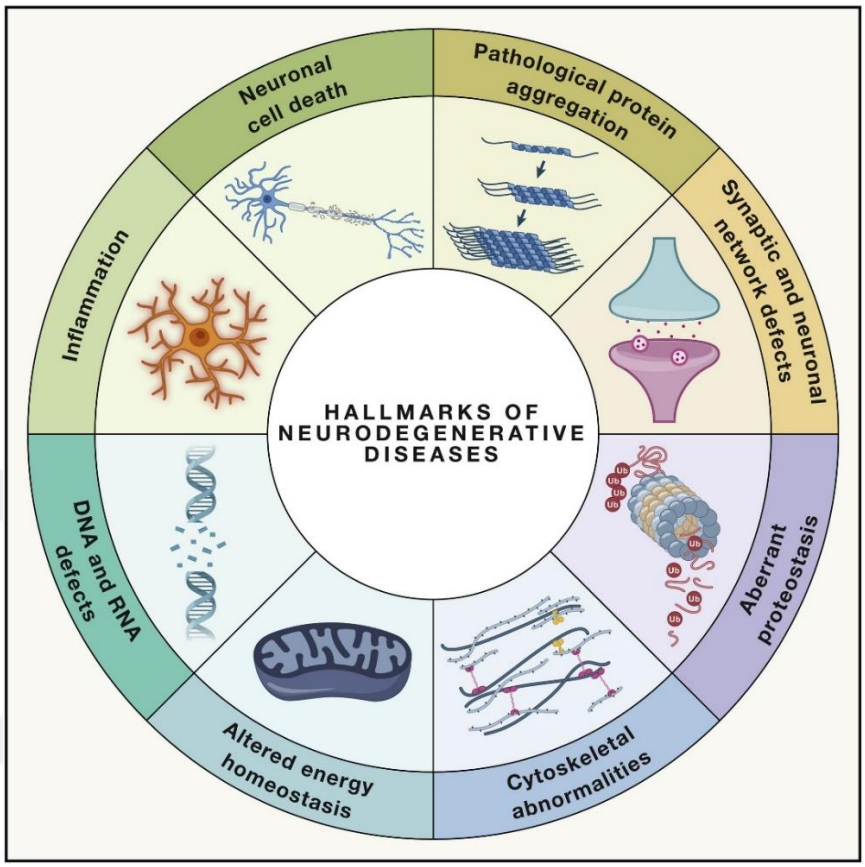

Figure 1. The hallmarks of neurodegenerative diseases (Wilson et al., 2023).

1.2. Alzheimer's Disease and its Pathology

Alzheimer's disease is a prevalent neurodegenerative disease that impacts almost 50 million individuals across the globe, and this figure will reach 78 million by 2030 (Gauthier et al., 2021). The risk factors associated with Alzheimer's disease involve both genetic and environmental influences. These factors include chronic stress, dietary patterns, physical activity levels, smoking habits, traumatic brain injuries, diabetes, toxic metals, industrial chemicals, pesticides, and other medical conditions (Cetin et al., 2022; Sehar et al., 2022; Slanzi et al., 2020).

Alzheimer's disease is characterized by the loss of synapses, leading to neuronal atrophy across the cerebral cortex, with the medial temporal lobe being the most severely affected (Chen et al., 2018; Sheng et al., 2012). The pathological process is first observed in the hippocampus and entorhinal areas, later propagating through the frontotemporal cortices. This progression extends to the striatum and thalamus, while typically preserving the cerebellum (Duara et al., 2008; Mann, 1991; McDonald et al., 2009). Macroscale MRI assessments demonstrate a shrinkage of these specific regions, as well (Perl, 2010) (Figure 2). Although the reason behind the disease remains incompletely elucidated, the distinctive neuropathological features of Alzheimer's disease include the existence of extracellular plaques, primarily made up of amyloid beta (Aβ) peptides, and intracellular tangles consisting of hyperphosphorylated accumulations of the microtubule-associated protein tau (NFT), which is not necessarily observed in all cases (Finder and Glockshuber, 2007) (Figure 2A). They are co-localized with neuronal debris and activate microglia. They initially appear in the frontal, temporal, and occipital lobes of the neocortex (Sheppard and Coleman, 2020). Then, these pathological markers are found throughout neocortical areas, the hippocampus, and the entorhinal region, followed by spreading throughout the cerebral cortex to the striatum and thalamus at the end of the disease stages (Figure 2B) (Braak and Braak, 1991).

The majority of Alzheimer's disease cases are sporadic and occur due to the inefficient removal of Aβ peptide (Kummer and Heneka, 2014). The cause of sporadic Alzheimer's disease (SAD) remains unknown; however, potential factors contributing to its development include aging, as well as the intricate interaction between genetic and environmental risk factors (Sehar et al., 2022). In contrast, familial Alzheimer's disease (FAD), which is less common, is caused by mutations in genes related to Aβ metabolism (Barber, 2012). This type of Alzheimer's disease is known as early onset and is usually inherited in a Mendelian fashion. FAD is an extremely rare autosomal dominant disease that occurs at a young age and is caused by mutations in the Amyloid precursor protein (APP) and presenilin genes, each of which plays a role in Aβ metabolism (Finder and Glockshuber, 2007).

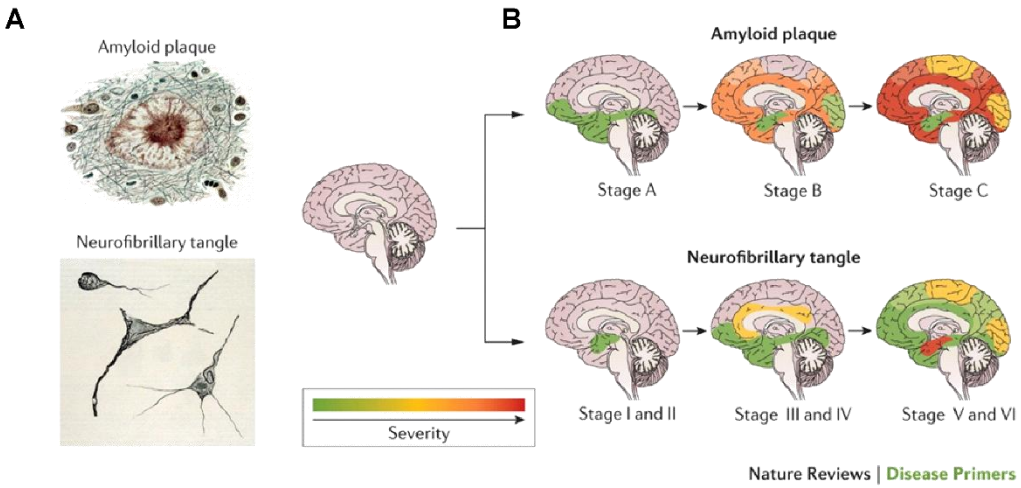

Figure 2. A) Aβ plaques and neurofibrillary tangles B) Brain atrophy, which correlates with a reduction in both synapses and neurons at an anatomical scale (Masters et al., 2015).

APP processing through non-amyloidogenic pathways involves the activity of α-secretase, an enzyme bound to the cell membrane (Figure 3). This enzyme cleaves the Aβ sequence within APP, generating two fragments: CTFα, which remains bound to the membrane, and sAPPα, which is released into the extracellular space. CTFα can undergo additional processing to produce P3 fragments that are found outside the cell, as well as the intracellular domain of APP (AICD) (Chen et al., 2017). In the amyloidogenic pathway, APP is processed by β and ϒ-secretases. β-Secretase (BACE-1) cuts APP into C-terminal fragment (CTF) and N-terminal soluble APP (sAPP). CTF is subsequently cleaved by ϒ-secretases to generate Aβ protein fragments and AICD (Chen et al., 2017; Tackenberg and Nitsch, 2019) . Depending on the cutting side of the γ-Secretase on APP change, the ratio of Aβ(1-42)/Aβ(1-40) increases. Long Aβ is more prone to form insoluble fibrils and is more likely to cause neurotoxicity. Aβ1-40 has 40 amino acids and is relatively soluble in aqueous media, while Aβ1-42 consists of 42 amino acid residues and is more prone to form aggregates.

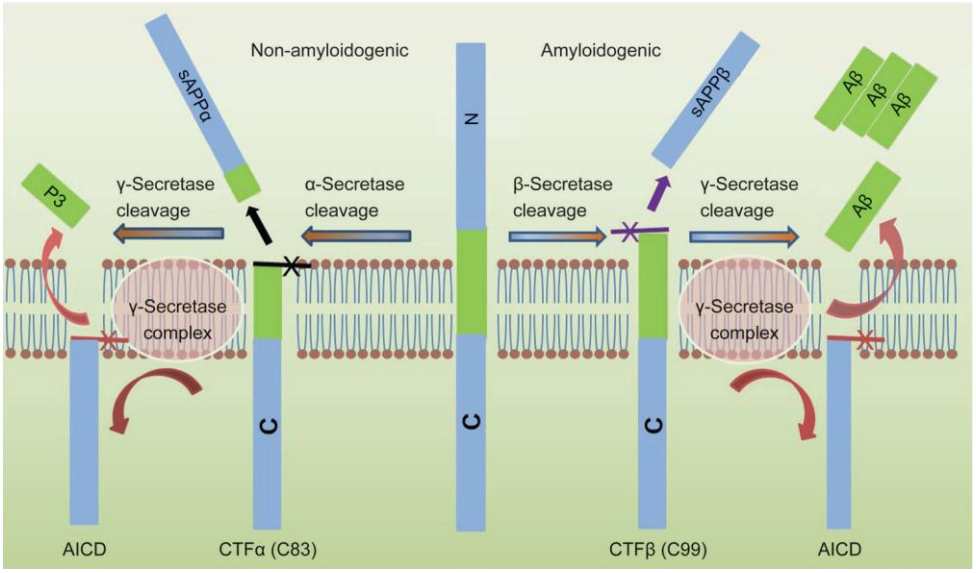

Figure 3. The schematic shows proteolytic pathways of human amyloid precursor protein (APP): non-amyloidogenic and amyloidogenic pathways (Chen et al., 2017).

Aβ fibrillation and associated neuronal damage begins with the cleavage of APP by β and γ secretases. This cleavage yields a peptide fragment that ranges from 39 to 42 amino acids, depending on the cleavage site. Subsequently, Aβ monomers begin to self-assemble, forming soluble toxic aggregates that eventually develop into insoluble fibrils (Figure 4). During this process, the formation of soluble oligomers from Aβ peptides occurs under *in-vitro* conditions, resulting in small, globular oligomers that range in size from trimers to 24-mers (Klein, 2002). Aβ protofibrils are identified as curvy structures with diameters between 4 and 10 nm and lengths reaching up to 200 nm (Harper et al., 1997; Walsh et al., 1997). These structures display a beaded appearance with a periodicity of 3 to 6 nm. Importantly, they are soluble and do not precipitate during centrifugation at moderate speeds of 16,000 to 18,000 x g. Protofibrils can further aggregate to form insoluble fibrils and are characterized by lengths greater than 200 nm, while their diameters remain similar to those of protofibrils (Walsh et al., 1997). These structures can be easily pelleted through centrifugation and bind to dyes such as Congo red, and Thioflavin T (Walsh et al., 1997). Research indicates that Aβ fibrils are composed of 5 to 6 protofilaments, with β-strands oriented perpendicular to the axis of the fiber, stabilized by hydrogen bonds (Serio et al., 2000). The strands are likely organized in a parallel configuration, creating a parallel-crossed β-sheet, with a turn occurring at residues 25 to

30. The majority of the amino acids within the core of the β-sheet are neutral and predominantly hydrophobic, except aspartic acid at position 23, which establishes a salt bridge with lysine at position 28 (Petkova et al., 2002). These fibrils are responsible for inducing synaptic dysfunction and neuronal cell death (Jokar et al., 2020).

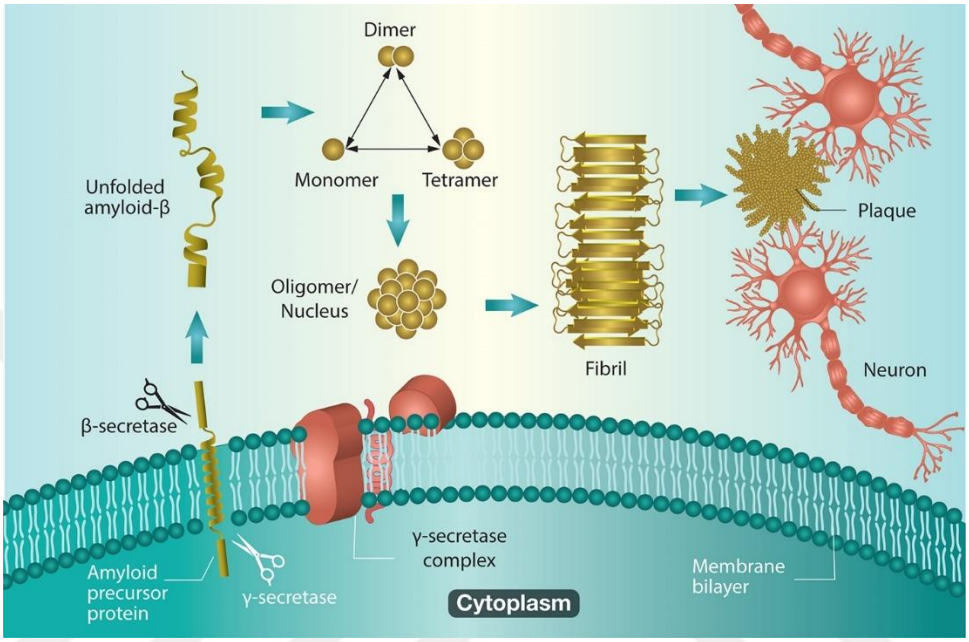

Figure 4. The aggregation mechanism of Aβ plaques (Jokar et al., 2020).

1.3. Diagnosis of Alzheimer's Disease

The early and accurate identification of Alzheimer's disease-related symptoms in clinical practice is a crucial but challenging advancement in Alzheimer's disease care. In the past, Alzheimer's disease was exclusively diagnosed postmortem until advancements in technology allowed for the detection of the underlying pathology of the disease through imaging and fluid biomarkers (Jack Jr et al., 2018). Despite promising results from trials conducted at single and multiple centers, the utilization and financial coverage for imaging and fluid biomarkers to assist in the diagnosis of Alzheimer's disease differ significantly across different countries (Porsteinsson et al., 2021). The advice categorizes

the diagnosis of Alzheimer's disease into the following phases: detection, evaluation/discrimination, identification, and treatment (Figure 5).

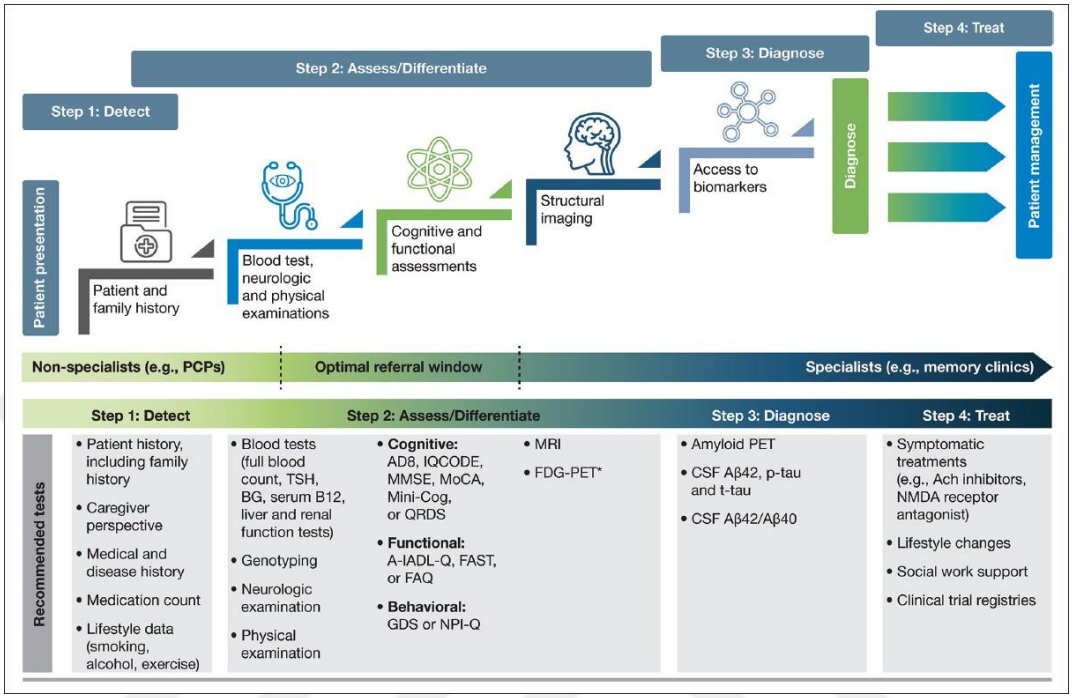

Figure 5. A visual representation illustrating the critical phases of the diagnostic process, in addition to the suggested tests to reinforce each phase (Porsteinsson et al., 2021).

1.3.1. PET Scanning for Aβ and Tau Detection

Recent developments have enabled physicians to visualize the proteins associated with Alzheimer's disease, which are Aβ and tau, using positron emission tomography (PET) scanning. Amyloid PET is currently the only imaging approach recommended by the Alzheimer's Association and the Amyloid Imaging Task Force to support the diagnosis of Alzheimer's disease. It utilizes tracers that specifically bind to Aβ within plaques (Frisoni et al., 2017). A positive amyloid PET scan shows increased cortical retention of the tracer in regions of Aβ deposition within the brain (Villemagne et al., 2018), confirming the presence of Aβ plaques (Clark et al., 2012; Villemagne et al., 2018)

and directly quantifying brain amyloid pathology (Wong et al., 2010). However, a positive amyloid PET scan alone does not definitively diagnose clinical Alzheimer's disease, and these results must be combined with other clinical assessments for an accurate diagnosis (Villemagne et al., 2018). It is important to note that amyloid PET is expensive and not readily reimbursed by health insurance providers (Frisoni et al., 2017); if it is not possible to access amyloid PET, biomarker confirmation can be assessed using cerebrospinal fluid (CSF).

1.3.2. CSF for Aβ Detection

An additional or alternate method to amyloid PET involves the collection and examination of CSF for biomarkers associated with Alzheimer's disease pathology. Patients displaying symptoms suggestive of Alzheimer's disease can undergo a lumbar puncture to analyze their CSF for specific Alzheimer's disease-related biomarkers (Jack Jr et al., 2018; Porsteinsson et al., 2021; Zhao, 2020). The strong correlation between CSF biomarkers and amyloid PET allows for them to be used in confirming Aβ burden (Hansson et al., 2018). Therefore, CSF biomarkers are widely accepted within the Alzheimer's disease community to support a diagnosis (Blennow et al., 2015). Alzheimer's disease biomarkers from the brain can be detected in CSF before the onset of overt clinical symptoms in early-stage Alzheimer's disease (Bateman et al., 2012; Jack Jr et al., 2018). When analyzing CSF results for a patient with suspected Alzheimer's disease, it is essential to note that decreased CSF Aβ42 levels and increased tau isoforms are commonly associated with the disease (Blennow and Zetterberg, 2018). The decline in CSF Aβ42 reflects an increase in Aβ aggregation and deposition in the brain (Blennow and Zetterberg, 2018). The concentration of CSF Aβ42 is directly correlated with the patient's amyloid status, such as the presence or absence of significant amyloid pathology and the total amount of Aβ peptides, including Aβ42 and Aβ40 (Blennow and Zetterberg, 2018).

1.3.3. MRI for Brain Volume

MRI (magnetic resonance imaging) is capable of detecting brain abnormalities that are connected to mild cognitive impairment. A brain MRI allows a healthcare provider to evaluate neurodegeneration in the early phases of the disease. In general terms, structural MRI in Alzheimer's disease can be divided into two categories: assessing atrophy (or volumes) and changes in tissue characteristics that lead to signal alterations on specific sequences. During the initial stages of Alzheimer's disease, brain MRI might show no abnormalities, but in the later stages, MRI may indicate a decrease in the size of different brain regions (Johnson et al., 2012).

1.4. Alzheimer's Disease Models

The intricate nature of Alzheimer's disease pathology has led to the development and enhancement of numerous preclinical disease models. These models encompass a range of approaches, including transgenic animals, two-dimensional (2D) cell cultures, and three-dimensional (3D) cell cultures. Their primary objective is to replicate the human brain environment closely, which is essential for insight into Alzheimer's disease pathology and the evaluation of new therapeutic strategies (Yanakiev et al., 2023).

Alzheimer's disease has been modeled by different approaches in the literature. Genetically induced SAD models employ induced pluripotent stem cells (iPSCs) obtained from individuals carrying the Alzheimer's disease APOE4 allele or utilize CRISPR/Cas9 technology to modify genomes to incorporate the ε4 isoform (Lin et al., 2018). In FAD-induced models, APP, PSEN1, and PSEN2 mutation led to Aβ accumulation within the cells. Following the development of cerebral organoids derived from stem cells that harbor one or more of these inherited mutations, models of FAD have been widely utilized to investigate various pathologies. On the other hand, there is another approach that models Alzheimer's disease by chemical induction way rather than utilizing mutations, namely Aβ-induced models (Bhattarai et al., 2018; Cai et al., 2020; Labour et al., 2016). This approach utilizes Aβ aggregates, which can be in oligomer or fibril form for

simulating neurotoxicity as observed in Alzheimer's disease. This alternative model offers distinct advantages and mechanisms that allow for the characterization of Alzheimer's disease without using genetic modifications of FAD or SAD.

1.4.1. Animal Models of Alzheimer's Disease

Animal models provide a unique opportunity to investigate physiological and behavioral mechanisms that many other alternatives do not offer. However, due to inter-species variations, the results obtained from these models may not always be directly applicable to preclinical drug screening for humans (Centeno et al., 2018). The utilization of animal models has limitations, including the inability to accurately represent human physiology and the difficulty in developing realistic disease models (Figure 6). For example, while there are equal proportions of neurons and glial cells in the human brain (Azevedo et al., 2009; Sreenivasamurthy et al., 2023), the glial/neuron ratio is 35.4% in mice (Erö et al., 2018; Sreenivasamurthy et al., 2023). Another difference is that although 97% of the wild mouse APP gene is similar to the human APP gene, Aβ plaques do not form in mice due to three amino acid differences in the APP sequence between mice and humans (Drummond and Wisniewski, 2017; Tanzi et al., 1987). These differences have changed the functioning and mechanism of Alzheimer's disease in the human and mouse brain. Alzheimer's disease was closely modeled in animals by creating FAD mutations, but it still does not represent the disease itself (Drummond and Wisniewski, 2017; Granzotto et al., 2024; Zhong et al., 2024). Also, the expected improvement was not achieved in these models; no correlation was observed between neural death and Aβ accumulation (Irizarry et al., 1997). Therefore, the FAD mutation could not provide a complete solution for modeling Alzheimer's disease in animals. The observation of neural death was possible with multiple mutations (FAD and frontotemporal dementia (FTD) tau mutation) not seen in Alzheimer's pathology (Cavanaugh et al., 2014; Choi et al., 2016; Drummond and Wisniewski, 2017). Although plaque formation and cognitive impairment are observed in these mouse models, one of the problems is that the development of cognitive impairment coincides with the onset of plaque development because plaque deposition is observed in 20 years before cognitive impairment in the

human brain (Bateman et al., 2012; Masters et al., 2015). In addition, regional brain atropia and neurodegeneration cannot be observed in these models as in humans (Drummond and Wisniewski, 2017). While neuronal cell death increases linearly with age in human Alzheimer's disease, brain shrinkage in transgenic mouse models occurs early in life before Aβ accumulation as in human Alzheimer's disease (Ranjan et al., 2018). As another approach, models with tau and APP mutant forms in mice carrying FTD mutations have been developed. However, these models do not fully represent the disease because these mutations do not cause Alzheimer's disease (D'Avanzo et al., 2015). According to the studies, mouse models cannot fully reflect the Alzheimer's pathology in the human brain (Duff and Rao, 2001; Sreenivasamurthy et al., 2023). One of the main reasons for this is the physiological and genetic differences between mice and humans (D'Avanzo et al., 2015).

Moreover, the investigation of Alzheimer's disease has expanded to include nonhuman primates, specifically rhesus monkeys (Macaca mulattas), stump-tailed macaques (*M.arctoides*), mouse lemurs (*M.murinus*), common marmosets (*C.jacchus*), and cynomolgus monkeys (*M.fascicularis*). These primate models present a valuable opportunity to study the effects of aging on primates that closely mirror the aging process in the human brain (Sreenivasamurthy et al., 2023). However, in these models, Aβ protein accumulation tended to accumulate in the cerebral, temporal, and limbic cortex instead of the hippocampus (Maclean et al., 2000; Sreenivasamurthy et al., 2023).

In conclusion, even though animal models provide valuable insights into Alzheimer's disease pathology, in practice, there is no animal model that mimics the disease pathology accurately due to their limitations. This highlights the requirement for alternative techniques in pre-clinical drug screening and disease modeling (Goldstein et al., 2015).

1.4.2. 2D In-vitro Models of Alzheimer's Disease

2D *in-vitro* cell cultures have been extensively utilized in scientific research for over a century (Sreenivasamurthy et al., 2023). These cultures involve the growth of cells in specialized wells or trans-wells that are often coated with substances like fibronectin,

laminin, and collagen (Hazel and Müller, 1997). These coatings enhance cell adhesion and facilitate cellular differentiation. One of the primary advantages of 2D models is their simplicity, cost-effectiveness, and ability to conduct high-throughput screening. However, neurons cultured in 2D cell culture environment can spread horizontally but lack vertical support, leading to incorrect apical-basal polarity instead of the desired morphology (Figure 6). Moreover, cells in 2D models are less precise, resulting in fewer connections between neurons and larger synaptic distances. Furthermore, these 2D models fail to accurately replicate the *in-vivo* cytoarchitectural organization and the synaptic connections present in the brain (D'Avanzo et al., 2015). Therefore, it is important to note that 2D models are inadequate for accurately representing the complexities of Alzheimer's disease pathology due to their inability to mimic the structure and functionality of the brain.

In 2D *in-vitro* models, various limitations hinder the accurate modeling of Alzheimer's disease. These limitations include inadequate cell-cell and cell-matrix interactions, inability to maintain culture for extended periods, and inability to replicate the accumulation of Aβ in the extracellular environment due to media refreshing (Cenini et al., 2021; D'Avanzo et al., 2015). Also, FAD-induced models in 2D don't allow aggregation of robust Aβ (Choi et al., 2014). Furthermore, when neurons interact with Aβ in a 2D culture, there is no disruption in the neuronal structure as observed in the human brain affected by Alzheimer's disease (Hasan and Trushina, 2022; Zhang et al., 2014).

Therefore, 3D cell culture techniques in modeling Alzheimer's disease have been accelerated due to problems experienced in animals and 2D *in-vitro* models.

1.4.3. 3D In-vitro Models of Alzheimer's Disease

3D *in-vitro* models closely resemble *in-vivo* environments, promoting faster neuronal differentiation and the formation of neural networks (Berthiaume and Morgan, 2010; Li et al., 2012; Liedmann et al., 2012; Ortinau et al., 2010; Tang-Schomer et al., 2014). In 3D cell culture, neurons exhibit more accurate gene expressions, including neuronal markers compared to 2D cell culture (Duval et al., 2017; Park et al., 2023). In this context, it is crucial to emphasize that 3D cell culture provides disease modeling more

reliably as it can better replicate the original tissue microenvironment. The development of 3D cell cultures can be approached through two main methods: scaffold-free and scaffold-based techniques. Scaffold-free techniques involve the cultivation of cells in 3D self-assembled spherical clusters, such as cell aggregates or spheroids, without incorporating external biomaterials. In this process, the extracellular matrix (ECM) is exclusively generated by the cells. On the other hand, scaffold-based 3D cultures are achieved through seeding cells into 3D matrices composed of natural, synthetic, or hybrid materials. These matrices serve to facilitate cell-matrix interaction and direct cell behavior. 3D *in-vitro* models offer a significant advancement in mimicking the complex microenvironment of the human brain. These models provide more accurate representations of neuronal behavior, gene expression, and disease pathology compared to traditional 2D cultures (Figure 6). These approaches have shown promise in replicating key aspects of Alzheimer's disease, such as Aβ accumulation and tau protein pathology. Moreover, these advancements not only improve our understanding of Alzheimer's disease but also open new avenues for developing drugs for Alzheimer's disease.

In the literature, there are various studies that have focused on developing 3D Alzheimer's disease models based on using different methods (Lee et al., 2016; Park et al., 2015; Seidel et al., 2012) (Table 1), and some studies specifically focus on spheroid-based models. In a reported study by Park et al. (2015) a microchip was developed to provide slow flow owing to a flow osmotic pump and mimic the brain microenvironment. Spheroids were obtained by culturing neural progenitor cells in hollow microwells. Longer neural networks were formed in neurospheroids in dynamic culture compared to statically cultured cells. It was also observed that Aβ significantly decreased the viability in dynamic culture and caused further destruction of neural networks. It was reported that the microfluidic chip developed based on 3D culture can be used as an *in-vitro* brain model and drug screening for neurodegenerative diseases (Park et al., 2015). In another study, Lee et al. (2016) developed a 3D human neuro-spheroid model of Alzheimer’s disease using iPSC derived from Alzheimer’s disease patients. The cells were differentiated into 3D neuronal cultures and the study evaluated Aβ peptide generation and drug response by treating 3D-differentiated neurons with BACE1 and γ-secretase inhibitors. While these inhibitors effectively reduced Aβ levels in 2D cultures, they exhibited significantly lower efficacy in 3D cultures, suggesting differences in drug penetration or cellular responses. Proteomic analysis further revealed variations in protein expression that might contribute to the differential drug effects. This study highlights the

importance of 3D neuronal models in Alzheimer's disease research, providing a more physiologically relevant system for evaluating disease mechanisms and potential therapies (Lee et al., 2016). In addition to these studies, an array platform consisting of PDMS was developed, and neurospheroids were generated by culturing ReN. Induced iPSCs containing FAD mutation were differentiated by seeding on Matrigel and used in a 3D Alzheimer's disease model. After 8 weeks of differentiation, Aβ and p-tau formations were observed in different sequences. It was reported that the developed PDMS array platform has the potential for rapid drug screening in neurodegenerative disease models (Jorfi et al., 2018). In another study, neurospheroids were produced by facilitating cell-cell interaction with an acoustofluidic chip. 3D cell culture was performed using N2A cell line, and 3D Alzheimer's disease model was developed by an Aβ-induced approach by adding aggregates to the cell culture. In the developed model, microglia cell activity was also examined, and it was observed that these cells migrated to surround Aβ aggregates. It was reported that a platform that can mimic the *in-vivo*-like brain microenvironment was developed (Cai et al., 2020). Another study investigated the effects of dynamic versus static systems on modeling Aβ-induced neuronal toxicity using a neural stem cell (NSC)-based spheroid system that simulates the brain microenvironment. The dynamic system, which uses an osmotic micropump for continuous medium flow, provided a more biomimetic environment, enhancing neuronal differentiation and complex neural network formation compared to the static system. Parameters such as cytotoxicity, cell viability, neuron/astrocyte differentiation, reactive oxygen species (ROS) production, neuron marker expression, and acetylcholine release were evaluated. Results indicated that the dynamic system supported cell viability and reduced ROS production, while Aβ exposure led to significant neuronal damage and dysfunction in both systems. Real-time impedance recording further highlighted the dynamic system's ability to monitor neural network connectivity and degeneration, demonstrating its potential for advancing neurodegenerative disease research and drug discovery (Liang et al., 2024).

In addition to the above-mentioned studies, scaffold-based approaches in 3D Alzheimer's disease model studies (Benwood et al., 2023; Choi et al., 2014; Labour et al., 2016; Park et al., 2018; Rouleau et al., 2020; Zhang et al., 2022) have recently increased (Table 1). In a prominent study, ReN cells containing FAD mutation in a scaffold composed of Matrigel were cultured by differentiating into neurons and glial cells within 3 weeks. Compared to the 2D model, Aβ 1-40 was produced 9-fold more, and Aβ 1-42

was expressed 17-fold more within 6 weeks. At the same time, Aβ-induced tau formation was observed. The developed 3D neuronal model successfully mimicked Aβ-induced p-tau pathology without the need for mutation (Choi et al., 2014). In another study, a collagen-based hydrogel was produced, and a neuronal model was established with differentiated SH-SY5Y and PC-12 cells. Cells were cultured in a scaffold containing Aβ 1-42 peptide and collagen. Aβ aggregates were visualized with Congo red and anti-Aβ biomarkers. Interaction of Aβ aggregates with cells resulted in the shortening of neurite extension. As a result, it was observed that Aβ aggregates have a cytotoxic effect on neurons. It was emphasized that it could be a potential model for understanding neuronal death in Alzheimer's disease in future studies (Labour et al., 2016). In another 3D Alzheimer's disease modeling study, a scaffold was fabricated from poly (lactic-co-glycolic acid) (PLGA) fibers using electrospinning. iPSC-derived neural cells carrying FAD mutation were cultured in 3D on the scaffold until the cells differentiated. At the end of the 19th day, Aβ 1-42 and p-tau (highly phosphorylated tau protein) expression were observed, and both were reported to be significantly increased compared to the 2D control. 3D cell culture on PLGA microfiber scaffold proved that FAD-iPSC-derived neuronal cells can show their characteristic features and are a successful *in-vitro* model (Ranjan et al., 2020). Apart from these, a few studies developed 3D Alzheimer's disease model using the bioprinting technique. In a study reported in recent years, a scaffold consisting of Matrigel and alginate to mimic neural tissue was produced by 3D bioprinting method. Subsequently, the aim was to develop a 3D Alzheimer's disease model using neural progenitor cells containing FAD mutation. After 14 days of culture, 8.2-fold more 4R-tau isoforms were observed in the 3D model in the scaffold produced by the bioprinting technique than in the 2D model. Additionally, there was a 1.6-fold greater formation and accumulation of Aβ aggregates in the 3D model. This model was reported to be more reliable for investigating Alzheimer's disease pathology than 2D cell culture (Zhang et al., 2022). In another study, fibrin-based Polycaprolactone (PCL) microsphere and cell-containing bioink were developed and bioprinted. In this study, human iPSCs derived from both healthy and patient-derived cells were differentiated into basal forebrain-like cholinergic neurons in the 3D model, and analyses were performed to evaluate cell viability, immunostaining, and electrical signals at days 1, 30, and 45 of 3D cell culture. It has been reported that the developed model can be used in the future to screen drug candidates and to facilitate personalized medicine with models developed by taking cells from patients (Benwood et al., 2023). Apart from this, there are also studies

using organoids to model Alzheimer's disease (Chen et al., 2021; Raja et al., 2016). One of them studies explored the use of 3D brain organoids to model Alzheimer's disease pathology more effectively than traditional 2D cell cultures. The researchers developed organoids from familial FAD patients carrying APP gene duplications or PSEN1 mutations and observed amyloid-beta aggregation, tau hyperphosphorylation, and endosomal abnormalities in an age-dependent manner. Additionally, treatment with β- and γ-secretase inhibitors significantly reduced Alzheimer's disease-related pathologies, demonstrating the potential of this system for drug discovery (Raja et al., 2016). In another study, APPSwe/Ind (APP) and PSEN1 (PS1) mutant genes were transfected into iPSCs from mice. Alzheimer's disease model consisting of cerebral organoids at various ages was developed without using modified serum. In the developed model, a high increase in Aβ40 and Aβ42 levels was observed. The proposed model has the potential to be used in many biomedical fields, including drug screening, stem cell transplantation, and neuronal tissue engineering (Fan et al., 2022).

Despite the contribution of scaffold-based and organoid models in modeling Alzheimer's disease, they also have limitations (Figure 6). For example, Matrigel is a commonly used material in both approaches (Benwood et al., 2023; Cenini et al., 2021; Choi et al., 2014; Cuní-López et al., 2024; Hernández-Sapiéns et al., 2020). Matrigel-derived scaffolds have difficulty accurately mimicking the mechanical, chemical, and biological features of the human brain tissue microenvironment and ECM (Cenini et al., 2021). These challenges are attributed to the nature of Matrigel itself, as well as issues related to poor characterization, batch variability, and heterogeneity (Hebisch et al., 2023). Moreover, the possible cytotoxicity associated with scaffolds and their limited degradation properties pose further challenges for the scaffold-based strategy (Louit et al., 2023; Zhou et al., 2024). On the other hand, organoid models are subject to significant drawbacks, characterized by limited reproducibility, labor-intensive methodologies, high financial requirements, and ethical considerations (Slanzi et al., 2020). In addition to that, although organoid models predominantly utilize iPSCs, studies have demonstrated that the pathogenic Aβ concentration in neuronal models derived from iPSCs is less than that found in the brains of patients with Alzheimer's disease (Choi et al., 2016; D'Avanzo et al., 2015). Generating iPSCs is significant as it involves a complete reprogramming of cells, effectively eliminating the aging-related phenotypes, including mitochondrial function and telomere length. This reprogramming returns the cells to an "embryonic-like" state (Mahmoudi and Brunet, 2012; Sen et al., 2016). Therefore, even when iPSC

lines are derived from SAD patients (Choi et al., 2014), the reprogramming may have erased a notable proportion of the epigenetic marks that contribute to a genetic background for the disease (Pavoni et al., 2018).

Thus, scaffold-free strategies have emerged as a significant tool to overcome these obstacles. These techniques eliminate the requirement for external scaffolding materials, facilitating the self-organization of cells and, eventually, the formation of spheroids. Among these techniques, Magnetic levitation (MagLev) technology has attracted considerable attention due to its rapid and easy operational process (Ashkarran et al., 2020; Gao et al., 2022; Onbas and Arslan Yildiz, 2021; Quagliarini et al., 2022; Türker et al., 2018). Recently, its use has been accelerated in 3D cell culture studies.

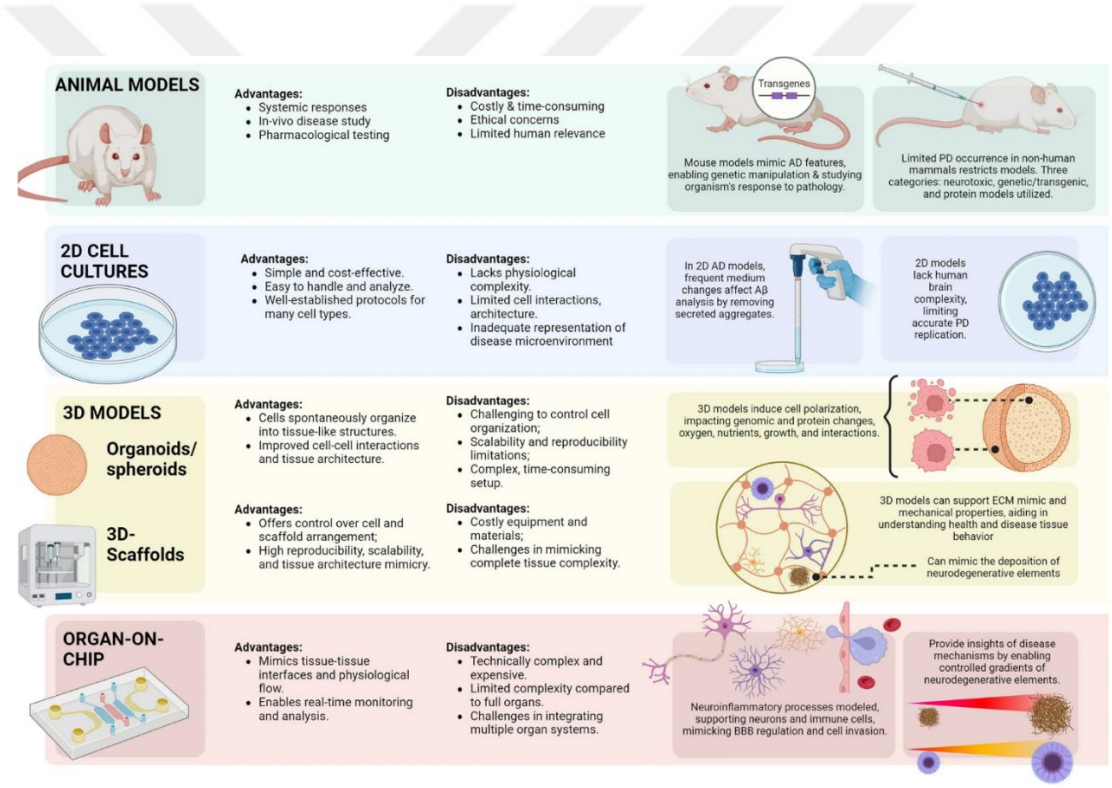

Figure 6. The advantages and disadvantages of *in-vivo* and *in-vitro* models in the diagram, showing the disadvantages and advantages of employing animal models, 2D or 3D, and organ-on-a-chip platforms (Balestri et al., 2024).

Table 1. Studies of Alzheimer's disease modeling utilizing 3D cell culture methodologies.

3D cell culture method	Cell type	Disease modeling approach	Pathology	Methodology/ material	References
Aggregate based	SH-SY5Y	Overexpress N-terminal EGFP-fused human tau (0N4R) variants	Tau	Organotypic-like spheroid culture	Seidel et al., 2012
Scaffold based	ReNcell VM (ReN) human neural precursor	FAD-induced model	Aβ and tau	Matrigel scaffold	Choi et al., 2014
Scaffold based	Human iPSC-derived neuroepithelial stem cells	Aβ-induced	P21-activated kinase modulation	Self-assembling peptide hydrogel matrix-based culture	Zhang et al., 2014
Aggregate based	Human iPSC derived from blood cells	SAD-induced model	Aβ and tau	Neuro-spheroid model obtained by ultra-low attachment plastic plates	Lee et al., 2016
Organoid	Human iPSC derived from fibroblasts	FAD-induced model	Aβ and tau	Embryoid bodies/Neural organoid culture	Raja et al., 2016
Scaffold based	PC-12 cells, SH-SY5Y cells	Aβ-induced	Aβ aggregates	Collagen matrix-based culture	Labour et al., 2016
Scaffold based	ReNcell VM (ReN) human neural precursor	FAD-induced model	Aβ and tau	Matrigel in a microfluidic chip	Park et al., 2018
Aggregate + Scaffold based	ReNcell VM human neural stem (ReN) cells and human iPSC-derived neural progenitor cells (hiPSC)	FAD-induced model	Aβ and tau	Neurospheroids suspended in Matrigel matrix	Jorfi et al., 2018

(Cont. on next page)

Table 1. (Cont.)

Scaffold based	Human iPSC-derived Neural Stem Cells	Aβ-induced	Aβ and tau	starPEG-heparin based hydrogels	Bhattarai et al., 2018
Scaffold free	N2A cell line	Aβ-induced	Aβ aggregates	Neurospheroids fabrication by acoustofluidic chip	Cai et al., 2020
Organoid model	Mouse iPSCs cells	FAD-induced model	Aβ aggregates	Matrigel scaffold	Fan et al., 2020
Scaffold based	iPSC-derived neural cells	FAD-induced model	Aβ and tau	Electrospinning of poly (lactic-co-glycolic acid) (PLGA)	Ranjan et al., 2020
Scaffold based	Human iPSC-patient-derived neural cells	SAD-induced model	Aβ and tau	Silk fibroin scaffold	Rouleau et al., 2020
Organoid model	Human iPSC-derived neural cells	SAD-induced model	Aβ and tau	Matrigel scaffold	Chen et al., 2021
Scaffold based	Human iPSC-derived neural cells	FAD-induced model	Aβ and tau	Bioprinting of Matrigel/Alginate	Zhang et al., 2022
Scaffold based	Human iPSC-derived neural cells	FAD-induced model	Aβ aggregates	Bioprinting of fibrin-based PCL microsphere	Benwood et al., 2023
Scaffold based	ReNcell VM (ReN) human neural precursor and MDMi (monocyte-derived microglia cell-like)	Aβ-induced	Aβ aggregates	Matrigel based	Cuní-López et al., 2024
Aggregate + Scaffold based	Rat neural stem cell	Aβ-induced	Aβ aggregates	Neurospheorid obtained from PDMS chip containing PLL/PLGA	Liang et al., 2024

1.5. 3D Cell Culture by MagLev

MagLev technology is one of the scaffold-free approaches that gained attention in 3D cell culture. The principles of MagLev, originally demonstrated recently on living objects by Geim's group (Berry and Geim, 1997), have found successful applications in chemistry, material science, and biochemistry, with implications for tissue engineering (Ge et al., 2020). MagLev is a newly developed, simple, and cost-effective methodology that can perform 3D assembly of cells. The underlying principle is applying a magnetic force to levitate objects in a paramagnetic medium. The gradient of the external magnetic field causes the diamagnetic material, like the cells, to move from areas of high magnetic fields to low magnetic fields, thereby positioning them based on their density differences (Cui et al., 2023). Ultimately, buoyancy, gravitational, and magnetic forces acting on the cell balance each other, and cells are levitated at a certain levitation height within the magnetic field. MagLev setup components typically comprise two permanent magnets (e.g., Neodymium Iron Boron - NdFeB) arranged in an anti-Helmholtz configuration, where the same poles are oriented towards each other. This configuration enables the generation of a magnetic field and magnetic field gradient.

Positive magnetophoresis involves labeling the cells with magnetic nanoparticles (MNPs) to gain magnetic properties in cells (Seo et al., 2023). The direct uptake of MNPs by cells can result in the development of magnetic sensitivity (Souza et al., 2010). However, the endocytic introduction of MNPs into cells has been shown to cause cytotoxicity (Tomitaka et al., 2011). Therefore, negative magnetophoresis can be an alternative way to positive magnetophoresis.

Negative magnetophoresis serves as an effective method for the 3D assembly of cells through the process of levitation (Costa et al., 2016). Negative magnetophoresis does not require labeling MNPs to cellular structures (Tepe et al., 2023). This method successfully mitigates challenges related to MNPs, such as cytotoxic effects. In this approach, cells are suspended in a solution of paramagnetic salts (Türker et al., 2018). Commonly utilized paramagnetic salt solutions include manganese (II) chloride ($MnCl_2$) (Mirica et al., 2009; Subramaniam et al., 2014), gadolinium (III) chloride ($GdCl_3$) (Mirica et al., 2010), and Gd (DTPA) (Guevorkian and Valles Jr, 2006; Mirica et al., 2010). These materials are easily accessible, cost-effective, and provide a transparent medium that

allows for the observation of samples (Onbas and Arslan Yildiz, 2021; Türker et al., 2018).

Recently, MagLev technology has emerged as a new tool for developing spheroids and 3D cellular structures. This technique utilizes the magnetic field to gather cells at a specific levitation height. Cell-cell interactions are enhanced by accumulating cells at the same levitation height, forming cellular aggregates and, eventually, spheroids. MagLev technology enables manipulating cells without physical contact and provides spatial control in a 3D environment that promotes cell-cell interactions. This allows cells to establish their ECM and facilitate the formation of more complex and heterogeneous 3D cellular structures.

MagLev technology offers several advantages in 3D cell culture over other scaffold-free techniques. While the hanging drop method is known for its simplicity, speed, and conventional approach to spheroid formation, it has significant limitations. One major drawback is its inability to refresh the culture medium, making it challenging to introduce chemicals at precise time intervals, such as those needed for differentiation protocols (Klingelhutz et al., 2018). Additionally, maintaining long term cultures with this technique is difficult due to its low working volume (Klingelhutz et al., 2018) and the risk of drop dislodgement (Lv et al., 2017). Bioreactors offer another scaffold-free option, extending culture duration and enabling high-throughput production. However, the continuous rotation involved in bioreactors can create shear stress on cells, leading to potential cell damage (Lv et al., 2017). Cell sheet engineering, another scaffold-free approach, mimics the architecture of native tissues, allowing for the creation of complex tissue structures (De Pieri et al., 2021). Despite this, it is limited by the achievable thickness due to poor vascularization, high demand for cell numbers, and considerable costs (De Pieri et al., 2021).

In contrast, MagLev technology supports spheroid formation with high circularity and precise control over spheroid size and area by adjusting various parameters. Obtained spheroids exhibit high cell viability even in the long term cultures. Also, MagLev technology provides high reproducibility and cost-effective biofabrication without any ethical concerns. This technique can be adapted to several cell types, such as adipose cells (Daquinag et al., 2013), aortic valve cells (Tseng et al., 2014), saliva gland-derived cells (Ferreira et al., 2019), and chondrocytes (Parfenov et al., 2020) for desired tissue targets. These studies showed that magnetically guided cells exhibited higher proliferation resembling *in-vivo* conditions compared to 2D cell culture (Souza et al., 2010; Tseng et

al., 2014). Therefore, MagLev technology, with its numerous advantages over other 3D fabrication methods, stands out as a particularly promising tool in this field. To date, various pioneering studies have explored using MagLev technology for creating 3D cultures across different tissue types.

Daquinag et al. (2013) utilized a ring magnet levitation (RM-LEV) tissue culture system, which is founded on the assembly of magnetic nanoparticles, to fabricate a model for the development and growth of white adipose tissue (WAT) in organoids known as adipospheres (Figure 7). This research demonstrated that levitated cell spheroids are suitable for prolonged multicellular studies and more faithfully mimic the spatial organization of cells than traditional 2D cell culture methods (Daquinag et al., 2013).

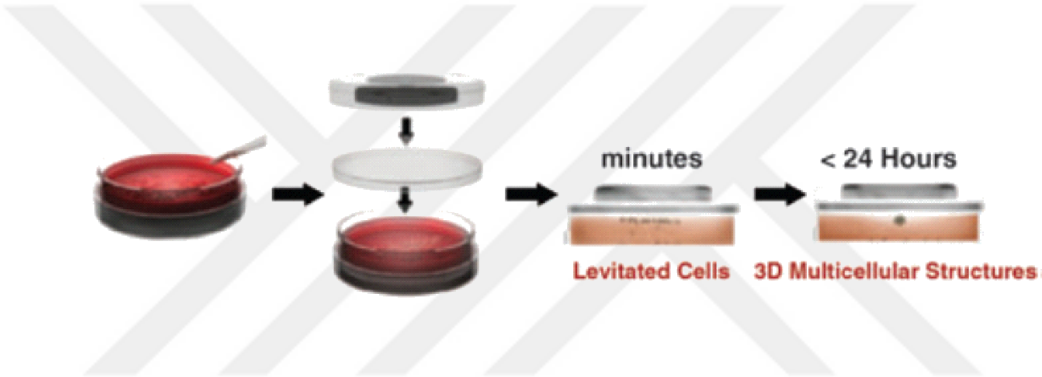

Figure 7. The setup and testing of a magnetic levitation system for 3D culture of adipocyte cells (Daquinag et al., 2013).

In addition, MagLev setup can be fabricated with different designs including 4 mirrors and poly (methyl methacrylate) (PMMA) holders. Türker et al. (2018) utilized a 4-mirror-based MagLev setup that allows monitoring of the 3D cell culture formation *via* mirrors under the microscope (Figure 8). In this study, MagLev setup was utilized for spheroid formation with NIH 3T3 and HCC 827 cells. The results indicated that the established MagLev system is a valuable method for non-contact cell manipulation and 3D cell culture formation (Türker et al., 2018).

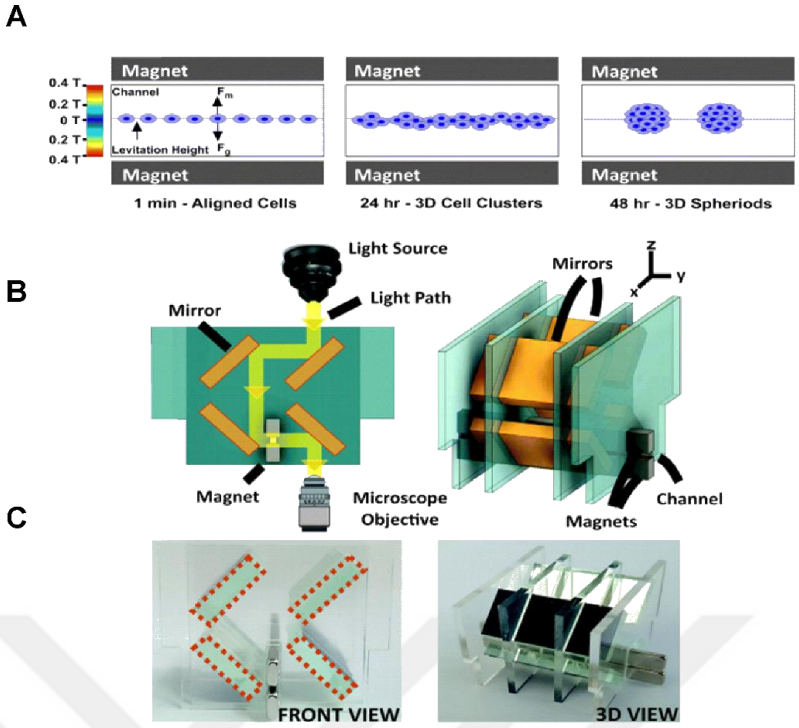

Figure 8. The illustration depicts A) MagLev technology and the formation of 3D cell cultures B) MagLev systems utilizing a four-mirror configuration are presented in 2D and 3D drawings. C) A frontal and 3D perspective of the MagLev components: mirrors, a capillary glass channel, and NdFeB magnets and transparent PMMA holders (Türker et al., 2018).

On the other hand, the magnetic force in the Maglev system can be adjustable, and it has been shown that a high magnetic field does not adversely affect cell viability as shown in the study performed by Parfenov et al. (2020) The aim of the study is to decrease the concentration of paramagnetic agents by increasing the magnetic field within the custom design of the MagLev setup (Figure 9). Spheroids were fabricated from the SW1353 chondrosarcoma cell line in MagLev setup, employing a gadobutrol salt solution containing 0.8 mM Gd^{3+} within a 19 T magnetic field. Also, an assessment of viability conducted after a one-hour exposure to high magnetic fields, with strengths of up to 30 T, revealed no significant cytotoxicity or changes in the morphology of the spheroids (Parfenov et al., 2020).

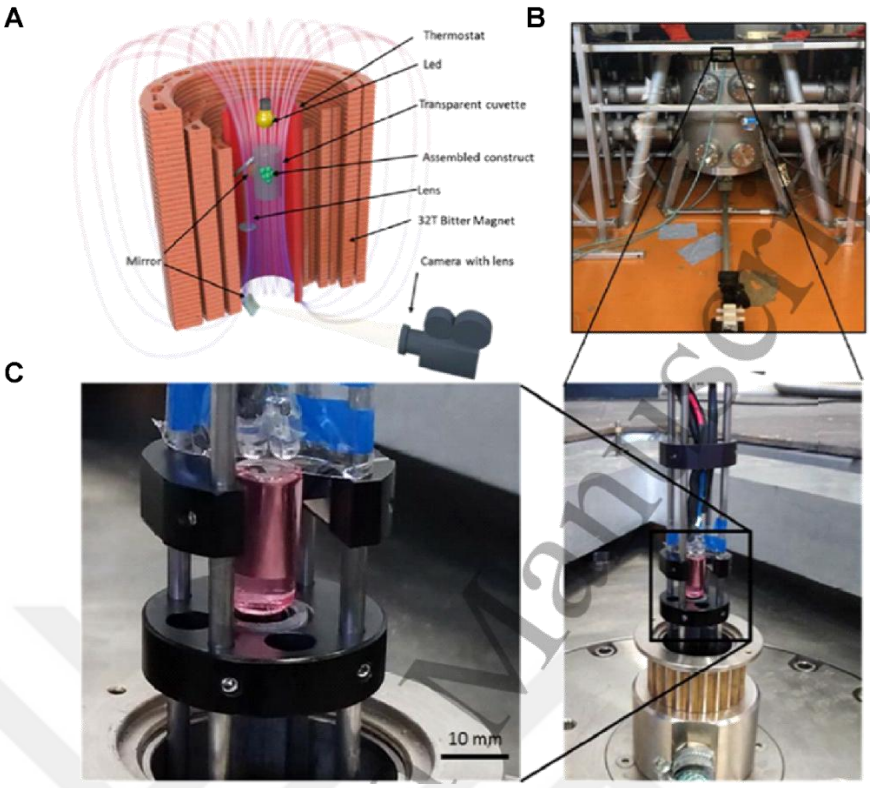

Figure 9. Illustration of the MagLev setup. A) 32T bitter magnet installation B) Image of the bitter magnet C) Cuvette with paramagnetic agent and medium, placed in the custom-designed setup (Parfenov et al., 2020).

In another study, Onbas and Arslan Yildiz (2021) developed another design of Maglev setup that allows for a tunable 3D cellular structure and spheroid formation (Figure 10). Also, this study showed that MagLev technology allows co-culture. Here, different cell lines with varied cell numbers and paramagnetic agent concentrations were carried out to show the adjustable size of 3D cellular structures and the effect of these parameters on cell viability and circularity of the 3D cellular structures. The methodology facilitates the production of adjustable spheroids, allowing adjustment in spheroid size, surface area, circularity, and the development of necrotic cores through the manipulation of cell seeding density, Gx concentration, and duration of culture. Also, it showed that Maglev methodology allows 3D cell culture utilizing different types of cell lines (Onbas and Arslan Yildiz, 2021).

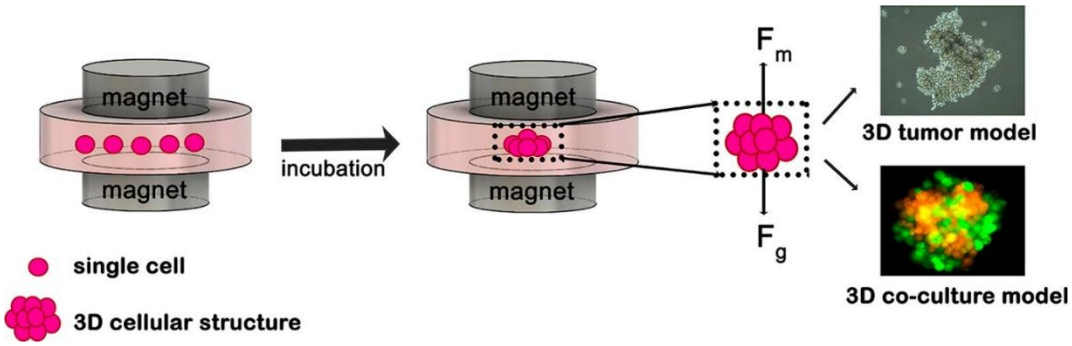

Figure 10. The illustration of the developed MagLev setup and formation of 3D cellular structures (Onbas and Arslan Yildiz, 2021).

Overall, these studies collectively demonstrate that MagLev technology is highly versatile, enabling 3D cell culture of a wide variety of cell types within setups that can be tailored with different design configurations. This technology not only facilitates the creation of complex 3D cellular structures by allowing precise adjustments to various parameters but also supports the maintenance of these cultures over extended periods with high cell viability. This makes it a crucial tool for researchers to conduct studies that require sustained high cell viability for specific research targets.

On the other hand, there are a few studies about neural tissue engineering using MagLev methodologies (Onbas and Arslan Yildiz, 2021). MagLev technology in 3D Alzheimer's disease modeling has not been explored in existing studies, indicating a significant gap in research within this field. This gap provides a valuable opportunity to advance the understanding of the disease through innovative modeling approaches.

1.6. Current Therapeutics for the Treatment of Alzheimer's Disease

To date, synthetic and natural sources of drugs have been developed for Alzheimer's disease; however, a few drugs have been approved by the Food and Drug Administration (FDA) for improving the symptoms of Alzheimer's disease. One mechanism involves cholinesterase inhibition, which reduces symptoms by improving the cholinergic function in neuronal synapses. These drugs act by blocking the hydrolysis

of the critical neurotransmitter acetylcholine. Only four drugs have been approved by FDA in this context up to now: Tacrine (1993, Cognex™), Donepezil (1996, Aricept™), Rivastigmine (2000, Exelon™), and Galantamine (2001, Razadyne™) (Dos Santos Picanco and Ozela, 2018; Park, 2010). Tacrine was a synthetic compound that was the first approved drug, having dose-dependent efficacy, short half-life, and high adverse effects such as hepatotoxicity (Engelhardt et al., 2005). Donepezil is another synthetic drug that was developed by a Japanese company and highly improves symptoms of Alzheimer's disease. However, it can interact with other drugs when it is used in combination (Engelhardt et al., 2005). Galantamine is a natural source-derived drug obtained from the bulbs and flowers of snowdrop *Galanthus woronowii* Losinsk (Park, 2010). It has a similar acting mechanism to Donepezil, but it requires caution when combined with another drug (Engelhardt et al., 2005). Rivastigmine is a synthetic drug that exhibits good activity and tolerance in patients with a neuroprotective effect and improves cognition (Rösler et al., 1999). The other mechanism involves memantine, which was approved in 2003. It is a synthetic drug that is a non-competitive N-methyl-D-aspartate (NMDA) channel blocker that reduces the activity of the neurotransmitter glutamate, which plays a crucial role in learning and memory by binding to the NMDA receptor (Park, 2010). Memantine decreases excessive glutamatergic neurotransmission and protects from Aβ-induced neurotoxicity. However, Memantine cannot improve people with moderate to severe Alzheimer's disease (Fox et al., 2012). On the other hand, these drugs can have serious side effects, such as nausea, vomiting, diarrhea, and dizziness (Hansen et al., 2008; Manap et al., 2019).

In addition, the current drug development pipeline is a strong reflection of ongoing research efforts with 32.5% of the 126 active clinical trials for Alzheimer's disease concentrating on either Aβ (30 trials, representing 23.8%) or tau (11 trials, accounting for 8.7%). Among the phase 3 trials, 52% (13 out of 25) are focused on these targets with 12 focused on Aβ and one on tau (Hara et al., 2019). While therapeutic strategies aimed at eliminating or reducing the production of Aβ have shown promise in preclinical and early-phase studies, they have largely failed to impact the progression of Alzheimer's Disease in later-phase clinical trials (Hara et al., 2019). it is essential to highlight that Aducanumab (Decourt et al., 2022), Blarcamesine (ANAVEX2-73) (Abdulraheem et al., 2024), ALZT-OP1a/b (Lozupone et al., 2022), CAD106 (Riviere et al., 2024), Crenezumab (Yoshida et al., 2020), and Elenbecestat (E2609) (Kocienski, 2022), targeting different mechanisms, constitute a considerable share of the drugs

undergoing phase III trials, representing 61% of the total. Besides, other targets, such as neurotransmitters, tau proteins, antioxidants, and anti-inflammatory processes, are also being explored in clinical studies (Long and Holtzman, 2019). Among these, two trials are concentrating on inflammatory pathways, indicating that neuroinflammation may be a significant factor contributing to the pathophysiology of Alzheimer's disease (Cummings et al., 2019; Singh et al., 2021).

Also, there are alternative natural compounds in which bioactive components are known to possess various beneficial biological effects that get the attention of researchers. Reports indicate that 63% of the low molecular weight drugs developed from 1981 to 2006 are classified as natural products or compounds derived from natural sources (Newman and Cragg, 2007). This finding suggests that natural products hold considerable promise for the development of biologically active compounds that might exhibit anti-Alzheimer's disease activity (Park, 2010). Several innovative therapeutic strategies derived from natural sources for Alzheimer's disease have been discovered up to date, and some of them concentrate on decreasing the levels of Aβ aggregates. Curcumin, also known as 1,7-bis(4-hydroxy-3-methoxyphenyl)-1,6-heptadiene-3,5-dione, is a naturally occurring yellow-orange pigment obtained from the rhizomes of Curcuma longa L. (Zingiberaceae) (Figure 11). It has several pharmacological features such as antitumor, anti-inflammatory, antioxidant, and neuroprotective effect (Ak and Gülçin, 2008; Menon and Sudheer, 2007). This compound has been found to have inhibitory effects on the formation of Aβ oligomers and fibrils, as well as it has ability to bind to plaques and reduce amyloid concentrations in the brains of animal models (Chen et al., 2017; Garcia-Alloza et al., 2007; Ma et al., 2013; Yang et al., 2005). Moreover, molecular dynamics simulation studies showed that the main factor in preventing oligomerization and promoting the formation of nontoxic aggregates is the distortion of protofibrils resulting from the interaction with Curcumin (Battisti et al., 2017; Kundaikar and Degani, 2015; Ngo and Li, 2012; Rao et al., 2015). In addition, Curcumin crosses the blood-brain barrier and binds to aggregates *in-vivo* owing to its symmetrical phenol groups (Rossi et al., 2008; Yang et al., 2005). These properties of Curcumin have attracted the attention of researchers, and recently, the use of Curcumin in Alzheimer's disease modeling has increased.

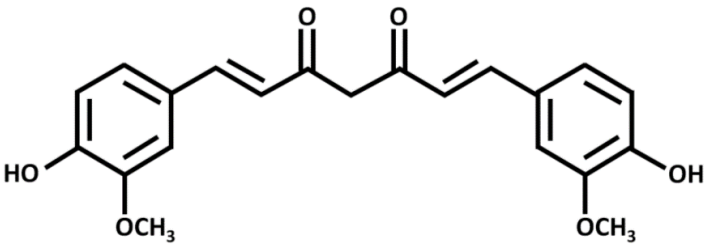

Figure 11. Curcumin's chemical structure: a beta-diketone compound containing two substituted aromatic rings linked by a seven-carbon chain and an aromatic ring with one hydroxy and one methoxy group (Zhai et al., 2020).

Recently, the neuroprotective effect of Curcumin has been investigated in 3D Alzheimer's disease modeling. For instance, Silveira et al. developed a herpes virus-induced Alzheimer's disease model on a silk-based scaffold. Twenty-one compounds, including Curcumin, were screened on the model. Results showed that Curcumin reduced aggregate formation at 10 μM, which was the minimum effective concentration (Silveira et al., 2022). In another study, Park et al. developed a 3D Alzheimer's disease model using patient-derived cells. Then, Curcumin was screened on this model, resulting in an anti-Aβ aggregate effect (Park et al., 2023). These studies highlight the importance of 3D culture systems in evaluating the neuroprotective effect of Curcumin, as they provide a more accurate representation of the complex cellular interactions and disease mechanisms that occur in the human brain compared to traditional 2D models.

1.7. Scope of the Thesis

This thesis aims to develop a novel 3D *in-vitro* experimental platform for Alzheimer's disease modeling using MagLev technology (Figure 12), whereas the platform provides screening of therapeutic interventions for Alzheimer's disease. Current animal and *in-vitro* models, often relying on 2D cell cultures, fail to capture the spatial and cellular organization of the brain, limiting their utility in understanding disease

mechanisms and testing therapeutic agents. This thesis addresses these limitations using MagLev technology to develop a more physiologically relevant 3D model.

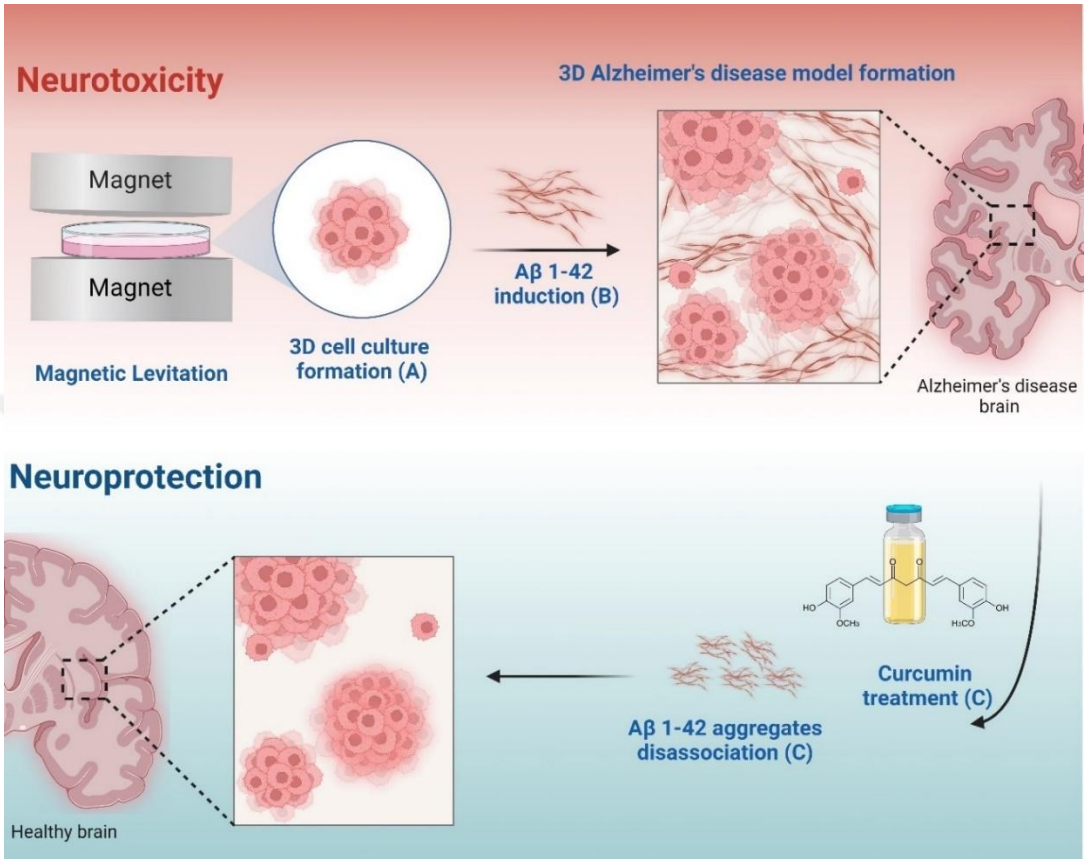

Figure 12. Depiction of the 3D Alzheimer's disease model formation (A) 3D cell culture formation via MagLev (B) Aβ 1-42 aggregates induction to 3D cell culture (C) Curcumin treatment and Aβ 1-42 aggregates disassociation (*The illustration was created by BioRender.com*).

The scope of this research encompasses the use of differentiated SH-SY5Y neuronal cells and PC-12 cells as key components in 3D cell culture formation (Figure 12A). MagLev technology facilitates the assembly of these cells into 3D structures without needing external scaffolds, relying instead on magnetic forces to position cells within a paramagnetic medium. This scaffold-free approach ensures that cells interact naturally with one another, promoting cell-cell and cell-matrix interactions. The thesis explores the application of MagLev technology in forming spheroids with high circularity

and uniform size, which are essential for achieving consistent experimental results. The study optimizes parameters such as Gx concentration and cell density for the initial step. By adjusting these parameters, the study aims to establish a reproducible method for generating 3D cell cultures that can be used for various experimental applications. A critical aspect of this research is the simulation of Alzheimer's disease conditions within the 3D model by inducing Aβ1-42 aggregates. This is achieved by introducing Aβ1-42 aggregates into the cell culture medium (Figure 12B), which induces neurotoxic effects. The study examines the impact of Aβ1-42 on neuronal viability.

In addition to modeling the disease, the thesis investigates the neuroprotective potential of Curcumin, known for its antioxidant and anti-inflammatory properties, and can disassociate Aβ aggregates. Curcumin is introduced into the 3D cell culture system to assess its ability to suppress Aβ1-42-induced neurotoxicity (Figure 12C). The research evaluates various concentrations of Curcumin to determine the optimal dosage for reducing Aβ-induced damage while maintaining cell viability. This aspect of the study not only explores Curcumin's potential as a therapeutic agent but also demonstrates the utility of the 3D model as a drug screening platform.

In conclusion, the scope of this thesis encompasses the development, optimization, and application of 3D *in-vitro* platform for Alzheimer's disease modeling using MagLev technology. The research aims to provide a reliable and reproducible method for studying Alzheimer's disease pathology and evaluating potential therapeutics.

CHAPTER 2

MATERIALS & METHODS

2.1. Standard 2D Cell Culture

SH-SY5Y (Human bone marrow neuroblastoma, ATCC® CRL-2266™) cell line was utilized in this study due to its extensive usage as a model cell line in Alzheimer's disease research (Abdul Manap et al., 2020; Calan et al., 2016; Krishtal et al., 2017; Manap et al., 2019). This cell line is of human origin; thereby, it can produce disease-related proteins in a cellular environment that reflects human protein and gene expression patterns (Strother et al., 2021). Also, it provides a homogeneous population that supports reproducibility, making it an appropriate choice for large-scale culture (De Conto et al., 2021). In this study, the cells were cultivated under standard conditions, which involved using DMEM (Gibco, USA), 15% FBS (Gibco), and 1% PenStrep (Gibco, USA) in a culture medium, and they were maintained at 37°C with 5% CO_2. Subsequently, the cells were employed for further investigations.

PC-12 is a cell line derived from rat pheochromocytoma (ATCC® CRL-1721 ™) and can synthesize nicotinic receptors (as a subtype of cholinergic receptors), which makes it an ideal model to study the pathology of Alzheimer’s disease (Xie et al., 2023). On the other hand, this cell line is more prone to be dopaminergic neurons after differentiation (Guroff, 1985; Jao et al., 2024; Srivastava et al., 2018) rather than the cholinergic neuron character. Therefore, in this study, PC-12 cells were not differentiated during 3D cell culture. In this study, PC-12 cells were maintained in a standard culture medium consisting of DMEM (Sakagami et al., 2017), 10% FBS, and 1% PenStrep at 37°C and 5% CO_2. Subsequently, the cells were employed for further studies.

2.2. MagLev Setup for 3D Cell Culture

3D cell culture of SH-SY5Y and PC-12 cells was carried out using MagLev technology, as depicted elsewhere (Onbas and Arslan Yildiz, 2021). This system consists of two permanent NdFeB N35 disc magnets (Mıknatıs Teknik Company, Turkey) with 40x5 mm dimensions arranged in an anti-Helmholtz configuration and replaced in poly (methyl methacrylate) (PMMA) holders (Figure 13). A Petri dish (Ibidi-80131, 35 mm) containing cells, cell medium, and the paramagnetic agent (Gadobutrol (Gx)/Gadavist, Bayer, Germany) was positioned between the magnets within the setup to conduct 3D cell culture experiments.

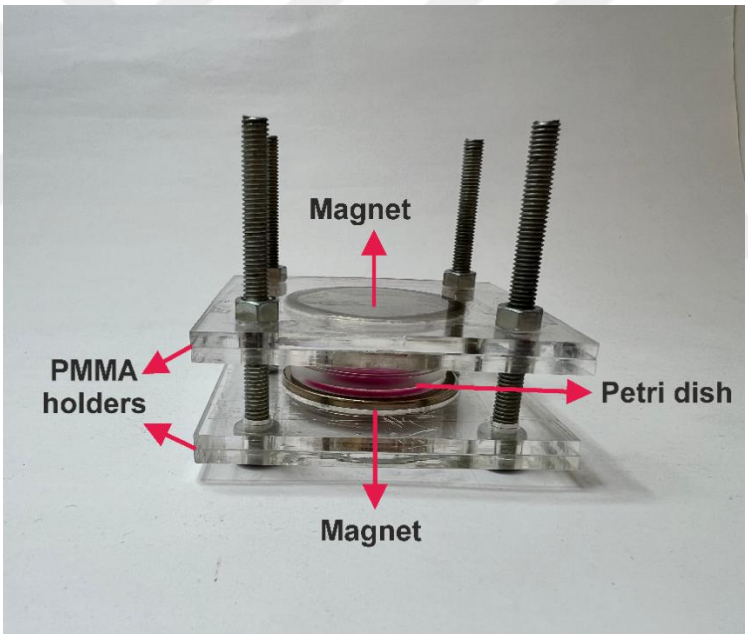

Figure 13. MagLev setup components: NdFeB N35 disc magnets, PMMA holders, and petri dish.

The optimal Gx concentration and cell number were determined for 3D cell culture formation. First, 10-100 mM Gx was investigated at $25x10^3$ cell number, then SH-SY5Y cell number optimization was conducted at 10 mM Gx, while PC-12 cell number optimization was done at 30 mM Gx for 5-100 $x10^3$ cells. Following 3D cell culturing,

structural changes of 3D cellular assembly were monitored by light microscopy, while cell viability was assessed by Live-Dead assay with Calcein Green/Propidium Iodide (PI) staining (ATT Bioquest, USA) for 9 days. Cell viability (%) and circularity versus area changes were characterized using Image J software (Onbas and Arslan Yildiz, 2021) (NIH). Circularity was measured based on the formula (Onbas and Arslan Yildiz, 2021).

2.3. Differentiation of SH-SY5Y Spheroids in MagLev Setup

Differentiation of SH-SY5Y proceeded on 2D cell culture for optimization before maintaining on 3D cell culture studies. The common protocol was utilized based on the literature (Bilginer Kartal and Arslan Yildiz, 2024; de Medeiros et al., 2019; Serdar et al., 2020), which applied Retinoic acid (RA, Across organics, Belgium) and Brain-derived neurotrophic factor (BDNF, MedChem, USA). Firstly, the cell number was optimized for differentiation using only RA before sequential treatment. For this purpose, $25x10^3$ and $50x10^3$ cell numbers were utilized. Following optimization, SH-SY5Y differentiation was carried out *via* RA-BDNF. Briefly, 10 μM RA that was dissolved in DMSO on day 1 was supplemented to cell culture with 1% FBS for 5 days by refreshing the medium every other day. On day 5, 50 ng/mL BDNF was supplemented into the cell medium; again, the medium was refreshed every other day until day 9. Cellular morphology and differentiation progress were monitored by Zeiss Axio Observer microscopy. Following the optimization of the differentiation protocol in 2D cell culture, the differentiation protocol was adapted to 3D cell culture, which was maintained in the MagLev setup.

The characterization of differentiation was carried out by the Neuron J program (NIH, USA), which traces and quantifies neurites for 2D cell culture. Also, immunostaining was performed for neuronal characterization to confirm β-III tubulin (ABclonal, USA) and neuronal nuclei (NeuN, ABclonal, USA) neuronal marker expressions in both 2D and 3D cell cultures. Fluorescence intensities of β-III tubulin and NeuN were measured for un-/differentiated cells in both models using Image J (NIH, USA) software.

2.4. 3D Alzheimer's Disease Modeling through Aβ 1-42 Induction

The primary aim of this investigation was to develop a 3D model of Alzheimer's disease induced by Aβ1-42 through the application of MagLev technology. The process involved generating Aβ1-42 aggregates by dissolving Aβ1-42 monomers (Royobiotech, China) in DMSO and incubating at 37ºC for 72 hours. The aggregate formation was confirmed using Congo red staining (Isolab, Germany), where 40 µM Congo red was added to Aβ1-42 aggregates ranging from 0 to 100 µM and incubated overnight. The spectral analysis was conducted by recording the Congo red spectrum between 400-700 nm with 10 nm intervals using a Multiskan™ GO microplate spectrophotometer (Feng et al., 2021; Klunk et al., 1999). Subsequently, the aggregates were examined under light microscopy after centrifugation at 14000 rpm. Additionally, scanning electron microscopy (SEM) analysis was employed to evaluate the formation of Aβ1-42 aggregates. Following the characterization of the aggregates, 5-15 µM Aβ1-42 aggregates were introduced to un-/differentiated SH-SY5Y and PC-12 in 2D cell culture to determine neurotoxic concentration before examining it on 3D cell culture. The aggregates were incubated in 2D cell culture environment for 24h, 48h, and 72h. The neurotoxicity of aggregates was evaluated by Live-Dead (Calcein AM-Propidium Iodide) and MTT (3-(4,5-Dimethylthiazol-2-yl)-2,5-Diphenyltetrazolium Bromide) assays. After establishing the effective neurotoxic concentrations in 2D models, un-/differentiated SH-SY5Y spheroids and 3D culture of PC-12 were incubated with Aβ1-42 aggregates at concentrations of 10-50 µM for 7 days for SH-SY5Y and 21 days for PC-12 to model Alzheimer's disease, as shown in Figure 14. This figure illustrates the experimental timeline for developing 3D Alzheimer’s disease models using SH-SY5Y and PC-12 cells through MagLev. For SH-SY5Y cells, cells were seeded in the MagLev setup, initially (day 0). Spheroid formation was obtained, and RA was applied to induce neuronal differentiation on day 4. BDNF was introduced to 3D cell culture to promote neuronal differentiation on day 9. Aβ 1-42 aggregates were introduced on day 13. and Alzheimer’s disease model was developed on day 20.

For PC-12 cells, the timeline also starts with cell seeding in the MagLev setup, initially (day 0). 3D cultured of PC-12 cells was then incubated with Aβ 1-42 aggregates from day 4 to day 25 for 3D Alzheimer’s disease modeling. Then, cell viability was

measured to evaluate neurotoxic parameters using Image J software. To further characterize the 3D Alzheimer's disease model, immunostaining of Choline acetyltransferase (ChAT, ABclonal, USA) was conducted to evaluate cholinergic neuron activity loss for differentiated SH-SY5Y spheroids and 3D cultured PC-12 cells after exposure Aβ 1-42 aggregates. The fluorescence intensities of ChAT were measured using Image J software, allowing for quantitative comparisons between control and Aβ-treated groups.

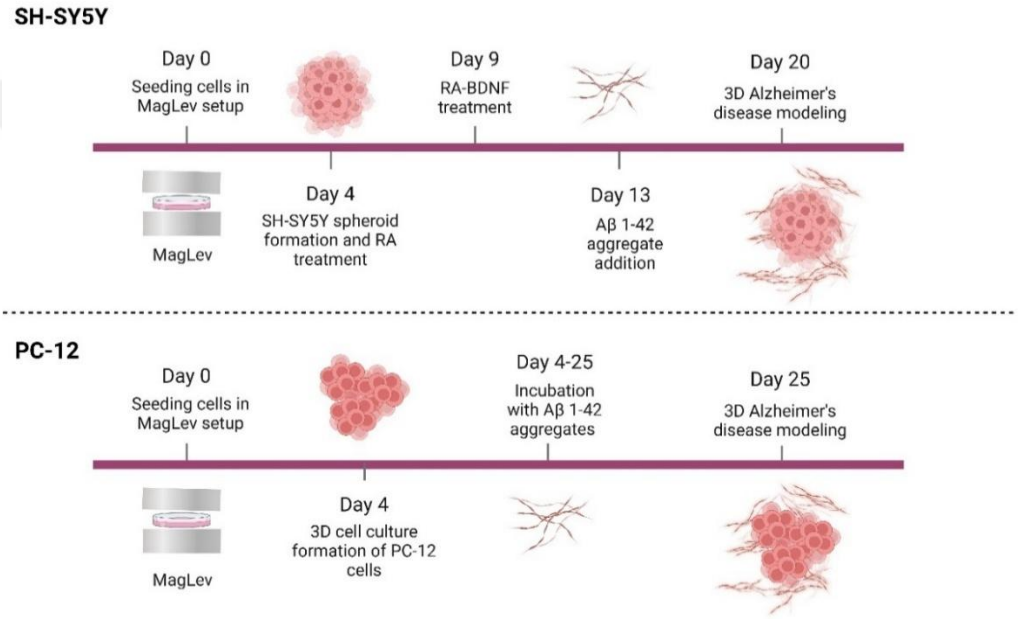

Figure 14. Depiction of 3D Alzheimer's disease protocol: SH-SY5Y cells formed spheroid and differentiated via RA-BDNF sequentially in MagLev, then induced by Aβ aggregates. PC-12 cells formed 3D cell culture and were induced by Aβ aggregates.

2.5. Curcumin Treatment on 3D Cell Culture

The potential of Curcumin to disassociate Aβ 1-42 aggregates was examined by utilizing Congo red (Isolab, Germany) and Thioflavin T (MedChemExpress, USA) assays

(Ding et al., 2024) before testing it on 3D Alzheimer's disease models. Curcumin was incubated at 25, 50, 75, and 100 μM with 50 μM Aβ 1-42 aggregates for 72h. Following this incubation, Congo red and Thioflavin T assays were conducted separately using a spectrophotometer (DaSilva et al., 2010; Zhu et al., 2007). Subsequently, Curcumin at 25, 50, 75, and 100 μM was introduced to SH-SY5Y and PC-12 cells on 2D cell culture to determine the proper concentration range for 3D cell culture. The cytotoxicity of Curcumin was evaluated by Live-Dead and MTT assays. Then, a similar investigation was done on SH-SY5Y and PC-12 in 3D culture using Live-Dead assay. Cell viability (%) was measured using Image J software. After optimization, 25-100 μM Curcumin (AFG Bioscience, USA) was screened on 3D Alzheimer's disease models of SH-SY5Y for 72h and PC-12 for 21 days (Durairajan et al., 2008; Lee et al., 2012; Xu et al., 2019). Then, Live-Dead assay was performed to determine cell viability, and cell viability (%) was evaluated using Image J software. Anti-Aβ biomarker (Proteintech, USA) was utilized in 3D Alzheimer's disease models to detect the presence of Aβ 1-42 in 3D cell culture environment before and after Curcumin treatment.

2.6. Statistical Analysis

The assessment of cell viability and proliferation was performed with at least three independent replicates, and the findings were expressed as mean ± standard deviation (SD). One-way and two-way ANOVA, along with Tukey's test for multiple comparisons, were conducted using GraphPad Prism 9 software (GraphPad Prism, Inc., San Diego). Statistical significance between groups was determined at $*p \leq 0.05$, $**p \leq 0.01$, $***p \leq 0.001$, and $****p \leq 0.0001$.

CHAPTER 3

RESULTS & DISCUSSION

3.1. Formation of SH-SY5Y Spheroids *via* MagLev

3.1.1. Optimization of Gx Concentration for 3D Cell Culture Formation of SH-SY5Y in MagLev Setup

MagLev setup facilitates the easy and rapid formation of SH-SY5Y spheroids using the magnetic levitation principle (Onbas and Arslan Yildiz, 2021). The optimization of Gx concentration and cell number is crucial for the formation of 3D cellular spheroids (Figure 15-18). For this purpose, the effect of Gx concentrations ranging from 10 to 100 mM on spheroid formation was analyzed over 24h. The magnetic, gravitational, and buoyancy forces aided in gathering cells, resulting in the observation of cell clusters starting from the 4^{th} hour, as shown in bright-field images (Figure 15). Over time, the size of these cellular clusters progressively increased, eventually leading to the formation of compact spheroids within 24h, even at low Gx concentrations. This can be attributed to the aggregation of cells through magnetic guidance, which enhances cell-cell interactions. Also, the upregulation of hemophilic cadherin and connexin expressions may contribute to this process (Cui et al., 2017; Lin and Chang, 2008) because these proteins have a crucial role in self-assembly (Bao et al., 2011). As cells aggregate, the contacts between cells are enhanced, and the behaviors associated with migration and aggregation during self-assembly are determined by the expression of cell adhesion proteins, including cadherins and surface adhesion molecules (Zhou, 2016).

Overall, the results of this study demonstrated that MagLev technology facilitates the rapid formation of spheroids within a 24h-period (Ferreira et al., 2019). In contrast, the scaffold-based approach requires an extended culture time to achieve spheroid

formation at a size of 200 μm (Srinivasan et al., 2017). Thus, MagLev technology significantly reduces the time needed to produce spheroids of comparable size (Tseng et al., 2013).

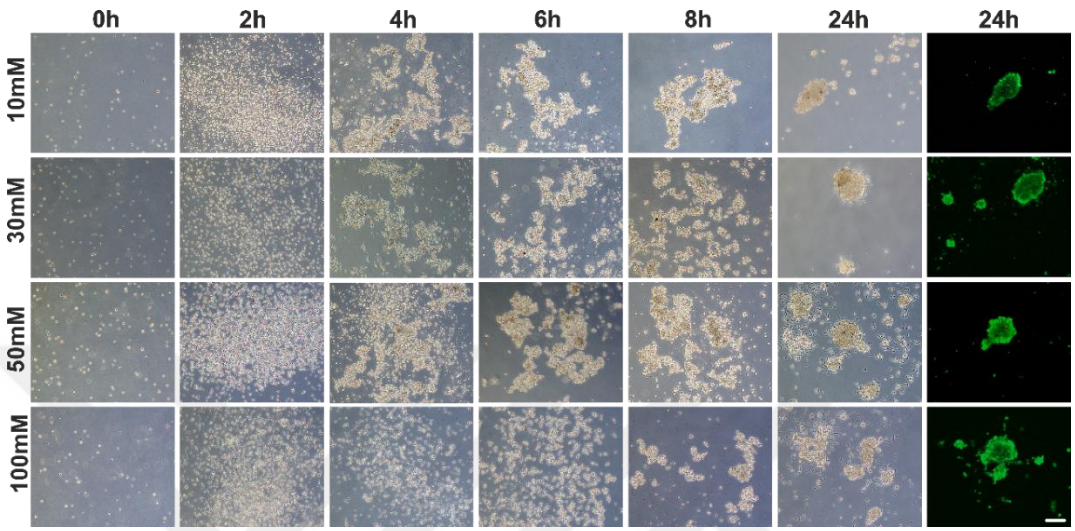

Figure 15. Bright-field and fluorescence microscopy images for SH-SY5Y spheroid formation at $25x10^3$ cell number between 10-100 mM Gx with for 24h (Scale bar: 200 μm, Green: Live, Red: Dead).

Moreover, the cell viability (%) measurements for Gx with varying concentrations are shown in Figure 16. SH-SY5Y spheroids were produced using the MagLev technology and exhibited remarkable cell viability, even at higher Gx concentrations. Cell viability remained at 98% and 96% for 10 mM and 100 mM Gx, respectively with no significant difference (ns). In conclusion, Gx does not have a considerable cytotoxic impact on cells during 24h observation, thereby affirming its biocompatibility.

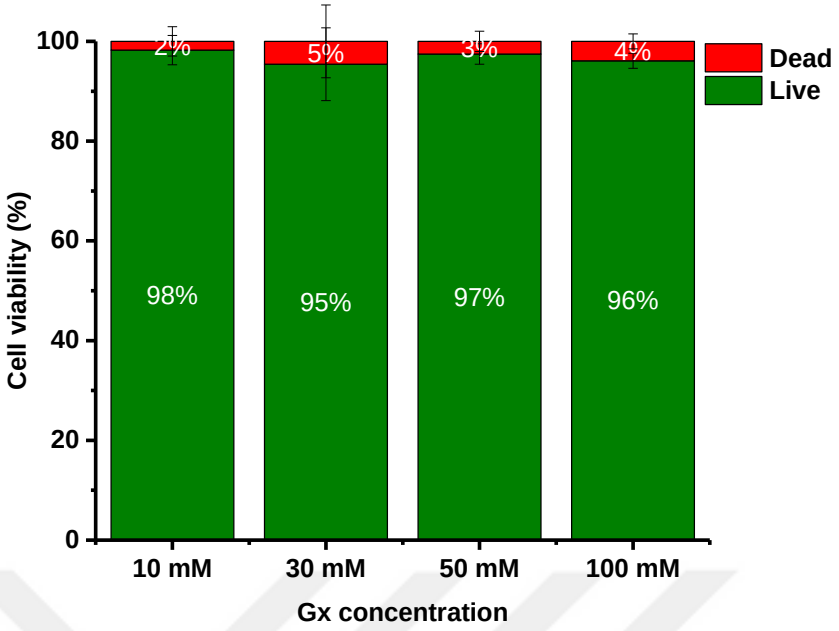

Figure 16. Cell viability results of SH-SY5Y spheroids between 10-100 mM Gx at $25x10^3$ cell number for 24h (n=6, there is no significant difference between groups, one-way ANOVA followed by Tukey's test).

3.1.2. Optimization SH-SY5Y Cell Number for 3D Cell Culture Formation in MagLev Setup

Next, cell number optimization was carried out at 10 mM Gx, which provided high cell viability and sufficient levitation of cells (Figure 17). 3D cellular clusters were observed starting from 4h and gained a more compact structure in time. 3D cellular structure formation was obtained at 24h, and the size and area of the cells increased with the increase in cell numbers. When $5x10^3$ cells were cultured, smaller spheroids were formed. $100x10^3$ cells were formed irregular and larger cellular clusters compared to the others.

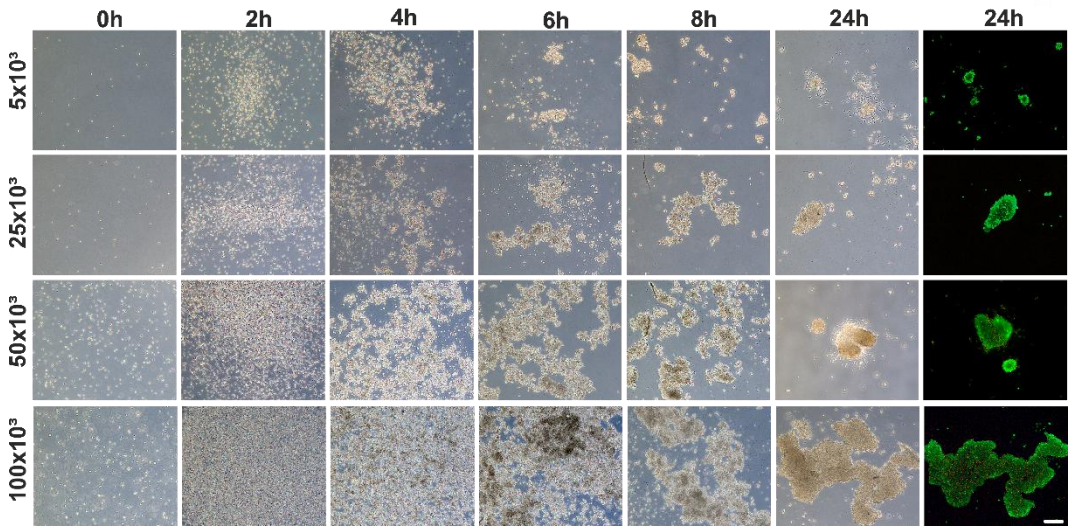

Figure 17. Bright-field and fluorescence microscopy images for SH-SY5Y spheroid formation between $5x10^3$-$100x10^3$ cell number at 10 mM Gx cells for 24h (Scale bar: 200 µm, Green: Live, Red: Dead).

Cell number optimization studies showed that cell number did not significantly influence cell viability, ranging between 100-94% (Figure 18). These findings showed that cell numbers have a high impact on the size of 3D cellular structures and morphology (Onbas and Arslan Yildiz, 2021). Also, cell numbers can influence cell viability for long term culture since spheroid size can limit oxygen and nutrient diffusion into the core of the spheroids (Lin and Chang, 2008). Therefore, a proper cell number is important for 3D cell culture, especially in the long term culturing.

Although there was no significant difference between $25x10^3$ and $50x10^3$ in terms of cell viability and morphological structure, subsequent studies were conducted using $25x10^3$ cells since lower cell number provides a more controlled environment, and spheroid formation parameters can be tuned in this way (Onbas and Arslan Yildiz, 2021), making it a suitable starting point for further investigations.

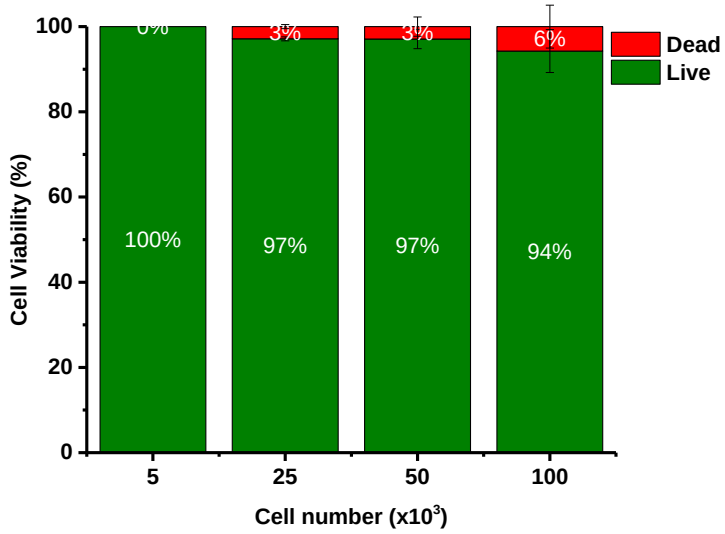

Figure 18. Cell viability results of SH-SY5Y spheroids between $5x10^3$-$100x10^3$ cell number at 10 mM Gx for 24h (n=6, there is no significant difference (ns) between groups, one-way ANOVA followed by Tukey's test).

3.1.3. Differentiation of SH-SY5Y Cells Using RA-BDNF

The differentiation of neuroblastoma cells is a crucial step in neuroscience, as it facilitates the development of similar morphological and biochemical properties *in-vivo* (Lone et al., 2016; Muñoz-Llancao et al., 2017; Sidell et al., 2003). This process is essential for both neural development and the establishment of models for neurodegenerative diseases, which are crucial for drug discovery and screening (Forster et al., 2016; Schneider et al., 2011). SH-SY5Y neuroblastoma cell line is extensively utilized in neuronal research, particularly in studies focused on differentiation (Costas-Rodríguez et al., 2019; da Costa et al., 2021) and modeling neurodegenerative diseases (Fiore et al., 2022; Kruger et al., 2020; Santillo, 2022). SH-SY5Y cells can possess cholinergic neuron character by expressing ChAT after differentiation (Adem et al., 1987; de Medeiros et al., 2019; Korecka et al., 2013; Kovalevich and Langford, 2013), which is important for Alzheimer's disease modeling studies (de Medeiros et al., 2019; Krishtal et al., 2017; Webberley et al., 2023).

In the literature, RA is commonly employed to differentiate SH-SY5Y cells, while BDNF is often used to enhance the effects of neuronal differentiation (de Medeiros et al., 2019; Encinas et al., 2000; Gimenez-Cassina et al., 2006; Murillo et al., 2017; Şahin et al., 2021; Schneider et al., 2011). During differentiation, significant biochemical and morphological changes occur, including the growth of neurites, alterations in the expression of neuronal markers and cell density, and accumulation of specific neurotransmitters, ultimately resulting in a phenotype closely resembling that of primary neurons (Cheung et al., 2009; Dwane et al., 2013; Encinas et al., 2000; Grover et al., 2011; Serdar et al., 2020).

3.1.3.1. Optimization and Characterization of Differentiation Protocol for SH-SY5Y on 2D Cell Culture

In this study, SH-SY5Y cells were sequentially differentiated with RA-BDNF, and characterized by neurite extension analysis and immunostaining of neuronal markers. First, cell number optimization was carried out when only RA was applied in 2D cell culture before differentiation of SH-SY5Y cells in 3D cell culture (Figure 19-20). As shown in Figure 19, there was a noticeable morphological change in SH-SY5Y cells regarding neurite extension. In undifferentiated cells, neurite extension was not observed, as expected. On day 5, the growth of neurites started to shorten, which can be attributed to the instability of RA beyond that time frame (Sharow et al., 2012; Temova Rakuša et al., 2021).

On the other hand, in groups containing 1% FBS and 1% FBS and DMSO, detachment of cells was observed due to a low amount of FBS (Strother et al., 2021). However, this was not observed for the RA-treated group; likely, RA increases survival factors in cells (Encinas et al., 1999). Also, this can be attributed to the increase in cellular adhesion molecules (CAMs) after differentiation with RA in neuroblastoma cell line (Melino et al., 1997). In addition, the cell density in the undifferentiated group increased, and the RA-treated group remained more stable. Differentiation induced a post-mitotic condition that generated a stable cell population, showing no noticeable increase in cell density over time (Dravid et al., 2021).

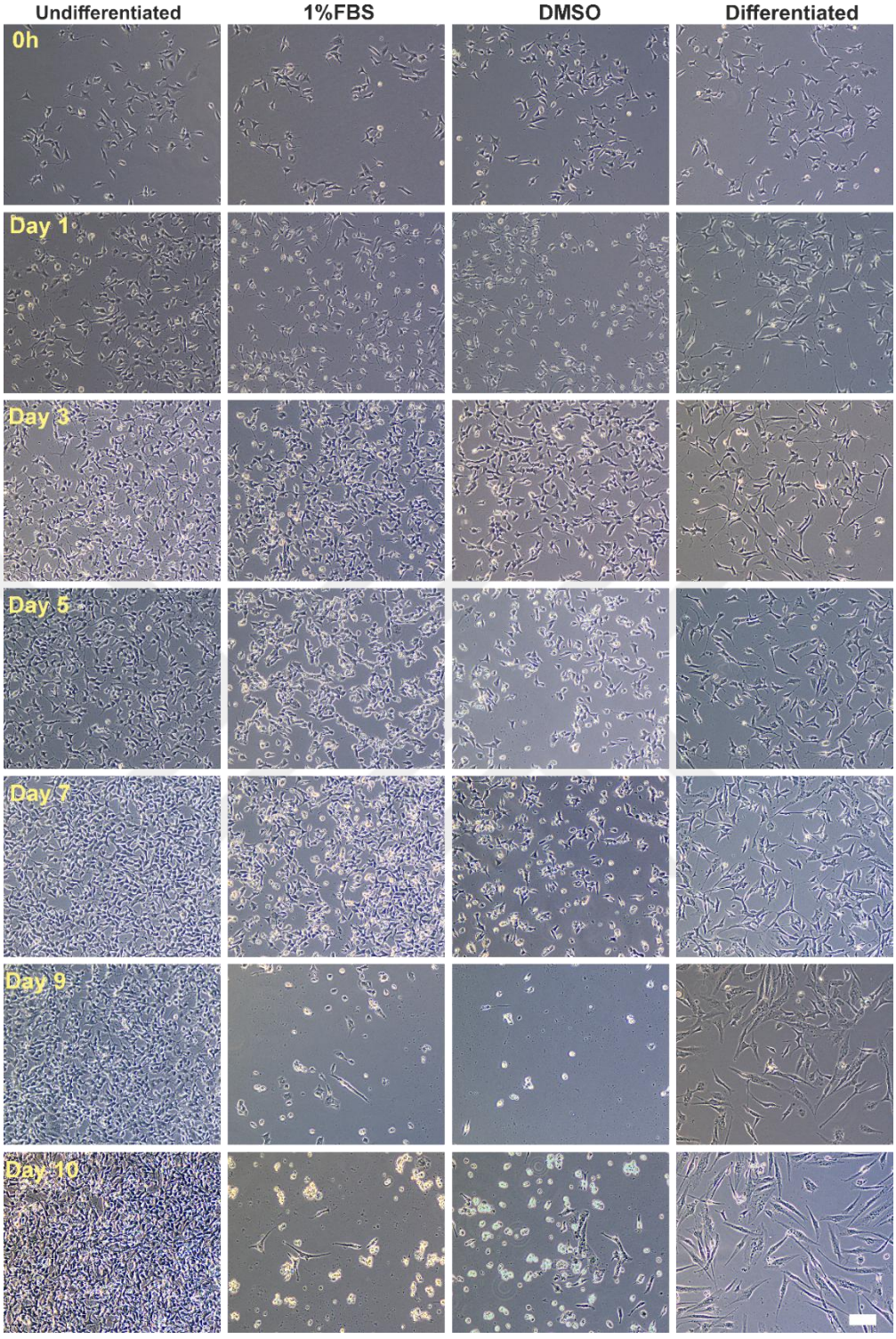

Figure 19. Differentiation of SH-SY5Y cells via 10 µM RA with high cell density ($50x10^3$) for 10 days (Scale bar: 100 µm).

A similar result was observed when differentiation was carried out with low cell density (Figure 20). On the other hand, neurite extension in low-density cultures was notably longer compared to differentiation performed at high cell densities. Neurite extension was observed after 24h, but it could be maintained until day 5, as it was observed in high cell density results. SH-SY5Y cell morphology changed after day 7, maintaining S-type (substrate-adherent) morphology instead of N-type (neuronal). While RA differentiation effectively promotes neurite outgrowth, its prolonged exposure leads to an increase in S-type cells. These findings underscore the critical role of differentiation conditions, such as initial cell density and RA treatment duration, in determining SH-SY5Y cell morphology and neuronal characteristics. Optimization of timing and dosing is essential to maintain a consistent neuronal phenotype, as variations in these parameters can significantly influence differentiation outcomes. For instance, initial cell density has been shown to impact not only cell viability but also neurite outgrowth and the expression levels of neuronal markers. In a study by Dravid et al. (2021), it was reported that differentiation under low cell density conditions allowed for a more precise and detailed analysis of neurite growth, facilitating better visualization and segmentation of individual neurites. However, this approach also posed challenges, as low cell density differentiation was associated with reduced cell viability, potentially due to decreased cell-cell interactions and support. (Dravid et al., 2021). The importance of cell density in differentiation efficiency was further highlighted in a study by Dwane et al. (2013), which investigated how varying initial cell densities influence cell attachment, adhesion dynamics, and differentiation outcomes. The study revealed that higher cell densities promote stronger cell adhesion, which is crucial for efficient differentiation, while lower densities may compromise these processes (Dwane et al., 2013). Another study provided valuable insights into the role of seeding concentration and spatial constraints on SH-SY5Y cell proliferation dynamics, highlighting the impact of initial cell density, chamber size, and available surface area on growth rates and aggregation tendencies (Kalwarczyk et al., 2024).

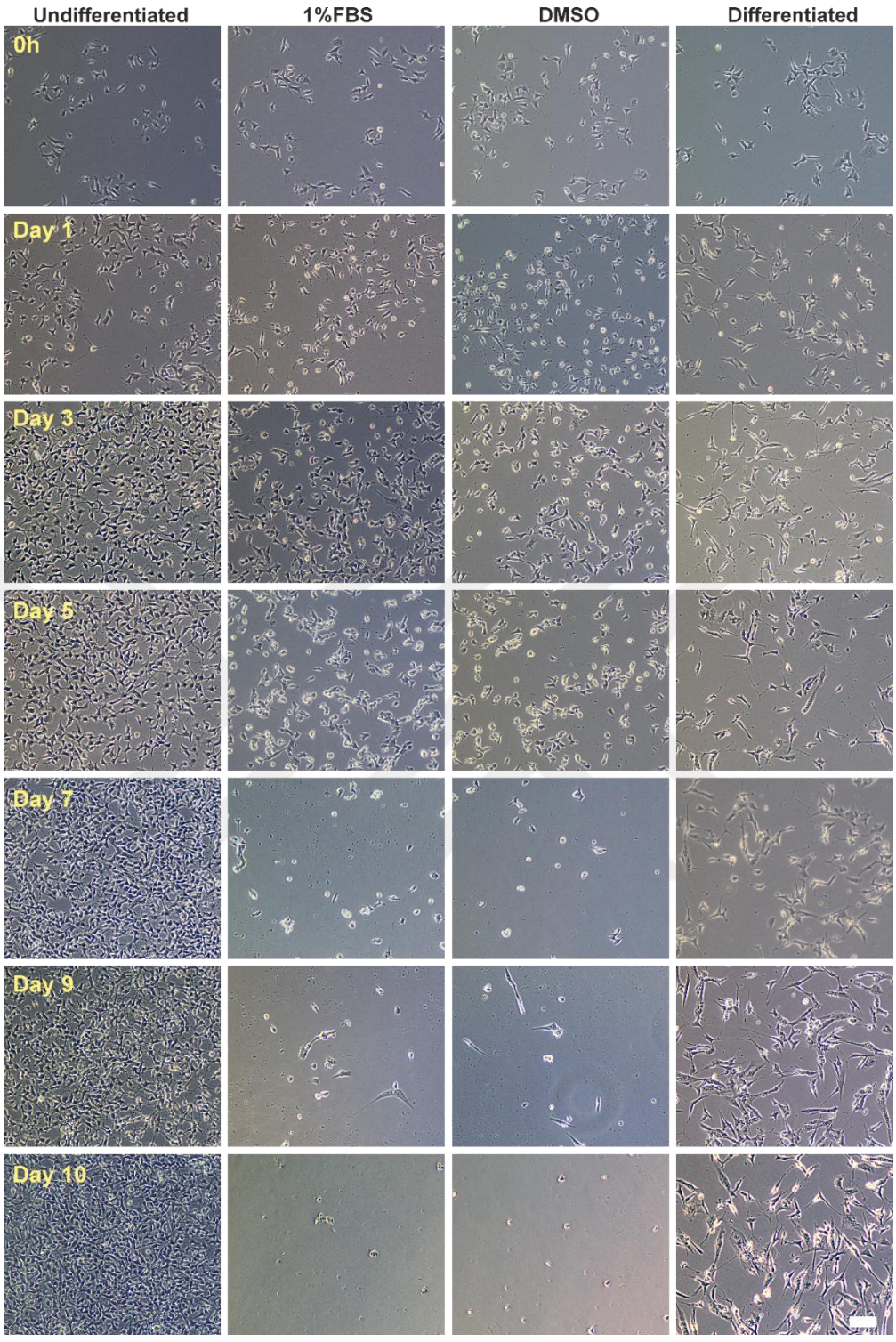

Figure 20. Differentiation of SH-SY5Y cells via 10 µM RA with low cell density ($25x10^3$) for 10 days (Scale bar: 100 µm).

Differentiated SH-SY5Y cells with RA exhibit neurite growth cones, including Focal adhesion kinase (FAK), which is necessary for neurite growth (Dwane et al., 2013). Therefore, differentiation was confirmed by measuring neurite growth using the Neuron J program, a widely used tool for assessing neurite outgrowth. Figure 21 shows neurite extension based on the cell density of SH-SY5Y after RA treatment. The findings revealed that the maximum neurite length for high cell density was observed on day 1 and day 3, which were 92 and 90 μm, respectively. The results in low cell density exhibited longer neurites, measuring 107 μm on day 5. Following these peak days, the neurite lengths for both cell densities declined until day 10.

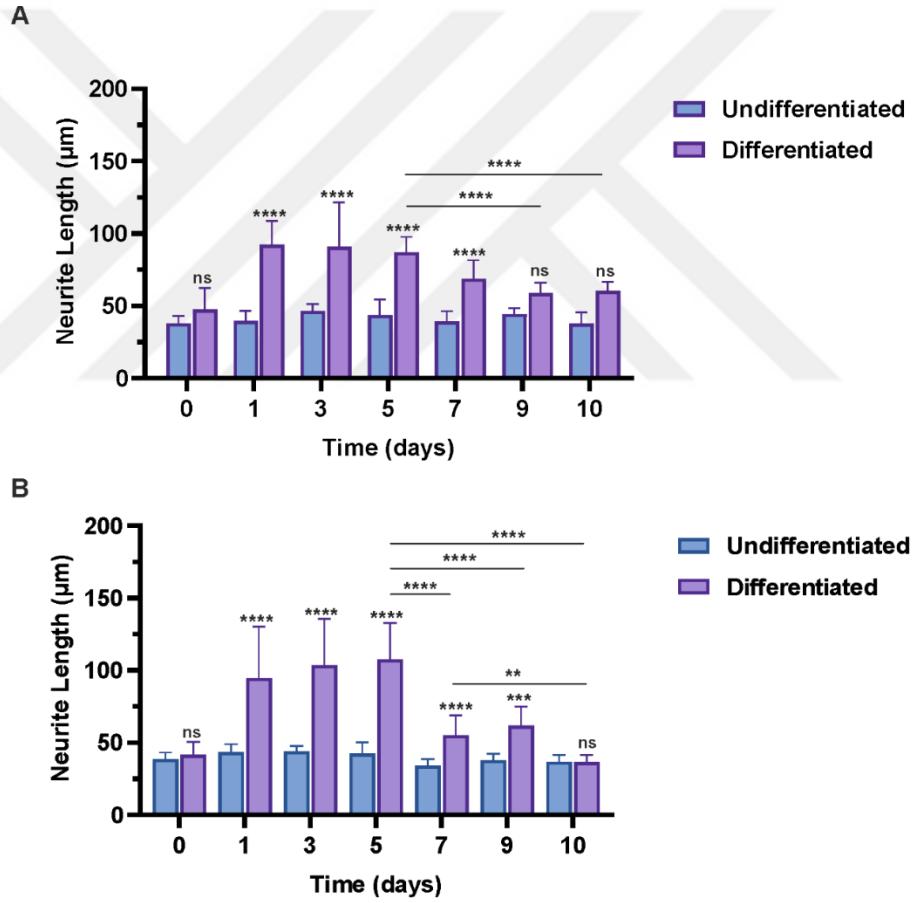

Figure 21. Neurite extension analysis of A) high ($50x10^3$) and B) low cell density ($25x 10^3$) for SH-SY5Y after differentiation via 10 μM RA for 10 days (n=10, ns:not significant, ***p <0 .001, ****p<0.0001 compared to the control of each group, two-way ANOVA followed by Tukey's test).

These results suggest that neurite length is influenced by cell density, likely due to the overcrowding associated with high cell density, which limits neurite extension owing to decreased surface area (Dravid et al., 2021). Conversely, in low cell density, the greater availability of space allows neurites to extend further, leading to longer lengths. Overall, the findings indicate that neurite length in differentiated SH-SY5Y cells is significantly influenced by cell density, with low-density cultures exhibiting longer neurites while high cell density limits neurite outgrowth. In addition, RA alone appears insufficient for maintaining long-term neurite length stability, as neurite lengths declined after the 7^{th} day, suggesting that additional differentiation factors are required to sustain neuronal morphology for extended periods (Riegerova et al., 2021; Strother et al., 2021). To address this limitation, BDNF supplementation was used, as it is widely recognized for its role in promoting neurite extension and neuronal differentiation. BDNF plays a key role in inducing a more stable and functionally mature neuronal phenotype, making it a preferred choice for long-term differentiation protocols (Riegerova et al., 2021; Strother et al., 2021). Thus, combining RA with BDNF supplementation represents a promising strategy for achieving more robust and stable neuronal differentiation in SH-SY5Y cells. For that reason, further studies were carried out with BDNF since the supplementation of BDNF allows for longer neurites over a prolonged time.

Following cell number optimization, SH-SY5Y cells were differentiated *via* RA-BDNF (Figure 22). Differentiation is a complex process influenced by various factors. RA triggers the expression of tyrosine kinase receptor B (TrkB), which is essential for binding BDNF (Kaplan et al., 1993; Ruiz-León and Pascual, 2003). Subsequently, BDNF activates PI 3-K and ERK pathways, which are crucial for cell survival and neuritogenesis (Encinas et al., 2000, 1999; Szobota et al., 2019). Therefore, neurite extension analysis was done to confirm RA-BDNF differentiation and to optimize the differentiation process. Neurite extension was observed from day 0 to day 5 after RA addition. The addition of BDNF on day 5 resulted in longer and more branched neurites, particularly on day 9, as expected. Moreover, it was observed that the cells within the RA-BDNF group did not proliferate as they did in the undifferentiated group due to the suppression of DNA synthesis after RA treatment (Qiao et al., 2012; Simões et al., 2021). Cells began to display a neuronal phenotype from day 5 onwards, confirming the differentiation induced by RA-BDNF. BDNF could enhance the differentiation of RA and cells maintained differentiated properties until day 9.

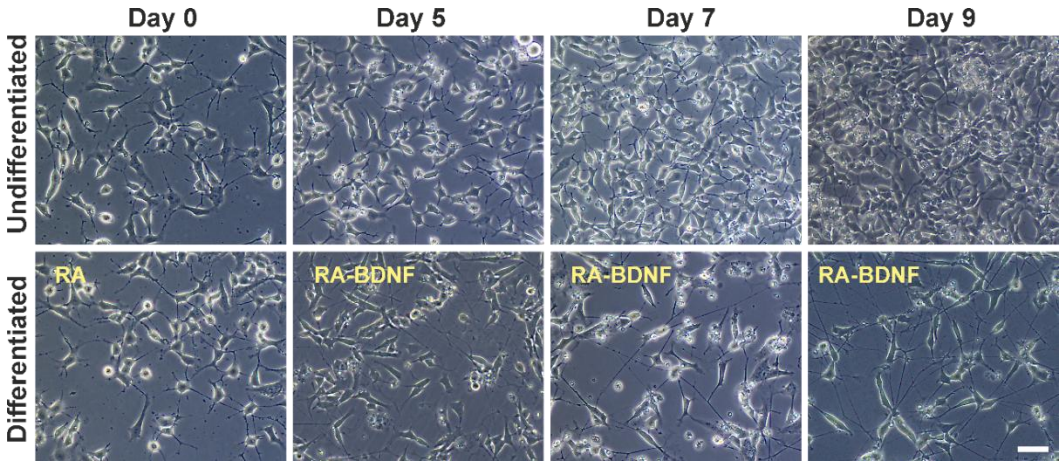

Figure 22. Morphology of un-/differentiated SH-SY5Y after sequential treatment with RA and RA-BDNF for 9 days (Scale bar: 50 μm).

Then, neurite lengths were measured using Neuron J software (Figure 23). A comparison of neurite lengths between undifferentiated and differentiated SH-SY5Y cells from day 0 to day 9 showed that differentiated cells had significantly longer neurites, reaching up to 150 μm while undifferentiated cells remained at 28-31 μm. BDNF, in combination with RA, has been shown to increase neurite length from 125 μm to 150 μm permanently. The sequential treatment of RA and RA-BDNF resulted in a nearly 4-fold increase in neurite lengths by day 9 compared to day 0, highlighting the differentiation potential of this combined approach. This finding aligns with a previous report indicating that neurite length was shorter in SH-SY5Y cells treated with RA alone compared to RA-BDNF (Serdar et al., 2020). In literature, it is reported that prolonged RA treatment for more than 5 days failed to maintain a homogeneous population of SH-SY5Y cells, leading to increased S-type cells. However, the addition of BDNF resulted in more branched and abundant neurites (Encinas et al., 2000). Conversely, another report found that RA treatment exceeding 3 days increased the percentage of apoptotic cell death (Yang et al., 2016). These findings collectively indicate that while RA treatment initiates the differentiation process, it is not efficient in differentiating cells when used alone. Therefore, a combined approach is necessary to achieve efficient neuronal differentiation, which results in stronger changes in the expression of neuronal markers (Riegerova et al., 2021). Apart from these studies, differentiated SH-SY5Y cells represent a suitable *in-vitro* model for neurodegenerative disease research, as they mimic several aging-related

characteristics, which are critical for understanding age-associated neuronal decline (Strother et al., 2021).

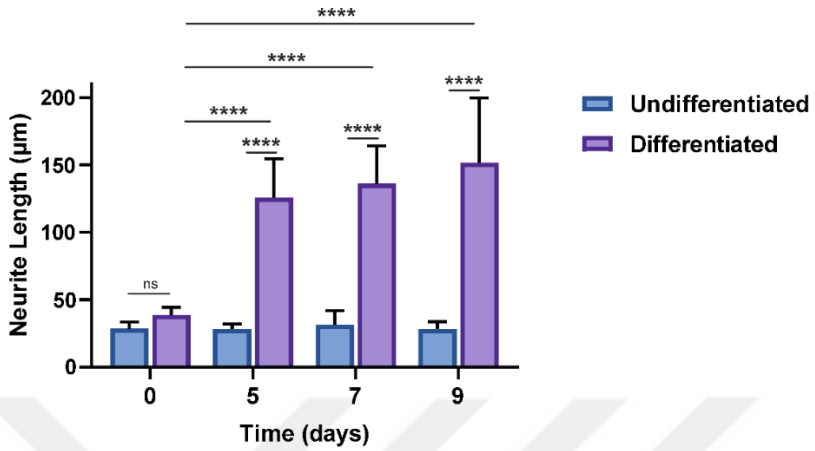

Figure 23. Neurite extension analysis of un-/differentiated SH-SY5Y cells after sequential treatment by RA and RA-BDNF for 9 days (n = 10, ns: not significant, ****p < 0.0001, two-way ANOVA followed by Tukey's test).

In addition to the neurite length analysis, immunostaining was also used for assessing cellular differentiation through the expression of neuronal markers. To confirm the neuronal differentiation of SH-SY5Y cells, β-III tubulin and NeuN immunostaining were performed. β-III Tubulin is a specific type of tubulin that is found in neurons, and its levels increase as neuronal differentiation occurs. Neuronal nuclei (NeuN) is only observed in cells that have undergone differentiation. Figure 24 illustrates the expression of β-III tubulin and NeuN in both un-/differentiated cells. β-III tubulin was slightly expressed in undifferentiated cells, but its expression was clearly observed in the differentiated groups (Figure 24A−24C). On the other hand, NeuN showed weak expression in undifferentiated groups, while its expression increased, especially on day 9 for differentiated cells (Figure 24A−24C).

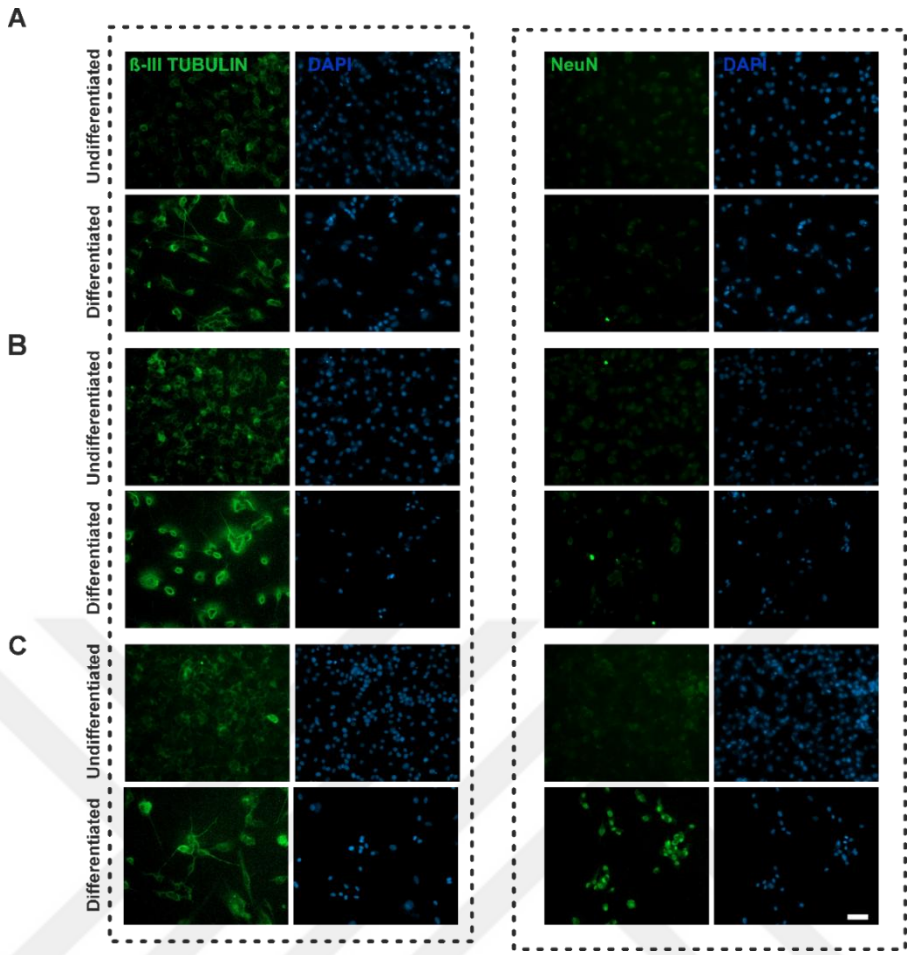

Figure 24. Immunostaining of β-III tubulin and NeuN for un-/differentiated SH-SY5Y cells on A) day 5, B) day 7, and C) day 9 (Scale bar: 50 μm, Blue: DAPI, Green: β-III tubulin and NeuN).

The relative fluorescence intensity (F.I.) of β-III tubulin was 2-fold higher for all time intervals in differentiated cells compared to the un-/differentiated control groups (Figure 25A). NeuN relative F.I. increased five-fold on day 9 in differentiated cells compared to the undifferentiated groups (Figure 25B). These findings are consistent with studies that have reported an increase in β-III tubulin and NeuN expression following the differentiation of SH-SY5Y cells, indicating the acquisition of neuronal characteristics (Dravid et al., 2021; Dwane et al., 2013; Serdar et al., 2020). This suggests that the differentiation process successfully induced a neuronal phenotype, confirming their utility as a model system for studying neurobiological processes and neurodegenerative diseases.

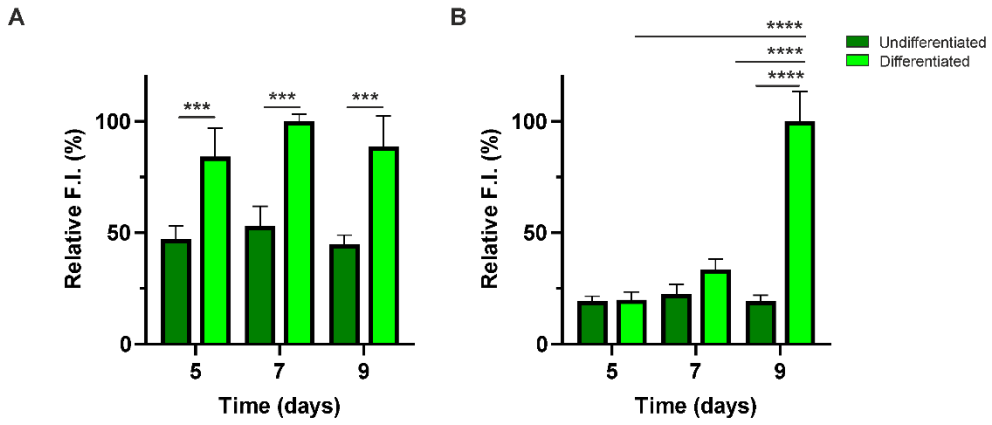

Figure 25. Relative fluorescence intensity (F.I.) of A) β-III tubulin and B) NeuN for un-/differentiated SH-SY5Y cells (n = 6, ns: not significant ***p < 0.001, ****p < 0.0001, two-way ANOVA followed by Tukey's test).

Overall, this study demonstrated that RA alone might be insufficient for sustained neuronal differentiation, as evidenced by temporary neurite extension and morphological changes after prolonged treatment. The sequential treatment of RA and BDNF resulted in significant improvements in differentiation, promoting longer, more branched neurites and maintaining neuronal properties for long time. Immunostaining revealed increased expression of β-III tubulin and NeuN, markers of neuronal differentiation, further confirming the successful differentiation of SH-SY5Y cells into a neuronal phenotype. Therefore, further studies were carried out using optimized parameters to differentiate SH-SY5Y in 3D cell culture.

3.1.3.2.3D Cell Culture in MagLev Setup while Maintaining Optimized Differentiation Protocol

Further, the differentiation process was adapted to 3D cell culture because neuronal cells cultured in a 2D environment cannot maintain the features of primary neurons (Fiore et al., 2022; Li et al., 2022). Therefore, in this study, SH-SY5Y cells were cultured in a 3D environment and differentiated using RA-BDNF (Figure 26-27). The

differentiation process was carried out simultaneously with MagLev setup. As previously described, the process involved the initial addition of 10 μM RA, followed by adding 50 ng/mL BDNF on the 5th and 7th days. To ensure long term maintenance of differentiated SH-SY5Y cells MagLev setup, 10 mM Gx was used, and the spheroids were evaluated in terms of structure and viability (Figure 26-27). It was observed that the addition of 10 mM Gx successfully created a paramagnetic cell culture environment, allowing for the levitation of both un-/differentiated spheroids for 9 days, which aligns with findings in the literature (Onbas and Arslan Yildiz, 2021). Moreover, this concentration of Gx provided high cell viability for un-/differentiated spheroids, as evidenced by fluorescence microscopy images (Figure 26).

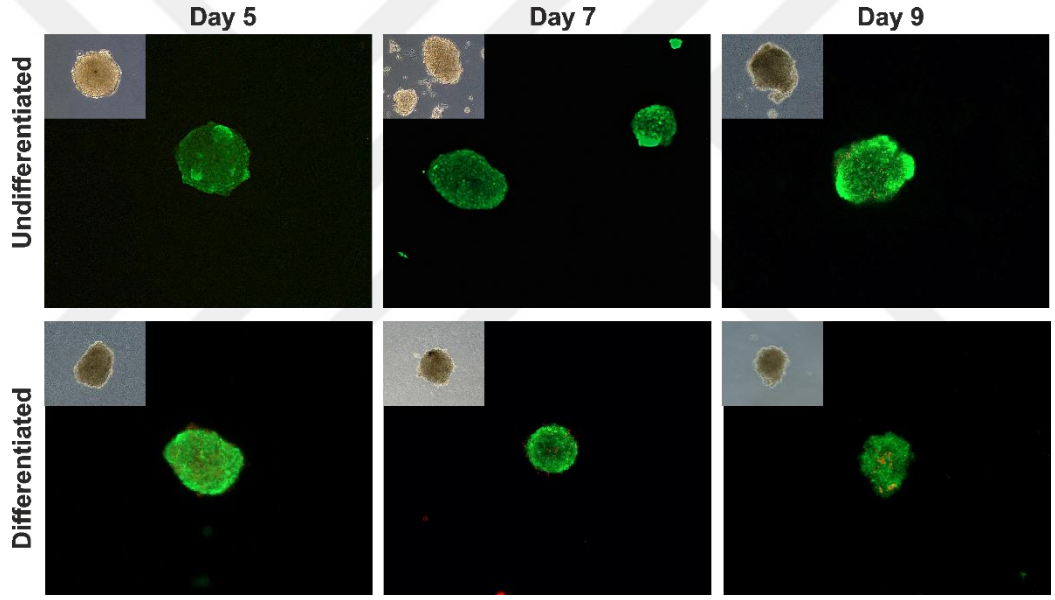

Figure 26. Bright-field and fluorescence microscopy images for un-/differentiated 3D SH-SY5Y spheroids analyzed by Live-Dead assay on day 5, 7, and 9 (Scale bar: 200 μm, Green: Live, Red: Dead).

The cell viability measurements demonstrated a high survival rate in both undifferentiated and differentiated spheroids, with viability ranging between 94-95% in undifferentiated spheroids and 98-100% in differentiated spheroids, showing no statistically significant difference (Figure 27A-27B). The slightly higher viability observed in differentiated spheroids can be attributed to the activation of the PI3-K/Akt

pathway, which plays a crucial role in cell survival, growth, and metabolic regulation, particularly in response to BDNF (Strother et al., 2021).

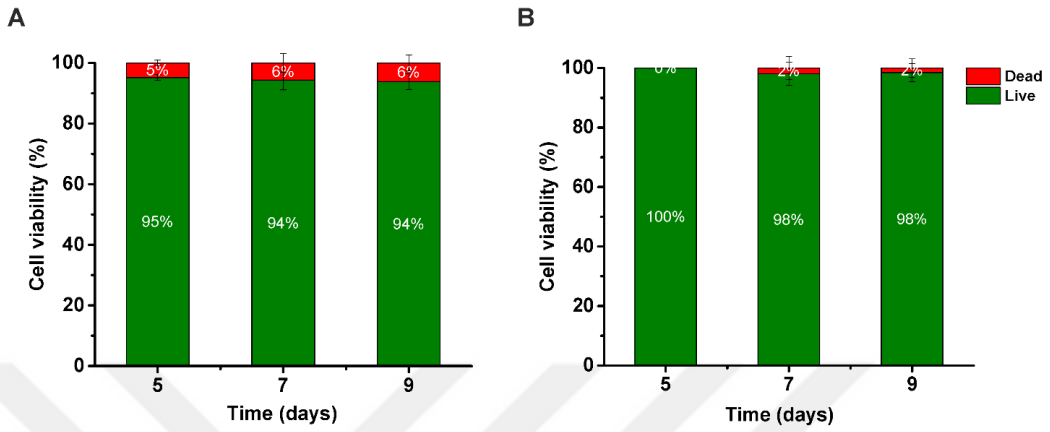

Figure 27. Cell viability results of A) undifferentiated and B) differentiated SH-SY5Y spheroids for days 5, 7, and 9 (n=3, there is no significant difference between groups, one-way ANOVA followed by Tukey's test).

Overall, un-/differentiated spheroids maintained their circular and compact structures. This compact form of the spheroid can be associated with MagLev technology, as it allows for a more efficient 3D cellular formation relative to other conventional methods (Moncal et al., 2022). Furthermore, differentiated spheroids exhibited a more compact structure compared to undifferentiated ones. The increased compactness in differentiated SH-SY5Y spheroids can be attributed to the elevated levels of cell adhesion molecules present in them compared to undifferentiated spheroids (Jung et al., 2013). As a result, MagLev technology offers a significant advantage in 3D neuronal culture systems, providing a controlled and efficient method for spheroid formation. These findings showed that MagLev is an effective, powerful, and biocompatible method for 3D cell culture formation. It enables efficient 3D neuronal differentiation while maintaining high cell viability, even under long-term culture conditions, making it a promising approach for neurodegenerative disease modeling applications.

The circularity and area analysis were also carried out to characterize the structural features of un-/differentiated SH-SY5Y spheroids, which were influenced by

factors such as Gx concentration, cell number, and incubation time. Therefore, circularity and area were measured based on the incubation time for un-/differentiated spheroids. The circularity of undifferentiated spheroids reached 0.87 on day 9, while differentiated spheroids reached 0.89 (Figure 28A). In addition to circularity, the spheroid area was analyzed and there was a notable difference between the two groups (Figure 28B). Undifferentiated spheroids showed an increase in spheroid area, indicating ongoing cell proliferation and expansion, whereas differentiated spheroids maintained a relatively stable area, exhibiting a more compact structure throughout the 9-day period. Specifically, the area of undifferentiated spheroids ranged between 0.162-0.224 mm^2, whereas the differentiated spheroids remained within a smaller range of 0.09-0.107 mm^2. This observation may be attributed to RA treatment, which induces p21 activation (Qiao et al., 2012; Simões et al., 2021), resulting in the inhibition of cell proliferation due to cell cycle arrest in the G1 phase, and inhibition of DNA synthesis (Qiao et al., 2012) .

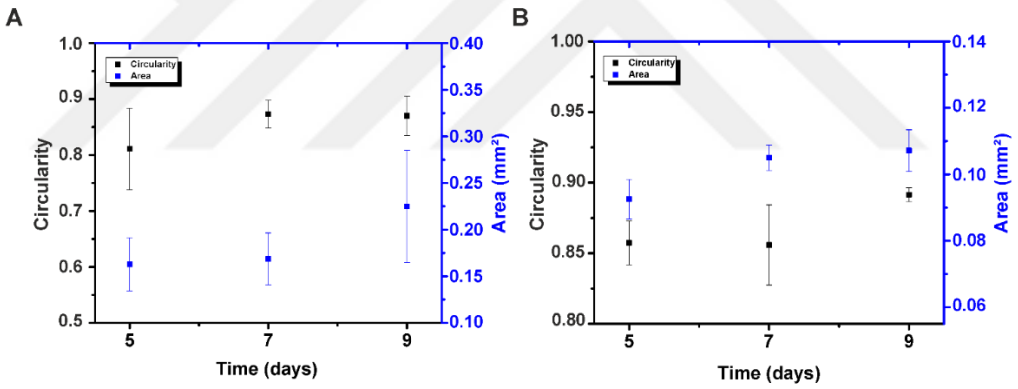

Figure 28. Circularity and area analysis of A) undifferentiated and B) differentiated SH-SY5Y spheroids on days 5, 7, and 9.

Moreover, cells that were differentiated in 2D and then cultured in MagLev formed cell clusters with low cell viability rather than spheroids (Figure 29). This observation suggests that the transition of differentiated cells from a 2D cell culture environment to a 3D cell culture may disrupt normal cellular organization and cell survival. This can be attributed to the replating of the differentiated cells, which can damage neurite extension (Dravid et al., 2021). Therefore, inducing differentiation

directly within a 3D culture system, such as MagLev, is a more effective strategy for generating 3D-differentiated spheroids with higher cell viability. Overall, the findings highlighted that differentiation of cells in MagLev setup results in proper spheroid size with remarkable cell viability, indicating the suitability of MagLev system for potential use in 3D neuronal differentiation. Differentiation in MagLev setup is a superior approach for achieving optimal spheroid size, enhanced cell viability, and sustained neuronal function. This highlights the suitability of the MagLev system for 3D neuronal differentiation, making it an efficient platform for neuroscience research, regenerative medicine, and drug discovery applications.

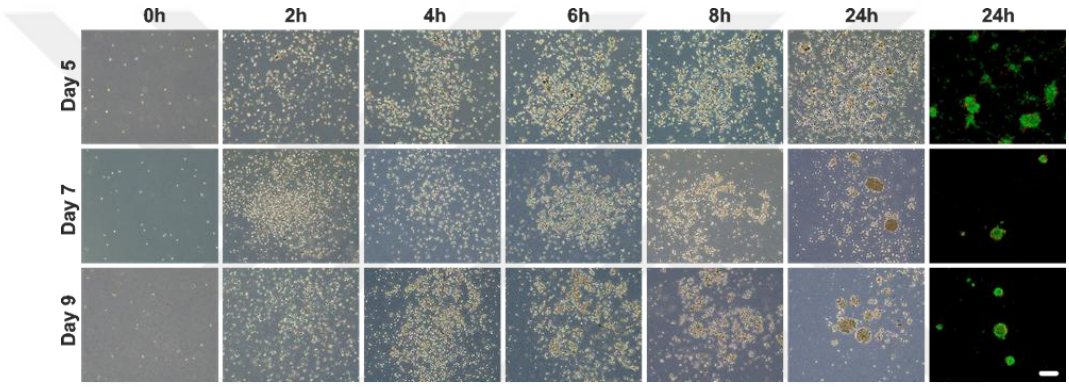

Figure 29. Bright-field and fluorescence microscopy images of SH-SY5Y cells differentiated in 2D and cultured in MagLev (Scale bar: 200 µm, Green: Live, Red: Dead).

Moreover, immunostaining of β-III Tubulin and NeuN was performed to evaluate the neuronal differentiation in 3D SH-SY5Y spheroids, following a similar approach as in 2D cell cultures. These markers were assessed to confirm the neuronal differentiation of spheroids under 3D cell culture conditions. Figure 30 shows fluorescence microscopy images of β-III Tubulin and NeuN immunostaining, comparing undifferentiated and differentiated SH-SY5Y spheroids. The β-III Tubulin expression was analyzed across different time points, revealing its presence in both un-/differentiated groups. The highest β-III Tubulin expression was observed in differentiated groups on day 9 (Figure 30A-30C). Despite its presence in undifferentiated spheroids, its elevated expression in

differentiated groups suggests that RA-BDNF treatment successfully promoted neuronal markers in 3D cell culture. On the other hand, NeuN expression was slightly detected in undifferentiated spheroids, it was significantly increased in differentiated spheroids (Figure 30A-30C).

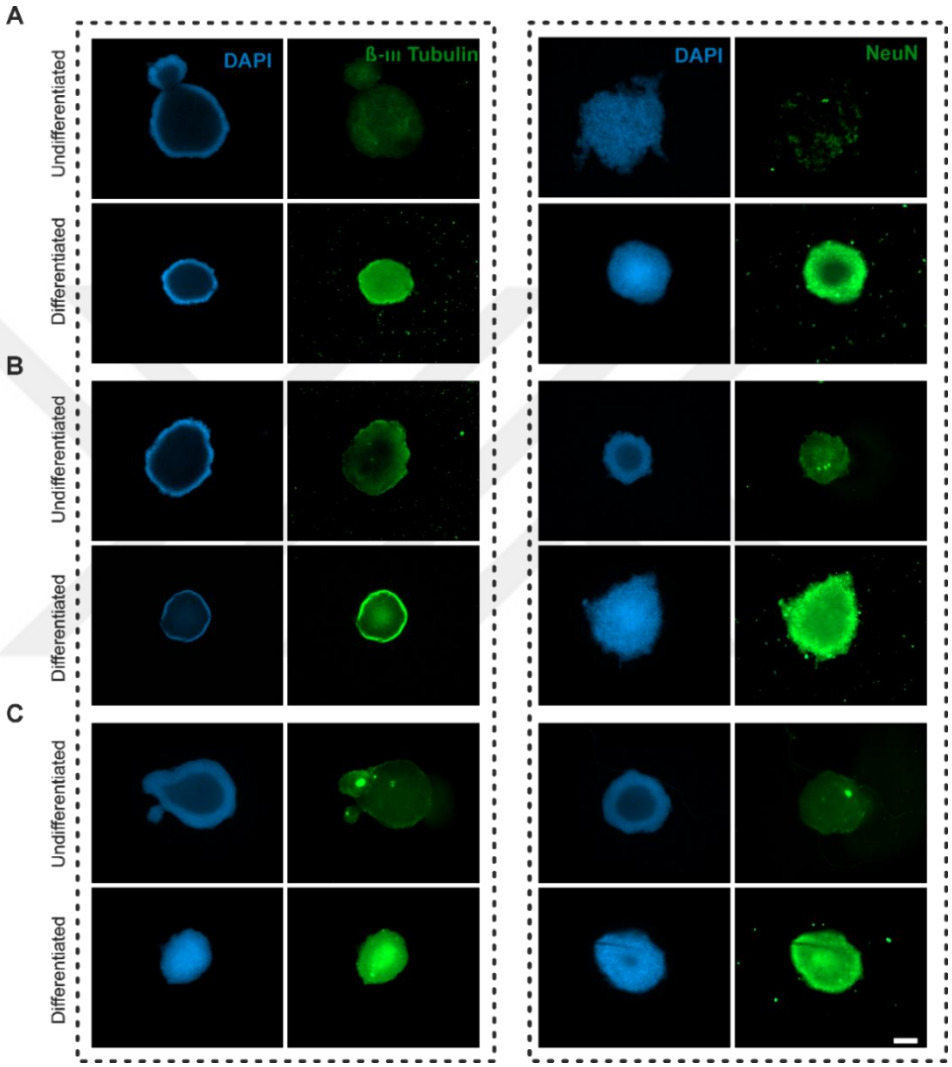

Figure 30. Fluorescence microscopy images of β-III tubulin and NeuN for un-/differentiated SH-SY5Y spheroids on A) day 5, B) day 7, and C) day 9 (Scale bar: 100 µm, Blue: DAPI, Green: β-III tubulin and NeuN).

The F.I. of β-III Tubulin exhibited 6.8, 1.5, and 2.3-fold increases when comparing un-/differentiated spheroids on days 5, 7, and 9, respectively (Figure 31).

Notably, the highest F.I. for β-III Tubulin was recorded on day 9 within the differentiated group. Significant differences were observed between day 9 and both day 7 and day 5 within differentiated groups. On the other hand, F.I. of NeuN demonstrated 34-fold, 4-fold, and 11.7-fold differences between the un-/differentiated groups on days 5, 7, and 9, respectively. These findings affirm that differentiated 3D spheroids maintained neuronal features (de Medeiros et al., 2019; Serdar et al., 2020; Simões et al., 2021).

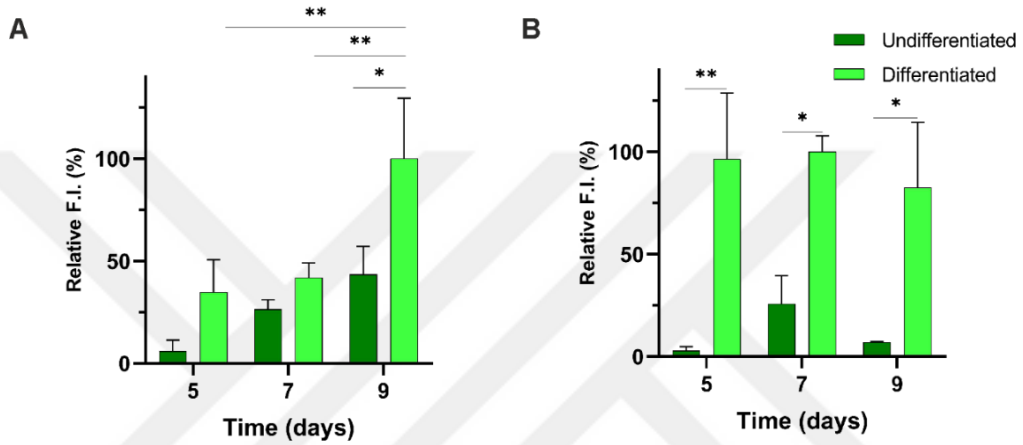

Figure 31. Relative fluorescence intensity (F.I.) of A) β-III tubulin and B) NeuN for un-/differentiated SH-SY5Y spheroids (n = 3, *p <0 .05, **p < 0.01, two-way ANOVA followed by Tukey's test).

These results highlight the effectiveness of RA-BDNF sequential treatment in promoting neuronal differentiation within 3D SH-SY5Y spheroids, as evidenced by the increase in β-III Tubulin and NeuN expression over time, underscores the applicability of the differentiation protocol in 3D cell culture. The successful implementation of this protocol in 3D culture opens new avenues for research in neurodevelopmental studies, drug screening, and disease modeling

3.2. Utilizing SH-SY5Y Spheroids to Model Alzheimer's Disease in 3D

3.2.1. Formation and Characterization of Aβ 1-42 Aggregates

Aβ 1-40 and/or Aβ 1-42 peptides are commonly encountered in Alzheimer's pathology, and associated with neurotoxicity; thereby, they have been utilized as tools for Alzheimer's disease modeling (Abdul Manap et al., 2020; Calan et al., 2016; Park et al., 2015). However, Aβ 1-42 is insoluble, prone to aggregate formation, and more toxic than Aβ 1-40 (Evin and Weidemann, 2002; Portelius et al., 2010) ; thus, it has been commonly employed in modeling Alzheimer's disease (Calan et al., 2016; Choi et al., 2013; Labour et al., 2016; Park et al., 2015). In this work, Aβ1-42 was used to model Alzheimer's disease. Prior to 3D Alzheimer's disease modeling, aggregate formation was confirmed by Congo red staining, (Klunk et al., 1999) and SEM analysis (Figure 32). Congo red interacts with the hydrophobic groove of the Aβ1-42 aggregates (Maiti et al., 2016), resulting in the observation of red staining. Congo red staining results of Aβ1-42 monomer and aggregates were given in Figure 32A-32B, respectively. As expected, no staining was observed for the monomers while Aβ1-42 aggregates were stained, confirming aggregate formation (Figure 32A-32B). Additionally, Aβ 1-42 aggregate formation was also observed by SEM analysis successfully as depicted in Figure 32C.

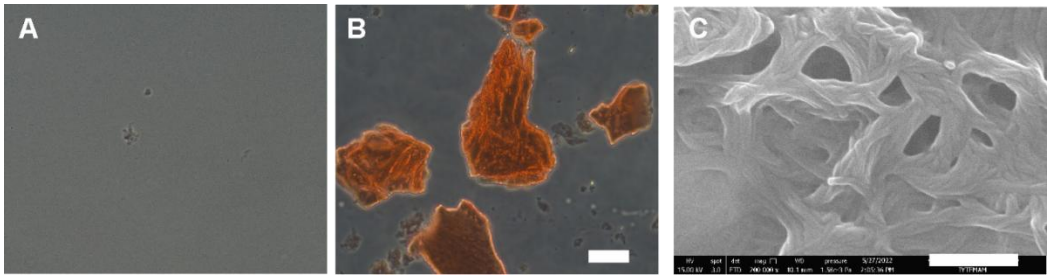

Figure 32. Monitoring Aβ 1-42 A) monomer and B) aggregates by light microscopy after applying Congo red (Scale bar 50 μm) C) Morphology of Aβ 1-42 aggregates monitoring by SEM (Scale bar: 500 nm).

Besides, formation of Aβ 1-42 aggregate stained with Congo red dye and it was investigated by spectrophotometric analysis (Wu et al., 2012). The absorbance maximum of Congo red was observed at 490 nm, which shifted to 540 nm after the formation of a complex between Aβ 1-42 aggregate and Congo red (Lee et al., 2019), especially at high concentrations of Aβ 1-42 aggregate, such as 75 and 100 µM (Figure 33).

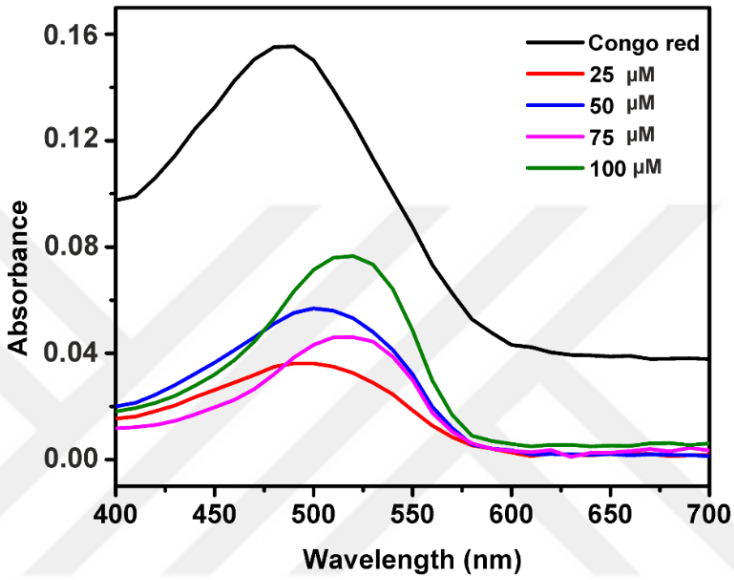

Figure 33. Spectrophotometric analysis of Aβ 1-42 aggregates formation through Congo red assay.

After confirming aggregate formation, the size distribution profile of Aβ1-42 aggregates was analyzed using light microscopy images, revealing that the aggregates frequently ranged between 20-60 µM (Figure 34). A detailed examination of these distributions demonstrated a consistent trend with previously reported findings in the literature, where Aβ aggregates in 3D *in-vitro* models typically vary between 40-80 µm, while those observed in post-mortem brain slices range between 20-60 µm (Armstrong, 2007; Labour et al., 2016). The similarity in size between the *in-vitro* aggregates and those present in brain tissue highlights the potential of the Aβ-induced 3D *in-vitro* model in mirroring the pathological conditions associated with Alzheimer's disease. Also, these

findings may contribute to future studies aimed at targeting specific aggregate sizes for therapeutic intervention.

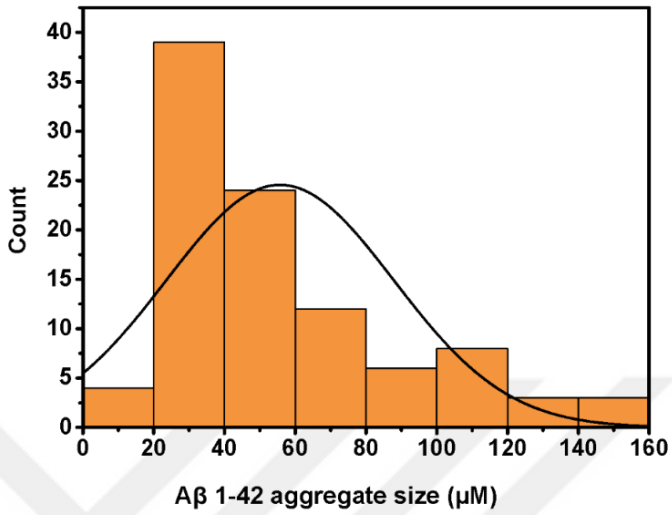

Figure 34. Size distribution profile of Aβ 1-42 aggregates by histogram graph (n=100).

3.2.2. Optimization of Aβ 1-42 Aggregate Concentration on 2D Cell Culture of SH-SY5Y Cells

Aβ 1-42 aggregates are key in Alzheimer's disease pathology by triggering neurotoxicity (Abdul Manap et al., 2019). A variety of *in-vitro* studies have identified several mechanisms that may lead to neuronal cell death in response to Aβ addition. These mechanisms include oxidative stress, alterations in Ca^{2+} homeostasis, microglial activation, nitric oxide production, mitochondrial dysfunction, and additional factors. Nevertheless, the specific mechanism that triggers these events is still not fully understood (Kumar et al., 2012).

Therefore, this study investigated the neurotoxicity of Aβ 1-42 aggregates on un-/differentiated SH-SY5Y spheroids. Prior to starting the application of Aβ 1-42 aggregates on 3D cell culture, optimization studies were carried out on 2D cell culture of un-/differentiated SH-SY5Y. Here, 1-15 μM Aβ 1-42 aggregates were introduced to

undifferentiated SH-SY5Y for 24h, 48h, and 72h (Figure 35A-35C). Bright-field images showed cell detachment correlating with increasing Aβ 1-42 aggregate concentration and incubation time. There were almost no cells on the surface, especially at 15 µM. There was no cell remaining at the end of 72h incubation, especially after 10 µM Aβ 1-42 aggregates.

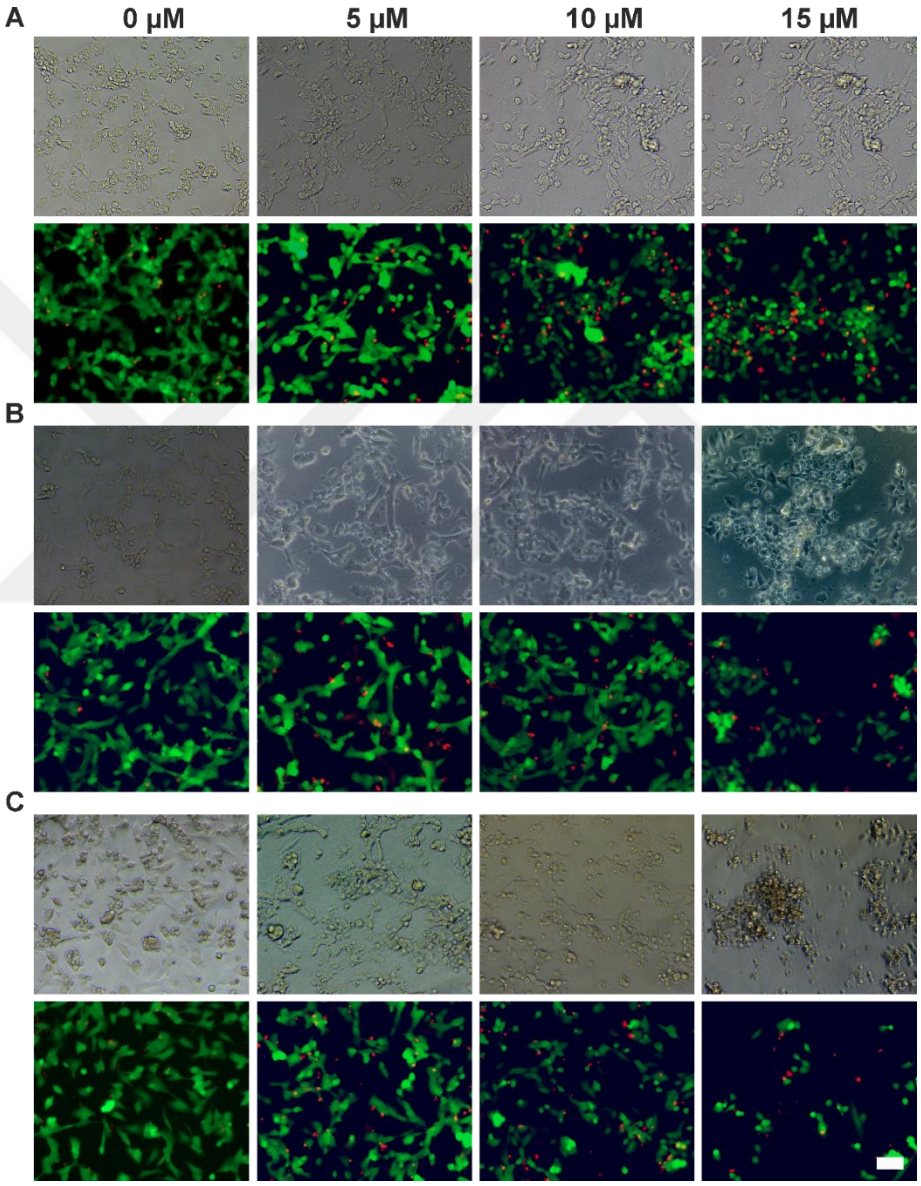

Figure 35. Bright-field and fluorescence microscopy images of SH-SY5Y cells after 0-15 µM Aβ 1-42 exposure for A) 24h, B) 48h, and C) 72h (Scale bar: 50 µm, Green: Live, Red: Dead).

In addition, the cell viability of undifferentiated SH-SY5Y cells was analyzed *via* MTT after addition of Aβ 1-42 aggregates (Figure 36). It was observed that cell viability decreased, correlating with Aβ 1-42 aggregate concentration and incubation time, which is in concordance with live-dead assay results. The cell viability decreased up to 46% at 10 µM for 72h with a significant difference, which was acceptable for modeling Alzheimer's disease *via* Aβ 1-42 induction. In literature, it was reported that Aβ aggregates reduced cell viability to around 44% at 25 µM (Lee et al., 2012).

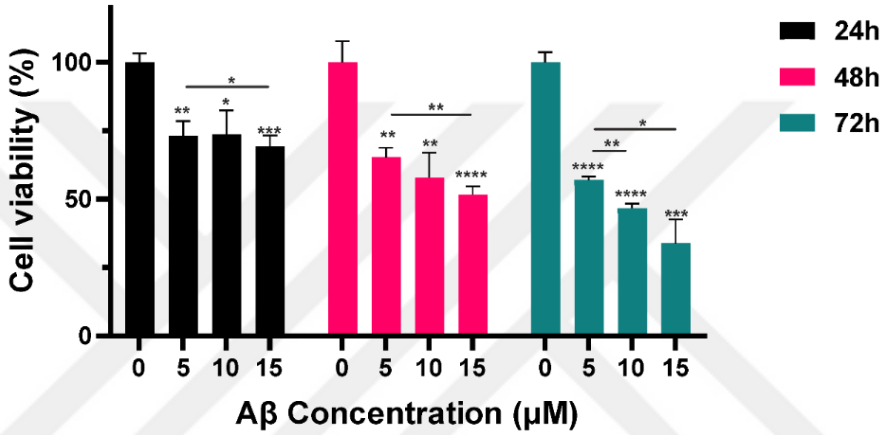

Figure 36. Cell viability measurement of SH-SY5Y cells after 0-15 µM Aβ 1-42 exposure for 24h, 48h, and 72h, analyzed by MTT (n=5, *p <0 .05, **p <0 .01, ***p <0 .001, ****p<0.0001 compared to the control of each group, two-way ANOVA followed by Tukey's test).

Then, differentiated SH-SY5Y was also exposed to Aβ 1-42 aggregates by applying the same protocol as it was done with undifferentiated SH-SY5Y for 24h, 48h, and 72h (Figure 37A-37C). When the concentration of Aβ1-42 was increased for all time intervals, the dead cell rate was accelerated. On the other hand, Aβ1-42 did not change cell morphology for 24h and 48h, but cell detachment was observed at a high concentration of Aβ1-42, such as 10 µM and 15 µM.

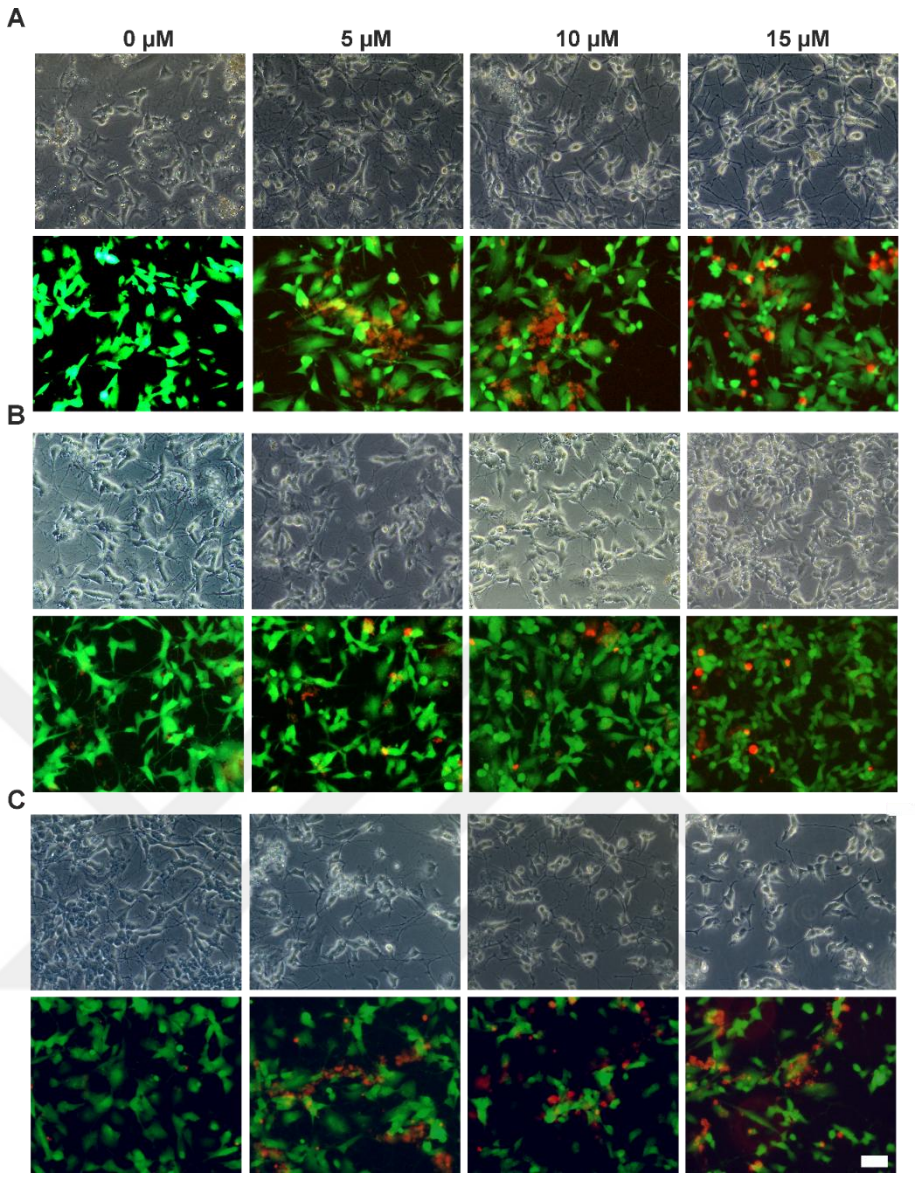

Figure 37. Bright-field and fluorescence microscopy images of differentiated SH-SY5Y cells after 0-15 µM Aβ 1-42 exposure for A) 24h, B) 48h, and C) 72h, analyzed by Live-dead assay (Scale bar: 50 µm, Green: Live, Red: Dead).

Next, MTT analysis was done to analyze cell viability quantitatively after exposure of 0-15 µM Aβ 1-42 aggregates. Cell viability of differentiated SH-SY5Y cells varied between 100-63% and 100-57% for 24h and 48h, respectively (Figure 38). At 72h, cell viability decreased to 47% at 10 µM with a significant difference, which can be an applicable concentration for modeling Alzheimer's disease (Thapa et al., 2016). In a literature, Aβ exposure decreased cell viability to 70% in SH-SY5Y cell line, whereas 5

days of incubation resulted in around 55% cell viability (Thapa et al., 2016). In another study, Aβ treatment decreased cell viability to around 70% in SH-SY5Y cells (Wang et al., 2012). These studies showed that the cell profile after Aβ treatment is in a suitable range for modeling Alzheimer's disease.

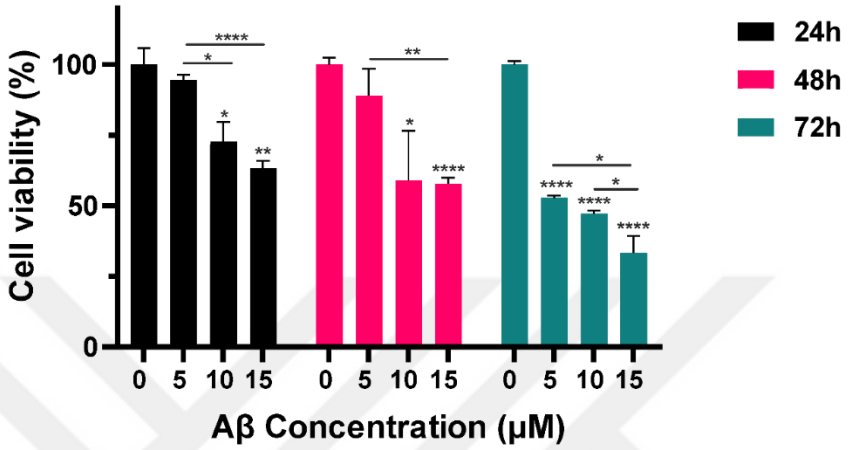

Figure 38. Cell viability measurement of differentiated SH-SY5Y cells after 0-15 μM Aβ 1-42 exposure for 24h, 48h, and 72h, analyzed by MTT (n=5, *p <0 .05, **p <0 .01, ***p <0 .001, ****p<0.0001 compared to the control of each group, two-way ANOVA followed by Tukey's test).

On the other hand, un-/differentiated SH-SY5Y cells displayed similar cell viability profile (Fernandez-Busquets et al., 2010), which is in line with some studies in the literature. Besides, some studies report that differentiated cells are more sensitive compared to undifferentiated in terms of cell proliferation profiles (Lambert et al., 1994). Overall, these findings indicated that 10 μM Aβ 1-42 aggregates exposed to SH-SY5Y cells for 72h are the appropriate condition for modeling Alzheimer's disease. As a result, subsequent studies focused on Alzheimer's disease in 3D cell culture models were initiated using these parameters of 10 μM for 72h incubation.

Then, the presence of Aβ 1-42 aggregates in the SH-SY5Y cell culture environment was tested *via* Congo red and Thioflavin T assays (Figure 39A-39B). The results showed that Congo red dye and Thioflavin T both bound to cells and Aβ 1-42 aggregates. Therefore, they could not be distinguished from each other and do not

specifically bind to Aβ1-42 aggregates. This indicates that neither dye is specific solely to Aβ 1-42 aggregates, as they also exhibit affinity for cellular components. This finding highlights potential limitations in using these dyes for the selective detection of Aβ1-42 aggregates in 2D and 3D cell culture, as cellular components may lead to false-positive signals or misinterpretation of aggregates. On the other hand, there are contrary results in the literature that show the presence of Aβ 1-42 aggregates in cell culture environment without binding to cells (Abdul Manap et al., 2020; Park et al., 2023).

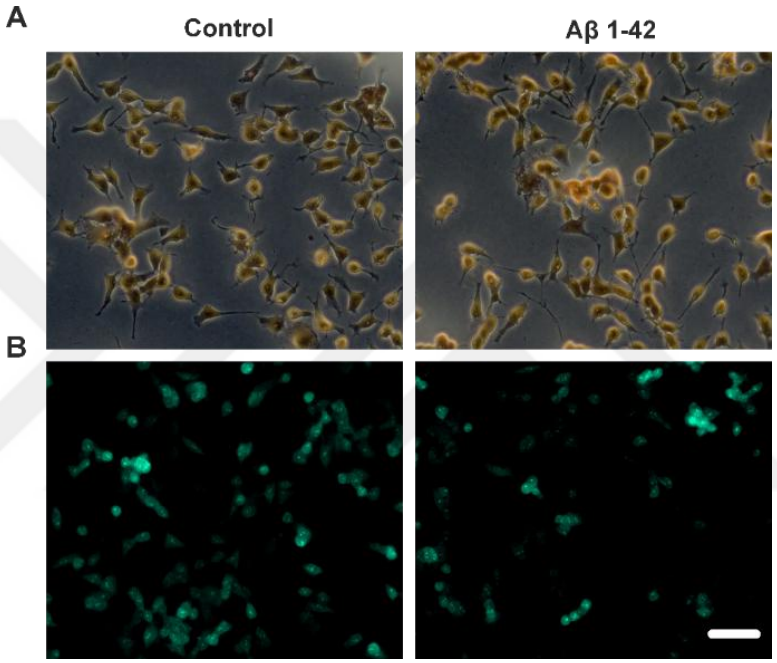

Figure 39. Aβ 1-42 aggregate staining in cell culture environment via A) Congo red and B) Thioflavin T assays (Scale bar: 50 μm).

3.2.3. Alzheimer's Disease Modeling via Aβ Induction Using SH-SY5Y Spheroids

Following the optimization of Aβ 1-42 induction on 2D cell culture, un-/differentiated spheroids were exposed to 10-50 μM Aβ 1-42 aggregates to determine neurotoxic parameters reducing cell viability around 50% (Calan et al., 2016; Zhang et

al., 2017). Spheroid structure and cell viability were monitored after exposing 10-50 µM Aβ 1-42 aggregates on un-/differentiated spheroids for 72h (Figure 40). A concentration-dependent decrease in cell viability was observed, with significant cell death occurring at 50 µM for un-/differentiated SH-SY5Y spheroids (Cai et al., 2020).

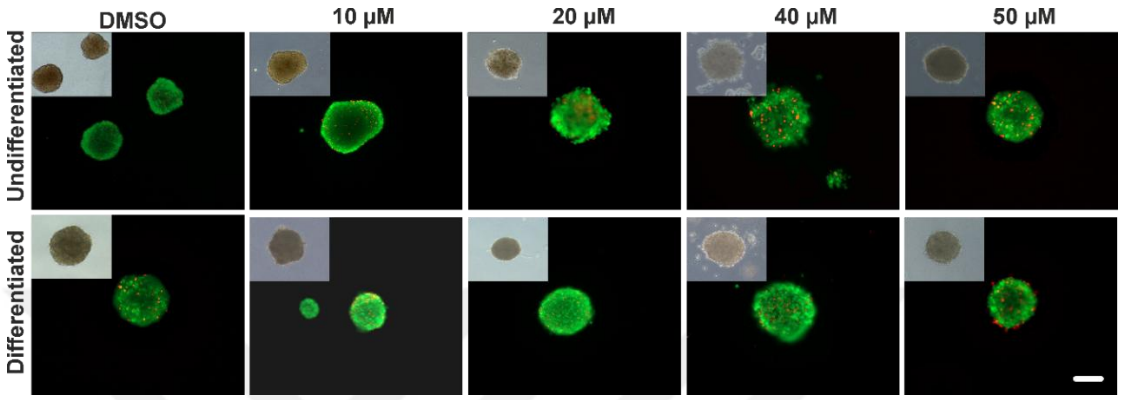

Figure 40. A) Bright-field and fluorescence microscopy images of un-/differentiated SH-SY5Y spheroids after 10-50 µM Aβ 1-42 aggregate exposure for 72h, analyzed by Live-dead assay (Scale bar: 200 µm, Green: Live, Red: Dead).

The cell viability of undifferentiated spheroids decreased from 96% to 71%, while it decreased from 96% to 68% in differentiated spheroids with a significant difference compared to control (Figure 41). It was 87% and 82% at 10 µM for un-/differentiated spheroids for 72h, respectively. This indicates that Aβ 1-42 aggregates resulted in different neurotoxicity profiles in 2D versus 3D cell cultures, as expected. This resistance in 3D cell culture against screened compounds, including Aβ 1-42 aggregates, arises from its more complex architecture, such as cell-cell and cell-matrix interactions (Calan et al., 2016; Gonzalez et al., 2018; Terrasso et al., 2015; Thapa et al., 2016; Wang et al., 2012).

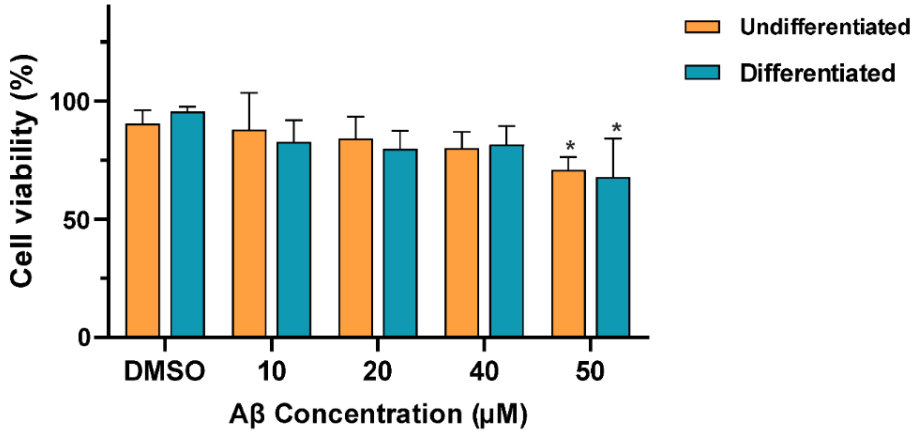

Figure 41. Cell viability of un-/differentiated SH-SY5Y spheroids after 10-50 μM Aβ 1-42 exposure for 72h (n=5, *p <0 .05, ***p <0 .001, ****p<0.0001 compared to the DMSO control of each group, two-way ANOVA followed by Tukey's test).

On the other hand, the findings showed that cell viability did not decrease to the targeted level, which is around 50%. Therefore, the incubation time with 50 μM Aβ 1-42 aggregates was extended from 3 to 7 days to be able to model 3D Alzheimer's disease realistically.

Furthermore, the neurotoxicity of 50 μM Aβ 1-42 aggregates was investigated based on incubation time (Figure 42). Cell death increased in correlation with the extended incubation time of Aβ 1-42 aggregates for both un-/differentiated spheroids. The findings revealed a time-dependent increase in cell death for both un-/differentiated spheroids, with a significant decline in cell viability observed on day 7, suggesting that prolonged exposure to Aβ1-42 aggregates increases their toxic effects. The results underscore the importance of incubation time as a crucial factor in studying Aβ-induced neurotoxicity.

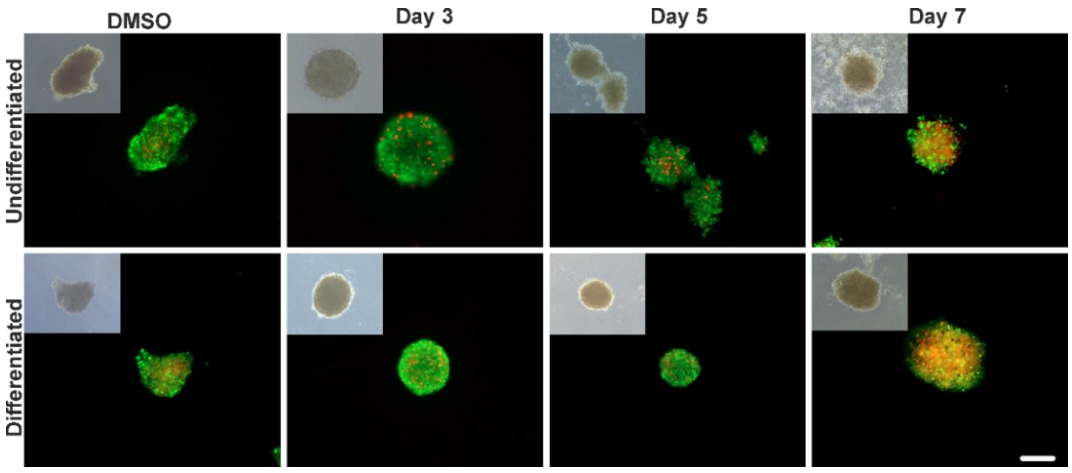

Figure 42. Bright-field and fluorescence microscopy images of un-/differentiated SH-SY5Y spheroids after 3-7 days of 50 µM Aβ 1-42 exposure, analyzed by Live-dead assay (Scale bar:200 µm, Green: Live, Red: Dead).

Cell viability results showed that it decreased from 92% to 65% for undifferentiated spheroids, while it decreased to 51% for differentiated spheroids (Figure 43), which are acceptable neurotoxicity profiles for modeling Alzheimer's disease on 3D cell culture (Calan et al., 2016; Thapa et al., 2016; Wang et al., 2012). Also, there is a significant difference in cell viability between un-/differentiated spheroids on day 7. This observation indicates that the neurotoxic effects of Aβ1-42 aggregates are influenced by both concentration and duration of exposure, where longer exposure times result in decreased cell viability. In addition, differentiated spheroids are more sensitive to toxins compared to undifferentiated spheroids, consistent with similar studies (Forster et al., 2016; Krishtal et al., 2017; Simões et al., 2021). This can be attributed to undifferentiated cells having smaller surface areas due to lacking longer neurites, resulting in smaller contact areas with Aβ 1-42 aggregates (Krishtal et al., 2017). Also, the findings support that differentiated spheroids are more suitable for studying 3D Alzheimer's disease model (Krishtal et al., 2017) due to the response to the Aβ 1-42 aggregates. Consequently, differentiated spheroids were utilized for 3D Alzheimer's disease modeling and investigating the neuroprotective effect of Curcumin for further studies.

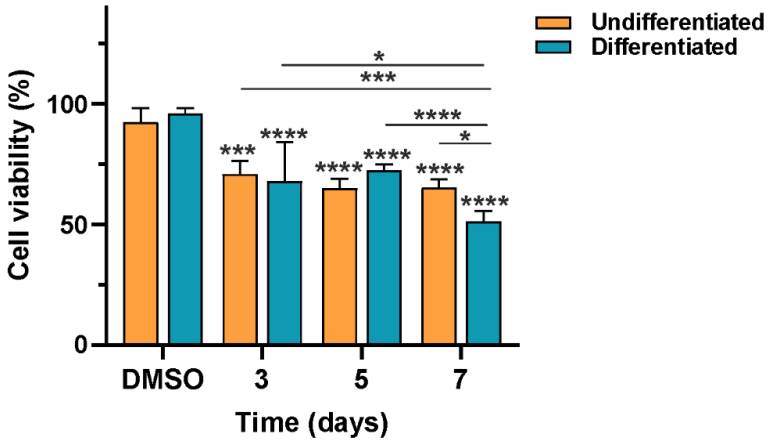

Figure 43. Cell viability of un-/differentiated SH-SY5Y spheroids after 3-7 days of 50 µM Aβ 1-42 exposure (n=5, *p <0 .05, ***p <0 .001, ***p<0.0001 compared to DMSO control of each group, two-way ANOVA followed by Tukey's test).

3.2.4. Characterization of 3D Alzheimer's Disease Modeling of SH-SY5Y Using Immunostaining

The cholinergic system is continuously affected, and significant loss of cholinergic neurons is observed in Alzheimer's disease. ChAT expression has been investigated in Alzheimer's disease models for cholinergic neuron activity (Bowen et al., 1976; de Medeiros et al., 2019; Wilcock et al., 1982). Hence, the characterization of 3D Alzheimer's disease model was carried out by immunostaining of ChAT (Figure 44). Fluorescence microscopy images showed that the control group expressed ChAT, while ChAT expression in 3D Alzheimer's disease model reduced significantly (Figure 44A). There is a 2.2-fold decrease in ChAT relative fluorescence intensity in 3D Alzheimer's disease model (Figure 44B), consistent with studies in the literature (Gil-Bea et al., 2005). These findings indicate that 3D Alzheimer's disease model was successfully developed, offering a valuable tool for studying Alzheimer's disease and testing potential therapeutic candidates.

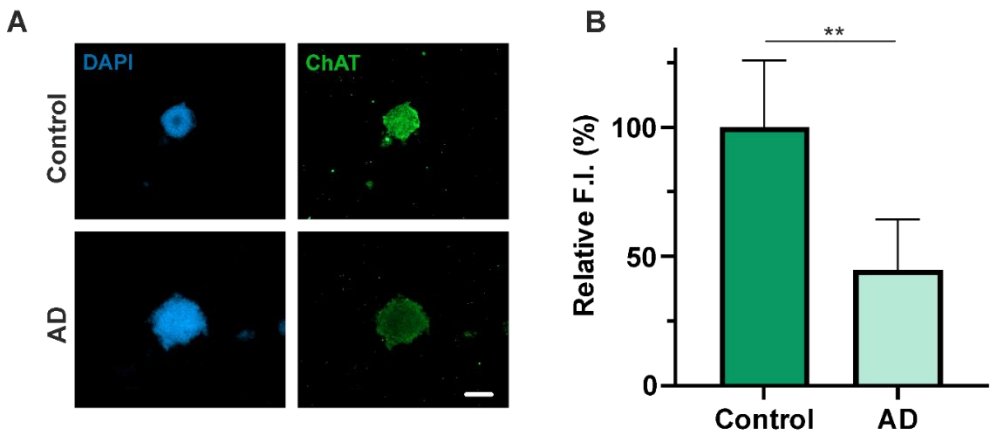

Figure 44. A) Fluorescence microscopy images of ChAT marker for 3D Alzheimer's disease model of SH-SY5Y spheroids B) Calculated fluorescence intensity (F.I.) of ChAT for Control and AD (Alzheimer's disease) model (Scale bar:200 µm) (Blue: DAPI, Green: ChAT) (n=4, **p <0 .0, t-test analysis).

3.3. Investigating the Neuroprotective Effect of Curcumin on 3D Alzheimer's Disease Model of SH-SY5Y

3.3.1. Evaluating the Disassociation Ability of Curcumin Against Aβ 1-42 Aggregates

Curcumin has shown potential as a neuroprotective agent for Alzheimer's disease by disassociating aggregates, and reducing neurotoxicity (Abdul Manap et al., 2020; Park et al., 2008; Yan et al., 2017). Moreover, studies reported that Curcumin can bind to Aβ plaques with different forms in post-mortem samples with high affinity (den Haan et al., 2018). Therefore, Curcumin can be a promising compound to suppress disease progression (Abdul Manap et al., 2020). For this purpose, Curcumin at varied concentrations was incubated with Aβ 1-42 aggregates for 72h exogenously (Figure 45). The samples were monitored by light microscopy then analyzed by Congo red and Thioflavin T assays. Bright-field images showed that Curcumin disassociated Aβ 1-42

aggregates effectively, while reducing their size with increasing Curcumin concentration. These results indicated that Curcumin possesses the ability to disassociate Aβ 1-42 aggregates by disrupting intra- and interstrand distances of preformed fibrils, as reported in literature, and reduced aggregate size and numbers (Silveira et al., 2022). It was also reported that Curcumin can change the Aβ fibrillar structure with a non-toxic form (Thapa et al., 2016).

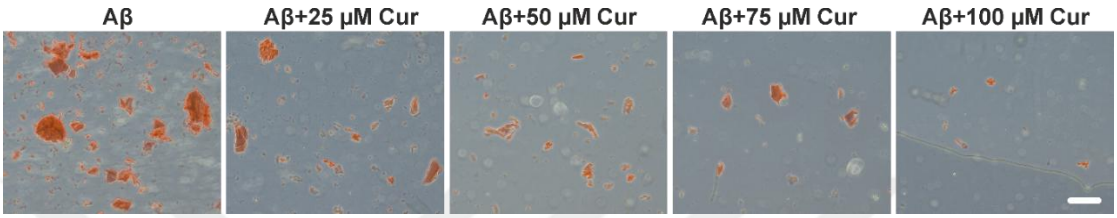

Figure 45. A) Monitoring Aβ 1-42 aggregates by bright-field microscopy following 0-100 μM Curcumin treatment for 72h (Scale bar: 200 μm).

Then, the size distribution of Aβ1-42 aggregates following Curcumin treatment was measured and analyzed as given in Figure 46, enabling a comparative analysis of aggregate size before and after treatment. Prior to Curcumin application, the majority of Aβ1-42 aggregates ranged between 20-60 μm. Additionally, although less frequently observed, larger aggregates measuring between 100-160 μm were also detected, indicating that in the absence of Curcumin. Following Curcumin treatment, a significant shift in Aβ1-42 aggregate size distribution was observed, particularly at 100 μM Curcumin concentration, where larger aggregates underwent disassociation, leading to the formation of smaller aggregates ranging between 20-50 μm (Figure 46A-46E). This reduction in aggregate size and frequency of large amyloid plaques indicates that Curcumin effectively disassociated with Aβ aggregation. These findings indicate the potential application of Curcumin as a neuroprotective agent, supporting its use in preventing Aβ aggregates neurotoxicity in Alzheimer's disease research.

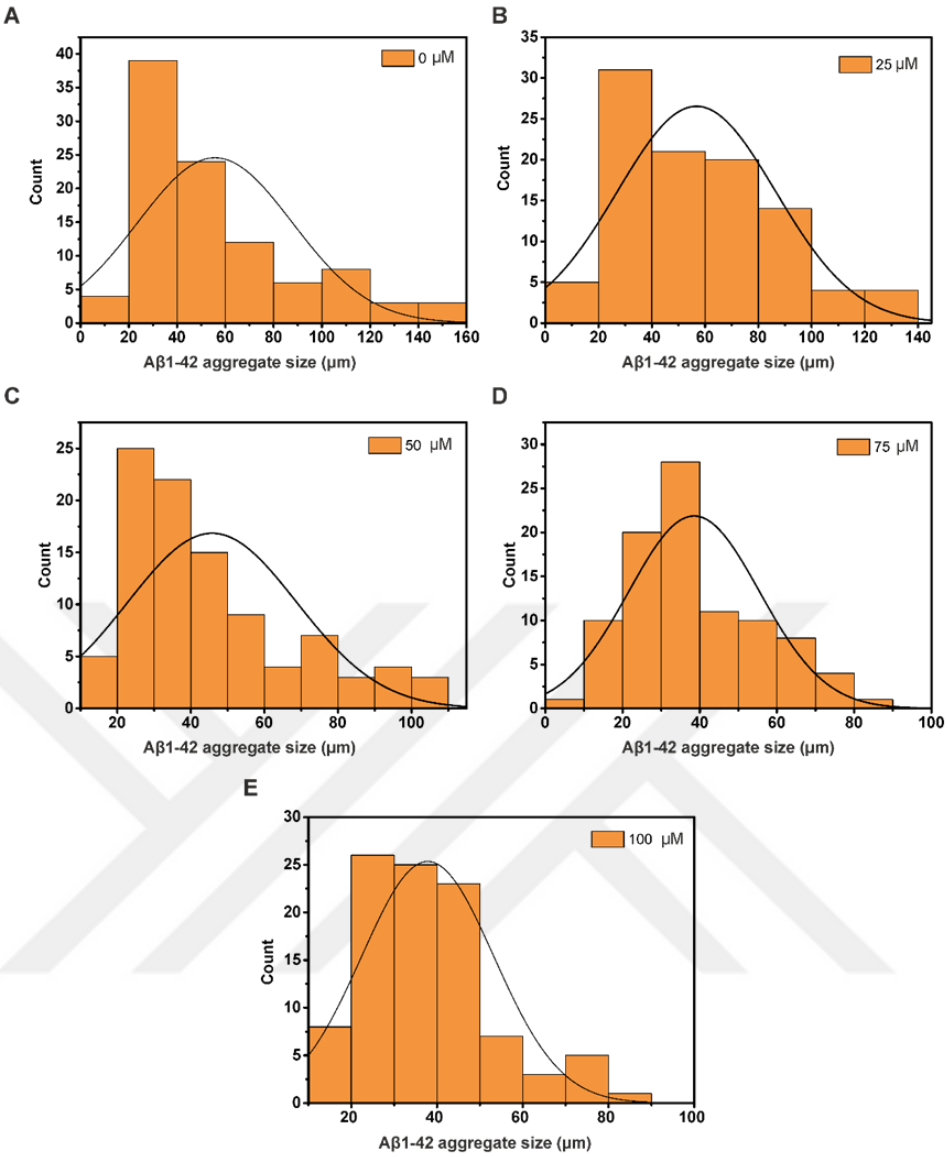

Figure 46. Size distribution profile of Aβ 1-42 aggregates after Curcumin treatment with varied concentrations A) 0 µM B) 25 µM C) 50 µM D) 75 µM and E) 100 µM.

Congo red assay provides quantitative evidence of Curcumin's effect in disassociating Aβ1-42 aggregates. Congo red dye specifically binds to the beta-sheet structures that are indicative of amyloid aggregates. This binding facilitates the spectral changes, serving as an indicator for the presence of Aβ aggregates (Klunk et al., 1999; Yakupova et al., 2019). Upon treating the Aβ1-42 aggregates with Curcumin, a noticeable decrease in relative absorbance intensity was observed, ranging between 55-60% with

significant differences, which indicates that Curcumin effectively disassociated the Aβ1-42 aggregates (Figure 47).

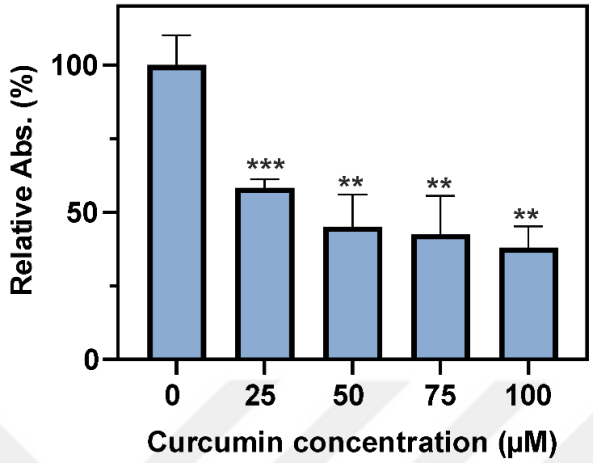

Figure 47. Relative absorbance (Abs.) values of Congo red staining following 0-100 μM Curcumin treatment for 72h (n=6, **p<0.01 ***p <0 .001, compared 0 μM (Aβ), one-way ANOVA followed by Tukey's test).

Thioflavin T assay is another assay for evaluating Aβ aggregate formation quantitatively (Zhu et al., 2007). Thioflavin T is a fluorescence dye that exhibits enhanced fluorescence upon binding to the β-sheet-rich structures of Aβ fibrils (Walsh et al., 1997). In the study, Thioflavin T assay was employed to evaluate the disassociation effect of Curcumin against Aβ 1-42 aggregates. Figure 48 shows that F.I. intensity decreased, ranging between 71-53 % after Curcumin treatment. Also, there is a significant difference between the control (0 μM) and Curcumin-treated group. A similar observation was reported in other studies in the literature. For example, Manap et al. (2019) screened Curcumin on the developed 2D Alzheimer's disease model *via* inducing Aβ 1-42 aggregates. Thioflavin T results showed that 49.1 μM Curcumin decreased F.I. almost 50% (Manap et al., 2019).

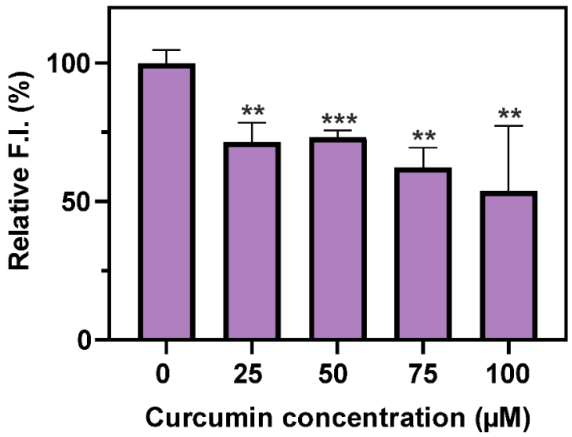

Figure 48. Relative fluorescence intensity (F.I.) of Thioflavin T assay following 0-100 μM Curcumin treatment for 72h (n=6, **p<0.01 ***p <0 .001, compared 0 μM (Aβ), one-way ANOVA followed by Tukey's test).

Overall, these results showed that Curcumin successfully disassociated Aβ 1-42 aggregates by some mechanism as mentioned in the literature. The aromatic rings of curcumin bind in parallel to the side chains of aromatic amino acids in Aβ fibrils. This bonding occurs by the overlapping of electron clouds and is referred to as π-π stacking interactions. This interaction impairs fibril stability by weakening the natural bonding between aromatic rings present in the fibril structure (Sarvestani et al., 2023). In addition, molecular docking and molecular dynamics simulations have shown that curcumin's keto-enol functional groups form hydrogen bonds with the backbone amide groups of the β-sheet. This interaction weakens the intra- and inter-strand hydrogen bonds that maintain the structural integrity of the fibril. For example, curcumin has been observed to bind within amyloidogenic sequences like the KLVFFA segment of Aβ fibrils, targeting critical residues through hydrogen bonding and hydrophobic interactions. These interactions induce perturbations in the β-sheet alignment, reducing the structural stability and leading to fibril disassembly or the formation of less toxic aggregates (Velander et al., 2017).

3.3.2. Optimization of Curcumin Concentration on 2D Cell Culture of SH-SY5Y

The cytotoxicity of Curcumin was investigated on SH-SY5Y in 2D cell culture to determine the proper concentration for 3D cell culture (Figure 49). Bright-field and fluorescence microscopy images showed that Curcumin has a cytotoxic effect at concentrations above 25 µM after 72h. These findings are consistent with other studies, such as one that reported Curcumin displaying significant cytotoxicity at a concentration of 100 µM (Silveira et al., 2022)

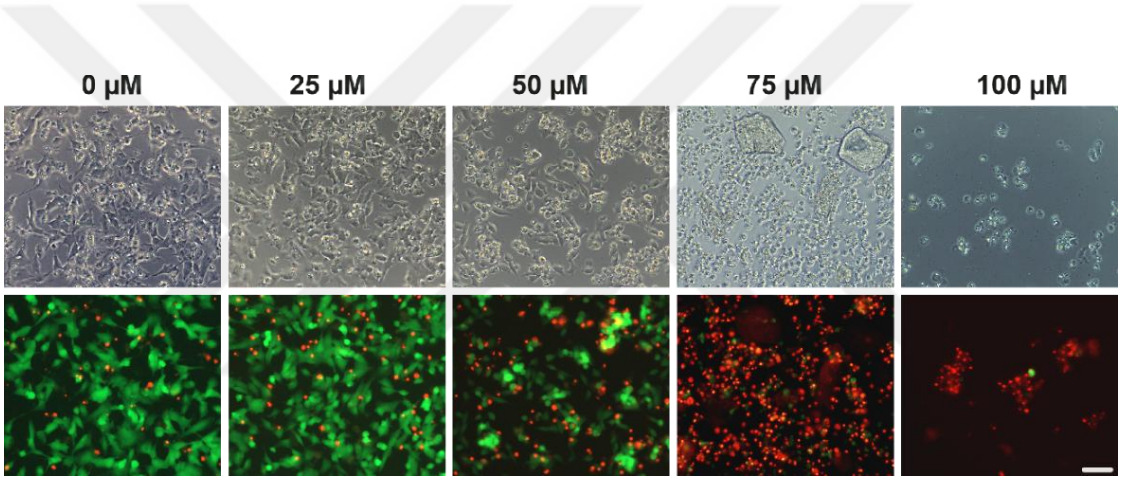

Figure 49. Bright-field and fluorescence microscopy images of SH-SY5Y after 0-100 µM Curcumin screening for 72h (Scale bar: 50 µm, Green: Live, Red: Dead).

Further studies were carried out between 25-100 µM Curcumin since 3D cell culture is more resistant to screened compounds due to its more compact and complex structure compared to 2D cell culture. Cell viability results in 2D cell culture showed that Curcumin exhibited high cell viability at 25 and 50 µM with 100 and 74%, respectively (Figure 50). However, there is a significant cytotoxicity after 50 µM.

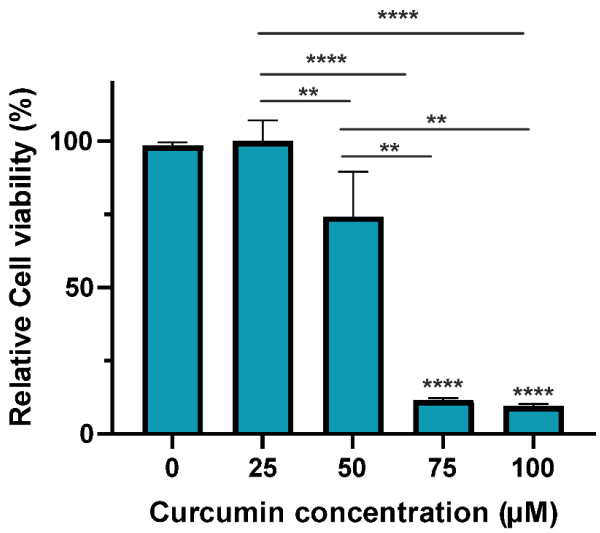

Figure 50. Evaluation of cell viability of SH-SY5Y after 0-100 µM Curcumin screening for 72h by MTT (n=6, **p<0.01, ***p <0 .001, ****p <0 .0001 compared 0 µM, one-way ANOVA followed by Tukey's test).

This finding is important because it suggests that Curcumin, despite being widely recognized for its neuroprotective effect, can induce cell death at certain concentrations (Silveira et al., 2022). The underlying mechanism of Curcumin-induced cytotoxicity has been attributed to its prooxidant properties, which is in contrast with its well-known antioxidant and anti-inflammatory effects at lower doses. (Banerjee et al., 2008; Shi et al., 2007). At elevated concentrations, Curcumin has been shown to induce apoptosis, trigger oxidative stress, and lead to DNA damage (Park et al., 2008). Therefore, determining the concentration of Curcumin is essential for its neuroprotective potential.

3.3.3. Investigating Curcumin Cytotoxicity on 3D SH-SY5Y Spheroids

The cytotoxicity of Curcumin was investigated on 3D SH-SY5Y spheroids fabricated by MagLev before 3D Alzheimer's disease modeling (Figure 51). The study involved treating SH-SY5Y spheroids with varying concentrations of Curcumin and assessing the effects on cell viability. The result showed that Curcumin did not exhibit a

cytotoxic effect as observed in 2D cell culture on SH-SY5Y spheroids. In contrast, spheroids exhibited high cell viability even at 100 µM of Curcumin, as expected.

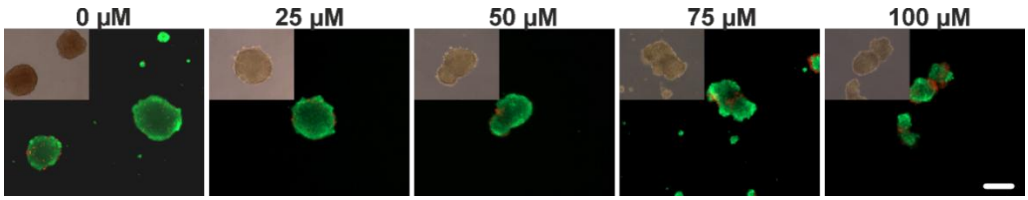

Figure 51. Bright-field and fluorescence microscopy images of SH-SY5Y spheroids after Curcumin cytotoxicity assessment by Live-Dead assay (Scale bar: 200 µm, Green: Live, Red: Dead).

Also, cell viability ranged between 91-72%, even at 100 µM Curcumin (Figure 52), indicating low toxicity of Curcumin on 3D cell culture. Following these findings, Curcumin was tested in the 3D Alzheimer's disease model of SH-SY5Y to evaluate its disassociation capability on Aβ 1-42 aggregates.

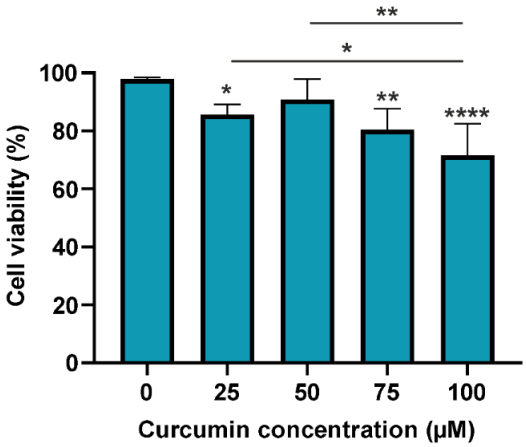

Figure 52. Cell viability measurement of SH-SY5Y spheroids after Curcumin cytotoxicity assessment by Live-Dead assay (n=6, *p <0 .05, **p <0 .01, ****p<0.0001 compared to the control of each group, one-way ANOVA followed by Tukey's test).

These results emphasize the differences in cellular responses between 2D and 3D cultures, as 3D spheroids better mimic the complex microenvironment of the brain, providing a more physiologically relevant model for drug testing. This suggests that toxicity assays on 2D cell culture may not fully capture cellular responses observed in 3D cell culture, further highlighting the importance of validating neuroprotective compounds in 3D models before translating findings to *in-vivo* studies.

3.3.4. Evaluation of the Neuroprotective Effect of Curcumin on 3D Alzheimer's Disease Model of SH-SY5Y

The evaluation of the neuroprotective effect of Curcumin was conducted on 3D Alzheimer's disease model of SH-SY5Y (Figure 53). Fluorescence microscopy images revealed that Curcumin significantly inhibited Aβ 1-42-induced cell death, highlighting its potential as a neuroprotective agent. Spheroids treated with Curcumin showed remarkably higher cell viability compared to untreated spheroids exposed to Aβ 1-42 aggregates, indicating that Curcumin inhibited the neurotoxic effects of Aβ 1-42 aggregates.

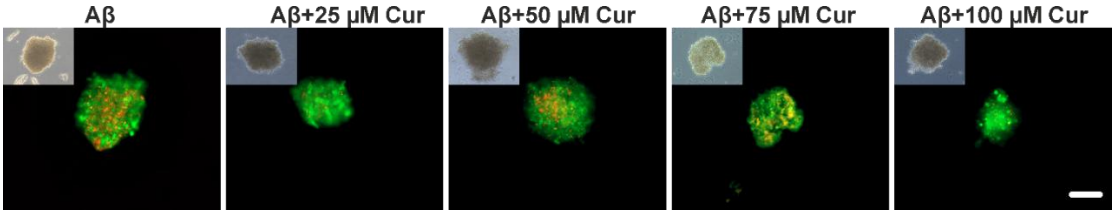

Figure 53. Investigating neuroprotective effect of Curcumin on Aβ 1-42 aggregates in 3D spheroids; Bright-field and fluorescence images of spheroids before and after 0-100 µM Curcumin treatment for 72h on Aβ–induced 3D Alzheimer's disease model (Scale bar: 200 µm, Green: Live, Red: Dead).

Cell viability results showed that Curcumin increased cell viability within a certain concentration range, particularly at 25 µM, which effectively inhibited Aβ-induced neurotoxicity. This resulted in an increase in cell viability from 51% to 94%, demonstrating a significant difference (Figure 54).

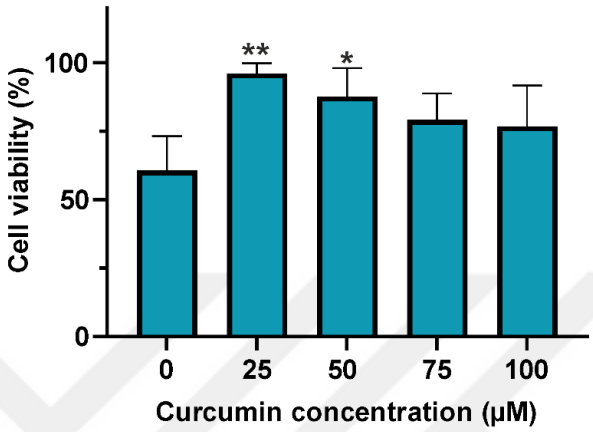

Figure 54. Cell viability after 0-100 µM Curcumin treatment for 72h in Aβ–induced 3D Alzheimer's disease model of SH-SY5Y (n=5, *p <0 .05, **p <0 .01, compared Aβ-treated group (0 µM), one-way ANOVA followed by Tukey's test).

In a similar study, Curcumin treatment increased cell viability from 45% to around 75% in the Aβ-induced model of SH-SY5Y (Thapa et al., 2016). The neuroprotectivity of Curcumin is attributed to the decreasing permeability of the cell membrane against Aβ after Curcumin treatment. In another report, it was found that the minimum effective concentration of Curcumin is 10 µM (Silveira et al., 2022), suggesting that even at lower doses, it can exert protective effects against Aβ neurotoxicity. In another study, 30 µM Curcumin exhibited a neuroprotective effect on 2D Aβ-induced model of SH-SY5Y cells (Yanagisawa et al., 2015). Another study investigated the neuroprotective effect of Curcumin against pesticide and Aβ-induced damage. Curcumin exhibited a neuroprotective effect by activating some mechanisms. For example, (i) Nrf2 protein, which activates the neuroprotective system in cells, (ii) APE1 activation, which takes a role in DNA repair, and (iii) inhibition of Aβ fibril formation (Sarkar et al., 2017). These

findings highlight Curcumin's potential as a neuroprotective agent that can inhibit Aβ-induced damage, offering a promising avenue for further research in Alzheimer's disease.

In addition, the disassociation of Aβ 1-42 aggregates within 3D cell culture environment was investigated by immunostaining before and after Curcumin treatment (Figure 55). Fluorescence images showed that Curcumin disassociated Aβ 1-42, and smaller fragments were observed after Curcumin treatment, as expected.

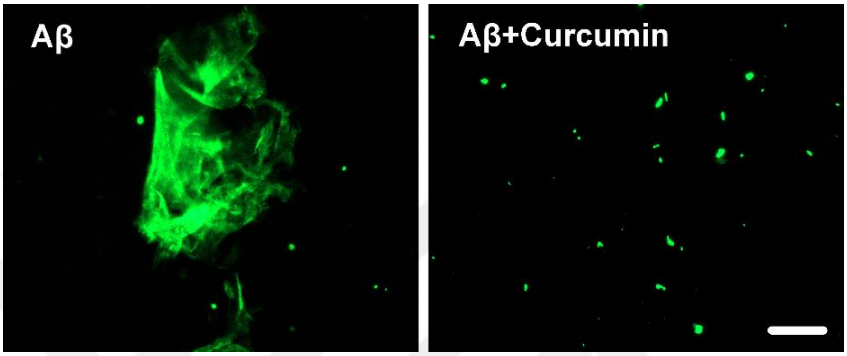

Figure 55. Fluorescence microscopy images of Aβ 1-42 aggregates in 3D Alzheimer's disease model before and after Curcumin treatment at 25 μM (Scale bar: 100 μm).

These findings strongly suggest that Curcumin's ability to disassociate Aβ aggregates plays a crucial role in reducing neurotoxicity, thereby protecting neuronal cells from Aβ-induced damage, supported by several studies (Abdul Manap et al., 2019; Yang et al., 2005; Yin et al., 2012; Zhang et al., 2018). Its neuroprotective effect can also be attributed to inducing PI3K, Akt, and Nrf2, which play a role in cytoprotecting (Yin et al., 2012). By both disassociation of toxic amyloid structures and activating protective signaling cascades, Curcumin shows promise as a therapeutic candidate for suppressing Alzheimer's disease progression, offering a multifaceted approach for preserving neuronal viability (Velankanni et al., 2019).

CHAPTER 4

4.1. Formation 3D cell culture of PC-12 via MagLev

4.1.1. Optimization of Gx Concentration for 3D Cell Culture Formation of PC-12 in MagLev Setup

PC-12 cell line is a commonly utilized cell line in neuroscience, particularly in Alzheimer's disease research. Recent studies have investigated the use of PC-12 for 3D cell culture in neuroscience(Javkhlan et al., 2024; Krokker et al., 2021). This study utilized PC-12 cells to fabricate 3D cell culture model *via* MagLev technology. A MagLev setup was used to facilitate the rapid and easy formation of 3D cell cultures. The study involved optimizing the concentration of paramagnetic agents and the number of cells for 24h culture time to form 3D cell cultures (Figure 56). Initially, the levitation capability and cytotoxicity of Gx were tested for 24 hours, revealing the formation of small aggregates and the acquisition of 3D cellular clusters after 4h.

The 3D cell culture formation displayed irregular shapes with increasing aggregate sizes by the end of the 24h culture period (Figure 56). This irregular shape may be due to the characteristics of endocrine tumor-type cell lines that do not naturally form spheroids and require an ECM (Krokker et al., 2021). Additionally, the size of compact 3D cell clusters increased with higher Gx concentrations. Gx with 10 mM resulted in smaller 3D cellular structures, while concentrations exceeding 10 mM led to larger clusters. This phenomenon can be attributed to the effect of magnetic guidance on cell aggregation, resulting in the development of larger 3D cellular clusters.

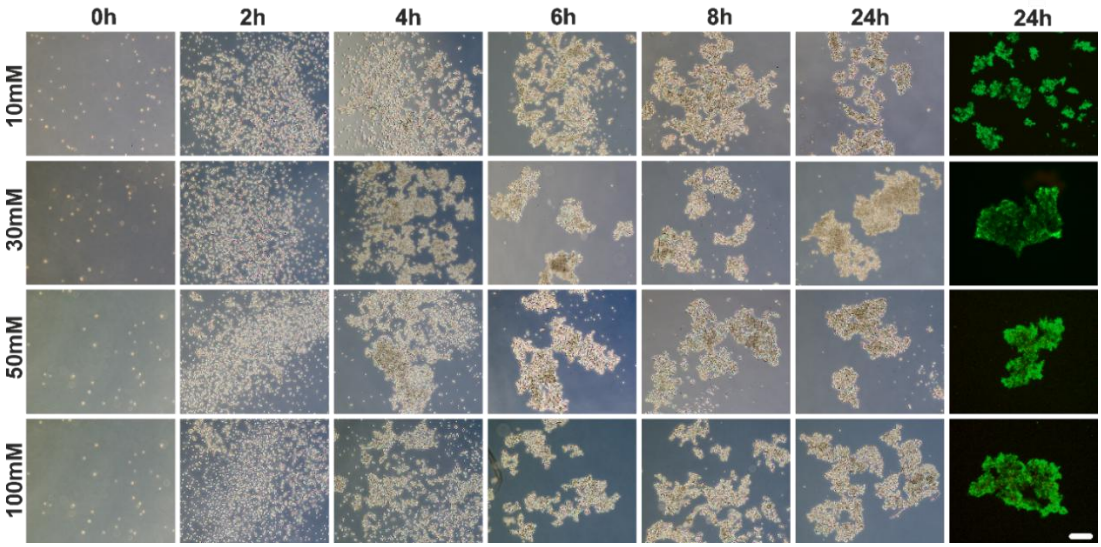

Figure 56. Bright-field and fluorescence microscopy images of 3D cell culture of PC-12 at $25x10^3$ cell number between 10-100 mM Gx for 24h (Scale bar:200 µm, Green:Live, Red:Dead).

Furthermore, 3D cell culture exhibited high cell viability even at high Gx concentrations. Notably, there was no significant change in cell viability from 10 to 100 mM, ranging from 93% to 92% (Figure 57). Further studies were carried out at 30 mM since 10 mM resulted in looser and smaller 3D cellular structure compared to the more compact and stable structures observed at 30 mM. Despite the differences in 3D cellular structures, no significant difference in cell viability was observed between 10 mM and 30 mM, indicating that the increase in Gx concentration primarily influenced the morphology of the 3D culture without affecting cell survival. In addition, there is no significant difference (ns) observed between other concentrations. This finding highlights the importance of optimizing Gx concentration not only for maintaining high cell viability but also for promoting the formation of robust and well-defined 3D cultures, which are essential for reliable *in-vitro* modeling.

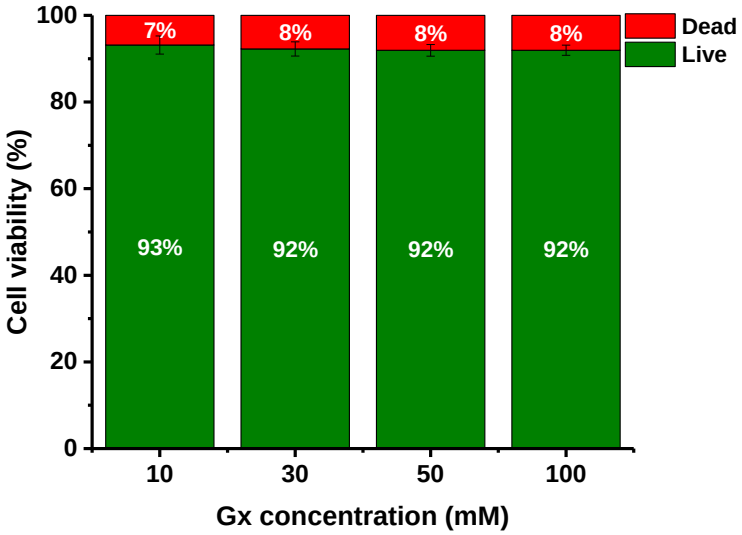

Figure 57. Cell viability results of 3D cultured PC-12 at 10-100 mM Gx with $25x10^3$ cell number for 24h (n=6, there is no significant difference between groups).

4.1.2. Optimization of PC-12 Cell Number for 3D Cell Culture Formation in MagLev Setup

Cell number optimization was conducted at 30 mM Gx concentration, as shown in Figure 58. During this process, cellular aggregation began to occur starting from 4^{th} h, with cells gradually coming together to form increasingly larger and more tightly structured aggregates over time. 3D cellular clusters formed at 24h, and their size increased from $5x10^3$ to $100x10^3$ cells. The progressive growth and tight structure of these aggregates underscore the importance of optimizing cell density, as these factors are crucial in promoting the development of 3D cellular structures.

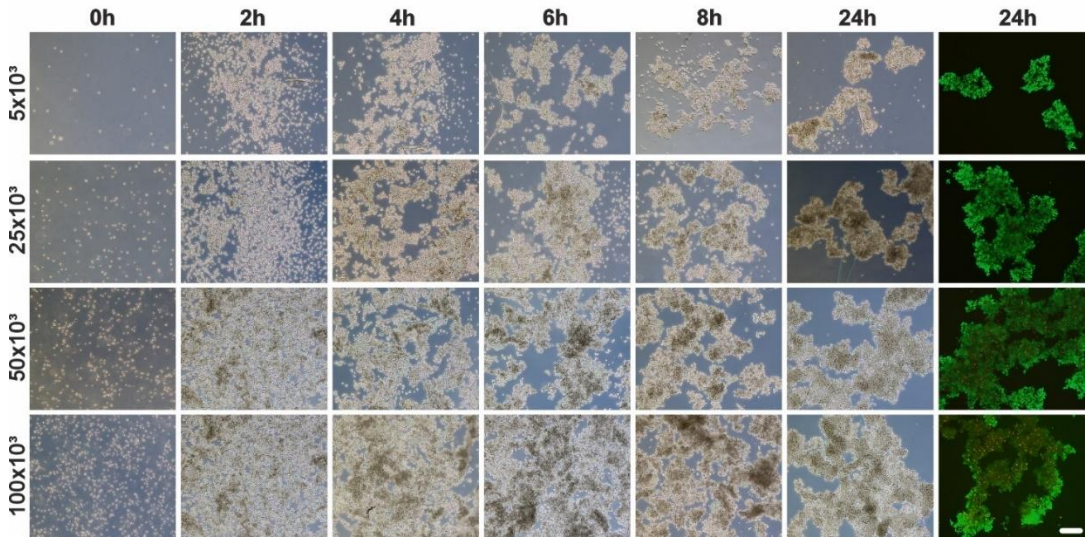

Figure 58. Bright-field and fluorescence microscopy images for 3D cell culture formation of PC-12 cells between $5x10^3$-$100x10^3$ cell number at 30 mM Gx cells for 24h (Scale bar:200 µm, Green: Live, Red: Dead).

In addition, high cell viability was observed, especially with 5 and 25 $x10^3$ cells, which was 96% and 93%, respectively (Figure 59). On the other hand, higher cell numbers resulted in 77% and 76% cell viability (Figure 59). This decrease in cell viability can be explained by the diffusion limitation of nutrients and oxygen, causing metabolic waste accumulation within the 3D cell culture structure exceeding a size of 200 µm (Lin and Chang, 2008). These findings indicate that maintaining a lower cell number leads to higher cell viability, whereas increasing the cell number tends to decrease cell viability (Onbas and Arslan Yildiz, 2021). Also, higher cell numbers led to faster formation of necrotic cores compared to lower cell numbers in 3D cell culture (Browning et al., 2021). Therefore, determining proper initial cell density is important for optimizing the balance between growth and viability in 3D cell culture. Selecting the appropriate cell number may prevent excessive aggregation, and minimize metabolic stress, all of which are crucial for maintaining viability of 3D cell culture, especially in long term culture.

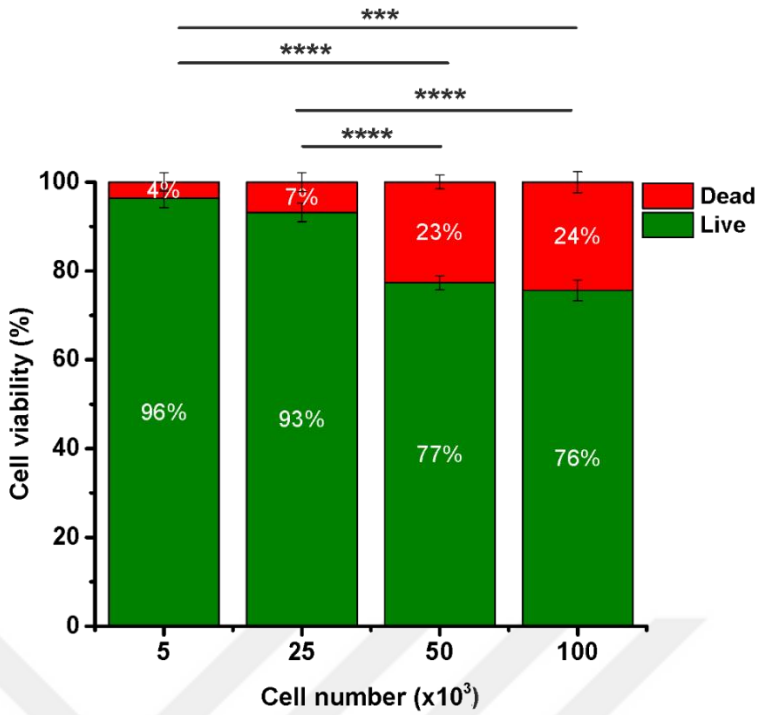

Figure 59. Cell viability measurement for 3D cellular structure of PC-12 between $5x10^3$-$100x10^3$ cell number at 30 mM Gx for 24h (n=6, ***p <0 .001, ****p<0.0001, two-way ANOVA followed by Tukey's test).

Next, the 3D cellular clusters of PC-12 cells were measured based on varying Gx concentrations and cell numbers, as depicted in Figure 60. It was observed that the cell area increased proportionally with the rise in Gx concentration. This phenomenon can be attributed to the increasing magnetic force acting on the cells (Onbas and Arslan Yildiz, 2021), which facilitates the aggregation of the cells into a more compact structure (Figure 60). In addition, the number of cells also played a significant role in the expansion of the 3D cellular area. As the cell number increased, there was a corresponding increase in the overall 3D cellular area, as expected. Overall, these findings highlighted the interplay between Gx concentrations and cell density in determining the 3D structure of the cell. MagLev technology allows for controlled cell aggregation and spatial arrangement, which is pivotal for the successful fabrication of tissue constructs. Further studies were carried out using $25x10^3$ cell numbers due to the forming of tight 3D cellular structures and high cell viability, while $5x10^3$ cells did not form 3D cellular structures, instead forming smaller aggregates.

On the other hand, circularity analysis was not done for 3D cultured PC-12 cells, since it formed irregular cellular clusters rather than spheroid formation. The irregular shape could be attributed to the nature of endocrine tumor-type cell lines, which typically do not form spheroids (Krokker et al., 2021).

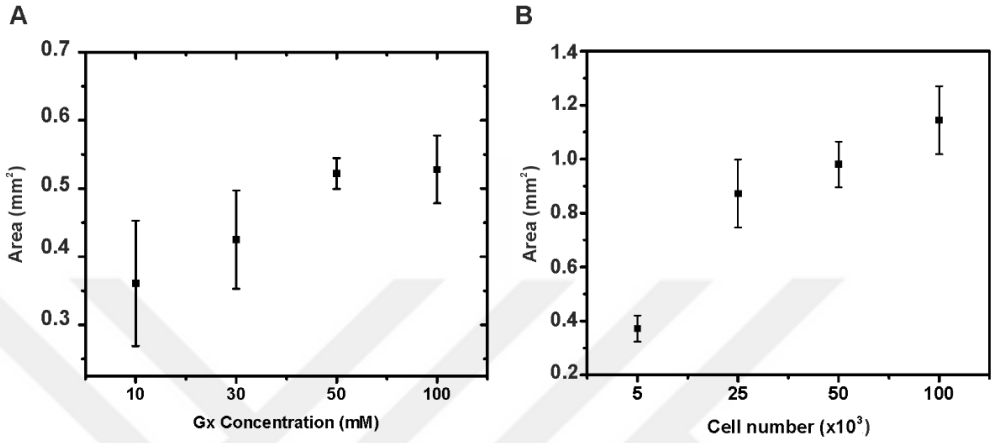

Figure 60. Area analysis of 3D cultured PC-12 cells based on A) Gx concentration and B) cell number for 24h.

4.1.3. 3D Cell Culture of PC-12 Cells in MagLev Setup for Long Term Culture

Furthermore, the long term culture of PC-12 cells *via* MagLev was further investigated to evaluate the levitation capability of the system and cytotoxicity of Gx (Figure 61). Bright-field images showed that PC-12 formed loose 3D cellular structure on days 1-3, forming a tight structure over time after day 3. This finding shows that different types of cells can show varying aggregation behavior in 3D cell cultures, which may result in either loosely formed aggregates or disconnected and floating cells (Leung et al., 2015). Moreover, the cell-to-cell junctions, particularly gap junctions, might impact on the compactness of the self-assembled structures when exposed to a magnetic field, as highlighted in the literature (McEvoy et al., 2020).

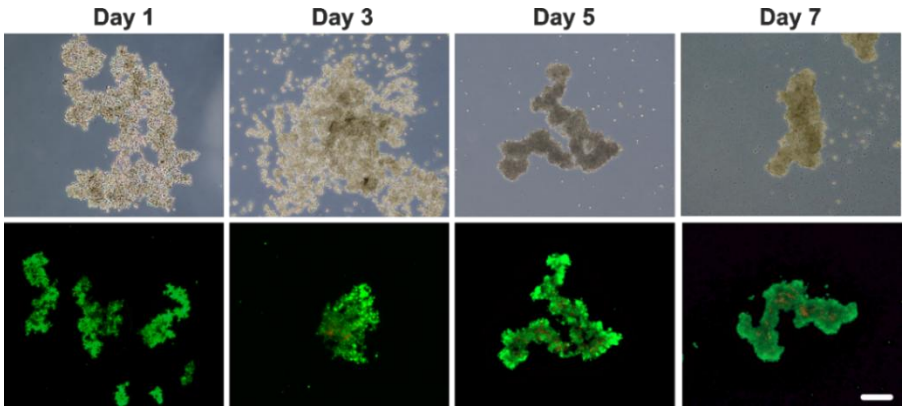

Figure 61. Bright-field and fluorescence microscopy images of 3D cell culture of PC-12 at $25x10^3$ and 30 mM Gx for long term culture (Scale bar:200 µm, Green: Live, Red: Dead).

3D cultured PC-12 cells showed high viability (99-97%), and Gx exhibited no cytotoxicity, even in long-term cultures (Figure 62). These findings confirmed that Gx is a reliable paramagnetic agent even during prolonged culture for the formation of 3D cellular structures (Onbas and Arslan Yildiz, 2021; Türker et al., 2018).

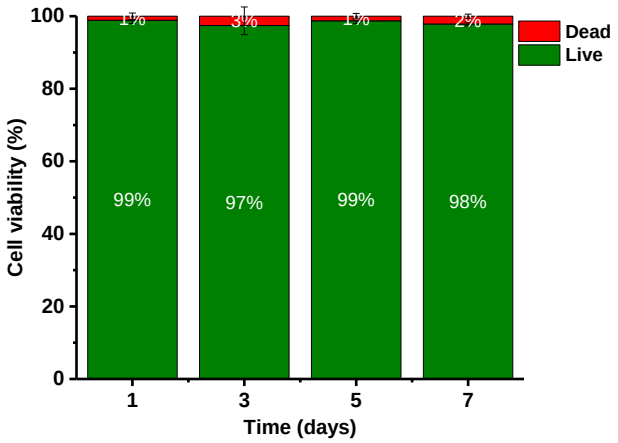

Figure 62. Cell viability measurement for 3D cellular structure of PC-12 12 at $25x10^3$ and 30 mM Gx for long term culture (n=6, there is no significant difference between groups).

Overall, the results indicated that MagLev method is a biocompatible method for 3D cell culture, demonstrating broad applicability across various cell types. Also, MagLev in 3D cell culture enhances cell aggregation, allows for the formation of larger structures, and promotes rapid 3D cell culture formation without inducing cytotoxicity, unlike traditional methods (Marques et al., 2022). Another significant advantage of MagLev is its ability to support long-term cell culture while maintaining consistently high cell viability (Moncal et al., 2022). Also, MagLev enables fabrication of 3D cell culture in a shorter time compared to scaffold-based approaches, further highlighting its potential in biomedical research.

4.2. Utilizing 3D Cultured PC-12 Cells to Model Alzheimer's Disease in 3D

4.2.1. Optimization of Aβ 1-42 Aggregate Concentration on 2D Cell Culture of PC-12 Cells

Here, a similar protocol that was used for un-/differentiated SH-SY5Y cells in 2D cell culture was applied to PC-12 cells to evaluate the neurotoxicity of Aβ 1-42 aggregates. Briefly, PC-12 cells were treated with varying concentrations of Aβ 1-42 (ranging from 1 to 15 μM) for different time periods (24 hours, 48 hours, and 72 hours). The impact of Aβ exposure on cell viability and cytotoxicity was assessed using live-dead assays and MTT assays in (Figures 63-64). The results revealed a concentration- and time-dependent increase in cell death following Aβ 1-42 exposure. Specifically, the number of dead cells significantly rose with higher concentrations of Aβ aggregates, particularly at concentrations exceeding 5 μM after 48 hours of treatment. This trend suggests that the toxic effect of Aβ 1-42 aggregates on PC-12 cells increases with higher concentration of Aβ and prolonged exposure times.

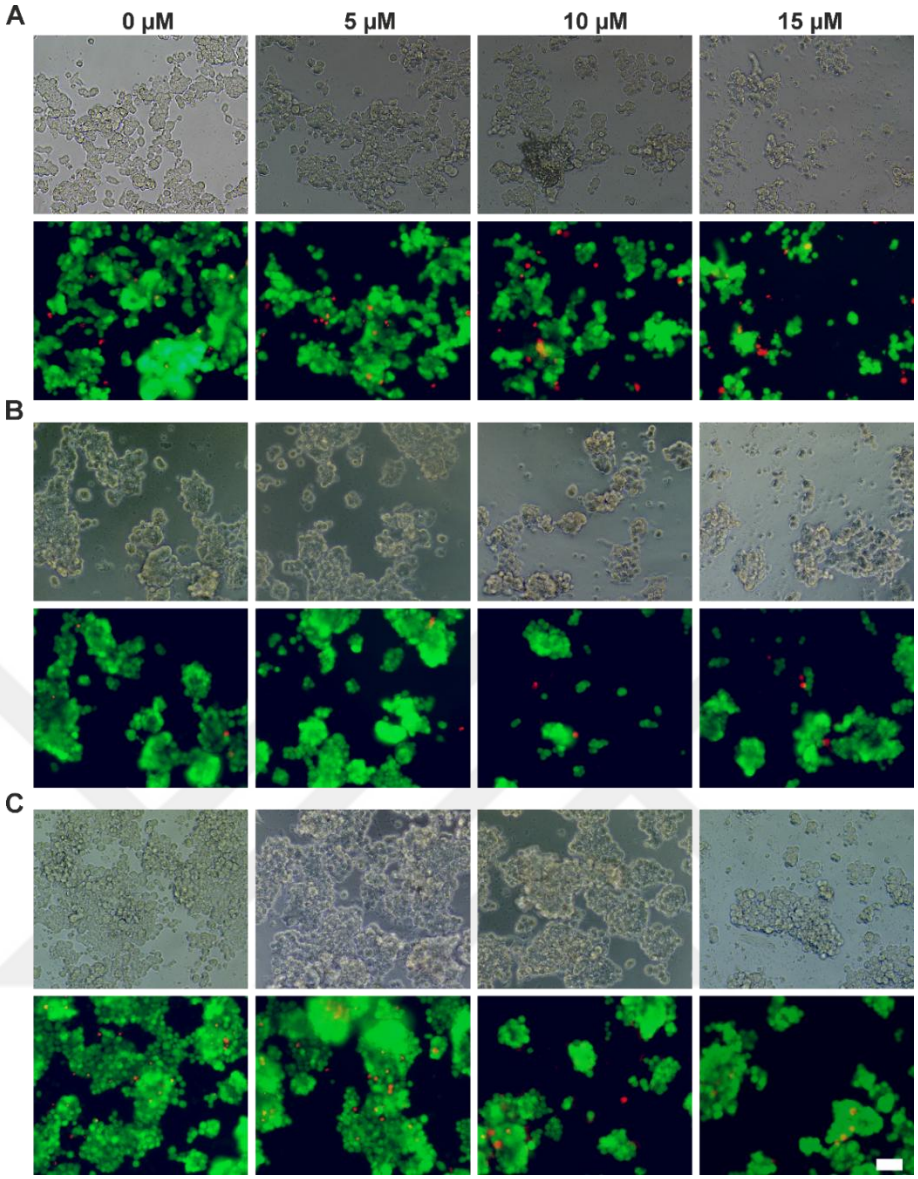

Figure 63. Bright-field and fluorescence microscopy images of PC-12 cells after 0-15 µM Aβ 1-42 exposure for A) 24h, B) 48h, and C) 72h (Scale bar: 50 µm, Green: Live, Red: Dead).

Furthermore, cell viability was quantitatively analyzed by MTT, resulting in a concentration-dependent decrease in cell viability for each time interval (Figure 64). However, cell viability increased at 72h compared to 24h and 48h, correlating with the results of Live-Dead assay. This increase may stem from the high proliferation rate of PC-12 cell line, which dominated the Aβ-induced cytotoxicity of 24h. In line with these findings, studies on Aβ-induced Alzheimer's disease model with PC-12 cells in the

literature have shown 75% viability at 10 µM Aβ (Xu et al., 2019), 72% viability at 0.5 µM Aβ (Jiang et al., 2018), and around 50% viability at 15 µM Aβ (Zhou et al., 2011).

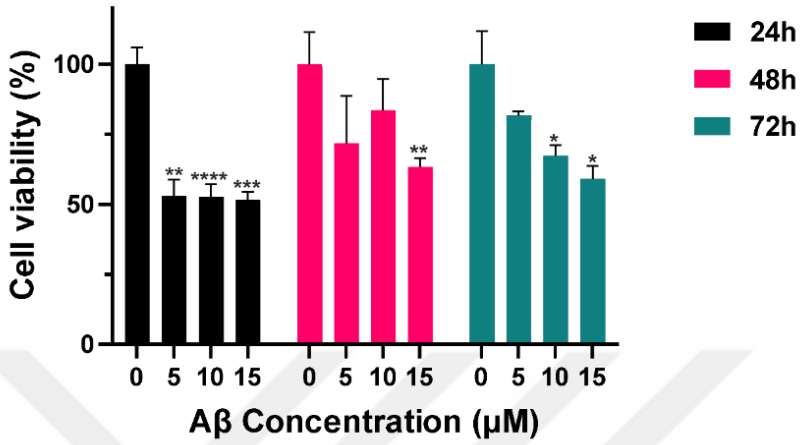

Figure 64. Cell viability measurement of PC-12 cells after 0-15 µM Aβ 1-42 exposure for 24h, 48h, and 72h, analyzed by MTT (n=6, *p<0.005, **p<0.01, ***p <0 .001, ****p<0.0001 compared to 0 µM, one-way ANOVA followed by Tukey's test).

4.2.2. Alzheimer's Disease Modeling via Aβ Induction Using 3D Cultured PC-12 Cells

Moreover, the neurotoxicity of Aβ 1-42 was investigated in 3D cell culture, and 10-50 µM Aβ 1-42 was applied to PC-12 cells to determine neurotoxic effects. The results demonstrated that exposure to Aβ 1-42 aggregates significantly increased the proportion of dead cells within the 3D cultured PC-12 cells (Figure 65).

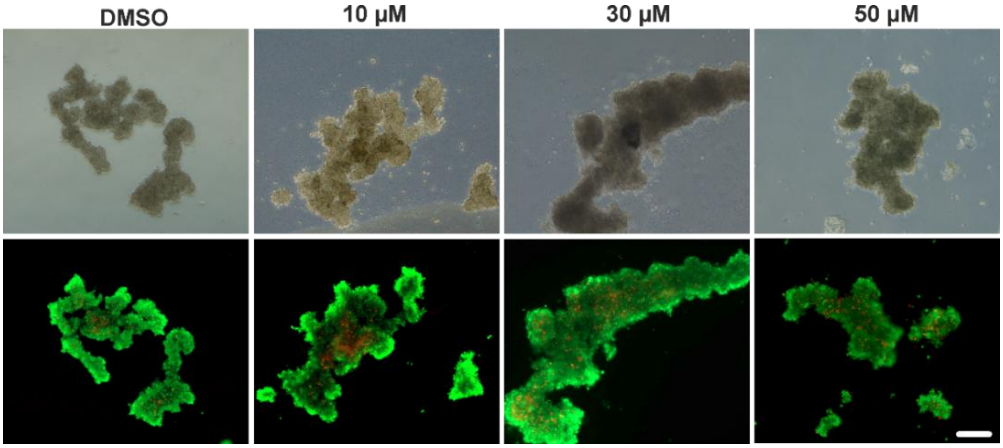

Figure 65. Bright-field and fluorescence microscopy images of 3D cultured PC-12 after 10-50 µM Aβ 1-42 exposure for 72h (Scale bar:200 µm, Green: Live, Red: Dead).

The cell viability exhibited a progressive decline, ranging between 94%-85%, following the application of Aβ 1-42 aggregates (Figure 66). Furthermore, a significant difference was noted between the DMSO control group and the 50 µM Aβ-treated group. Further studies were conducted using 50 µM Aβ 1-42 with an extended incubation time to observe the neurotoxic effect, targeting a cell viability reduction around 50%.

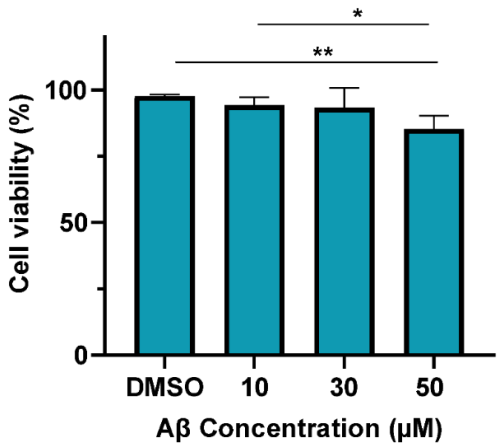

Figure 66. Cell viability measurement of 3D cultured PC-12 after 10-50 µM Aβ 1-42 exposure for 72h (n=6, *p<0.005, **p<0.01, one-way ANOVA analysis).

Furthermore, neurotoxicity of the Aβ 1-42 aggregates was investigated in 3D cell culture with extended incubation time (Figure 67). Notably, the most significant cell death was observed on days 15-21, indicating a progressive toxic effect of Aβ 1-42 aggregates over time. However, there is no remarkable difference in cell viability between days 15 and 21. The neurotoxicity of Aβ 1-42 on PC-12 cells has been investigated with different mechanisms by several studies. In one of the reports, it was observed that Aβ 1-42 aggregates on PC-12 cells are neurotoxic due to the interference of the nicotinic acetylcholine receptor by Aβ 1-42 aggregates (Li and Buccafusco, 2003). In another study, Aβ-treated PC-12 cells exhibited increasing p53 levels, involving the activation of Bax protein, which then coordinates with Bcl-2 to trigger a mitochondrial apoptotic pathway (Xie et al., 2015; Xu et al., 2019). Also, DNA fragmentation showed an increased apoptosis index in Aβ-induced PC-12 cells (Nishida et al., 2007) and Aβ disrupted the nuclear structure and cell integrity (Ding et al., 2024). Moreover, Aβ cytotoxicity was attributed to the increasing ROS activity in PC-12 cells (Zhu et al., 2007).

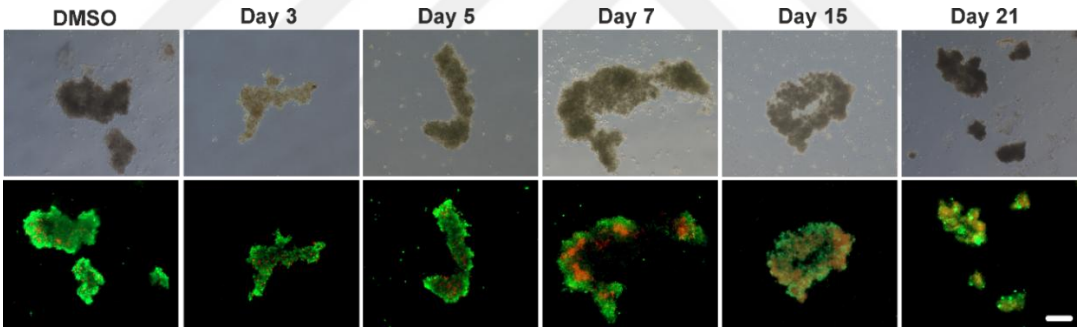

Figure 67. Bright-field and fluorescence microscopy images of 3D cultured PC-12 after 50 μM Aβ 1-42 exposure for 3-21 days (Scale bar:200 μm, Green: Live, Red: Dead).

Cell viability decreased up to 63% on day 15 for the Aβ-exposed group and there is no significant difference between day 15 and day 21 (Figure 68). This data underscores the importance of incubation time as a factor in neurotoxicity studies, particularly in mimicking the slow, progressive cellular damage seen in Alzheimer's disease. Also, this result showed that PC-12 cells are more resistant to Aβ neurotoxicity compared to other cell lines, which was an expected result due to native endocrine cell lines (Krokker et al.,

2021). The observed neurotoxicity in the 3D cell culture of PC-12 is within the appropriate range (20-50% inhibition) for studying Alzheimer's disease model when comparing the studies in the literature (Jayaprakasam et al., 2010; Zeng et al., 2017; Zhang et al., 2015).

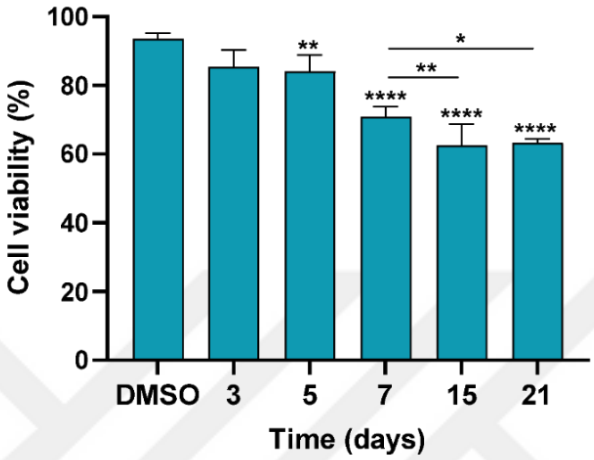

Figure 68. Cell viability measurement of 3D cultured PC-12 after 50 μM Aβ 1-42 exposure for 3–21 days (n=6, *p<0.005, **p<0.01, ****p<0.0001 compared to 0 μM, one-way ANOVA followed by Tukey's test).

4.2.3. Characterization of 3D Alzheimer's Disease Modeling of PC-12 Using Immunostaining

The cholinergic hypothesis is one of the primary models explaining the neurodegeneration observed in Alzheimer's disease. In particular, PC-12 cells can synthesize cholinergic receptors and have been extensively used in Alzheimer's disease model (Pokharel et al., 2018; Xie et al., 2023) because nicotinic receptors (as a subtype of cholinergic receptor) (Xie et al., 2023) in PC-12 cells have a high affinity with Aβ (Farhat and Ahmed, 2017). Moreover, ChAT expression of PC-12 cells has been previously investigated in Alzheimer's disease models, highlighting their relevance in studying cholinergic deficits and neuronal dysfunction (Rubenstein et al.,

1991). Therefore, ChAT immunostaining was performed to assess cholinergic neuron activity to further characterize 3D Alzheimer's disease model of PC-12 (Figure 69). The result showed that while the control group expressed ChAT, the Aβ-exposed group (AD) expressed it slightly (Figure 69A). On the other hand, F.I. of ChAT decreased to 2.8 in the AD group, indicating an almost two-fold decrease in F.I. (Figure 69B)

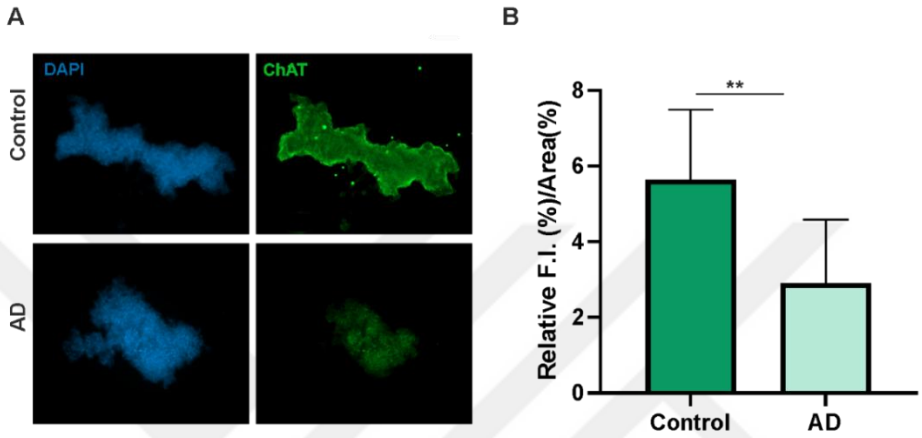

Figure 69. A) Fluorescence microscopy images of ChAT marker B) Calculated fluorescence intensity (F.I.) of ChAT based on the area (%) for Control and AD (Alzheimer's disease) model (Scale bar:100 µm) (Blue: DAPI, Green: ChAT) (n=4, **p <0 .01, t-test analysis).

These results overlap with the findings in the literature, which report an 18% activity decrease (Rubenstein et al., 1991). Overall, results showed that 3D Alzheimer's disease modeling using PC-12 cells was successfully developed, offering a valuable tool for studying Alzheimer's disease and testing potential therapeutic candidates. Consequently, Curcumin, a well-known neuroprotective compound, was selected for further investigation in this model to assess its potential therapeutic effects against Aβ-induced neurotoxicity.

4.3. Investigating the Neuroprotective Effect of Curcumin on 3D Alzheimer's Disease Modeling of PC-12

4.3.1. Optimization of Curcumin Concentration on 2D Cell Culture of PC-12

Here, the neuroprotective effect of Curcumin was tested in 3D Alzheimer's disease model of PC-12 with applying similar steps as it was done in SH-SY5Y model.

Curcumin cytotoxicity assessment was done on 2D cell culture of PC-12 for 72h before applying it on 3D cell culture. Bright-field and fluorescence microscopy images showed that Curcumin exhibited a cytotoxic effect at concentrations above 50 µM, as also observed in SH-SY5Y (Figure 70).

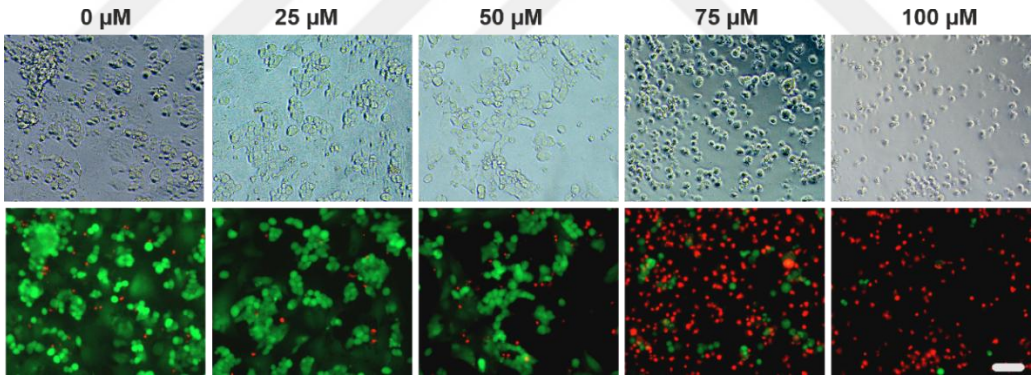

Figure 70. Bright-field and fluorescence microscopy images of PC-12 after 0-100 µM Curcumin screening for 72h (Scale bar: 50 µm, Green: Live, Red: Dead).

Then, relative cell viability was assessed in PC-12 cells following Curcumin treatment **(**Figure 71**).** The analysis revealed that cell viability remained at 92% when treated with 25 µM Curcumin**,** indicating that this concentration had a minimal cytotoxic effect**,** allowing for cellular survival and normal metabolic activity**.** However, beyond this concentration, a significant decrease in cell viability was observed, suggesting that higher

doses of Curcumin could exert cytotoxic effects, as observed in SH-SY5Y cells. Another report showed that exceeding 16 µg/mL (43.43 µM) caused cytotoxicity in PC-12 cells, highlighting that higher concentration may pose a risk of toxicity (Mendonca et al., 2009).

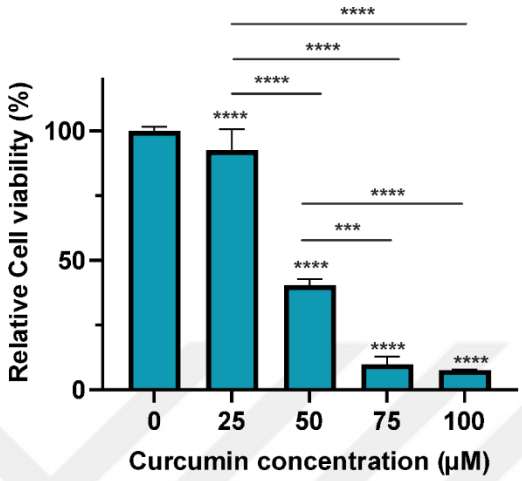

Figure 71. Cell viability measurement of PC-12 cells after 0-100 µM Curcumin screening for 72h (n=6, ***p <0 .001, ****p<0.0001 compared to the control of each group, one-way ANOVA followed by Tukey's test).

4.3.2. Investigating Curcumin Cytotoxicity on 3D Cultured PC-12 Cells

The cytotoxicity of Curcumin was tested on 3D cell cultured PC-12 before its application on 3D Alzheimer's disease model (Figure 72). Results showed that Curcumin did not have cytotoxicity on 3D cultured PC-12, and the Curcumin-treated group had similar cell viability with the control group, as well. The difference in the cytotoxicity of Curcumin between 2D and 3D cell cultures can be attributed to the resistance of 3D cell culture against compounds compared to 2D cell cultures.

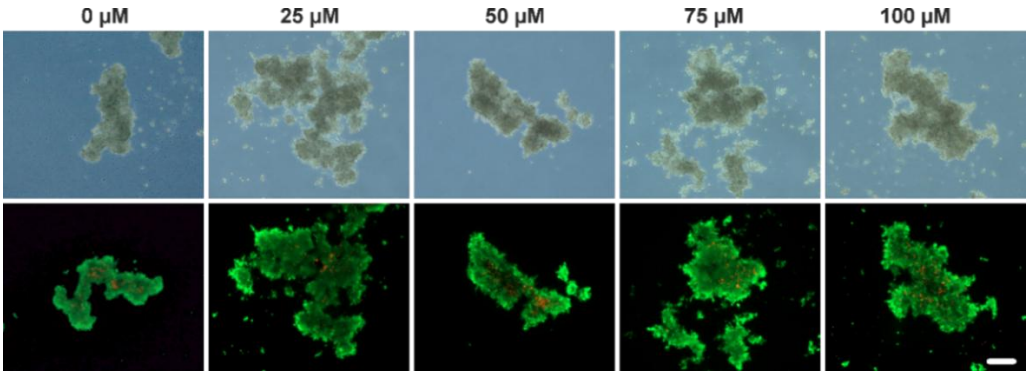

Figure 72. Bright-field and fluorescence microscopy images of 3D culture of PC-12 after Curcumin cytotoxicity assessment by Live-Dead assay (Scale bar: 200 µm, Green: Live, Red: Dead).

Then, the cell viability of 3D cultured PC-12 cells was measured to assess the cytotoxicity of Curcumin before screening it on 3D Alzheimer's disease model. Results demonstrated that high cell viability was observed, ranging between 96-91% with no significant difference (ns) (Figure 73).

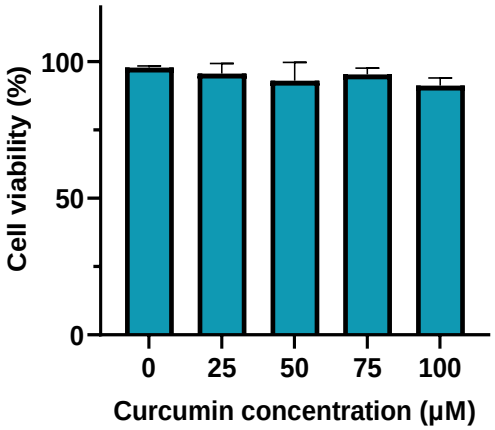

Figure 73. Cell viability measurement of 3D cultured PC-12 after Curcumin cytotoxicity assessment by Live-Dead assay (n=6, there is no significant difference between groups).

4.3.3. Evaluation of the Neuroprotective Effect of Curcumin on 3D Alzheimer's Disease Model of PC-12

Curcumin neuroprotective effect was evaluated on 3D Alzheimer's disease model (Figure 74). For this purpose, 0-100 µM Curcumin was screened on 3D Alzheimer's disease model for 72h culture time. Fluorescence microscopy images of cell viability assays demonstrated that Curcumin-treated groups maintained high cell viability.

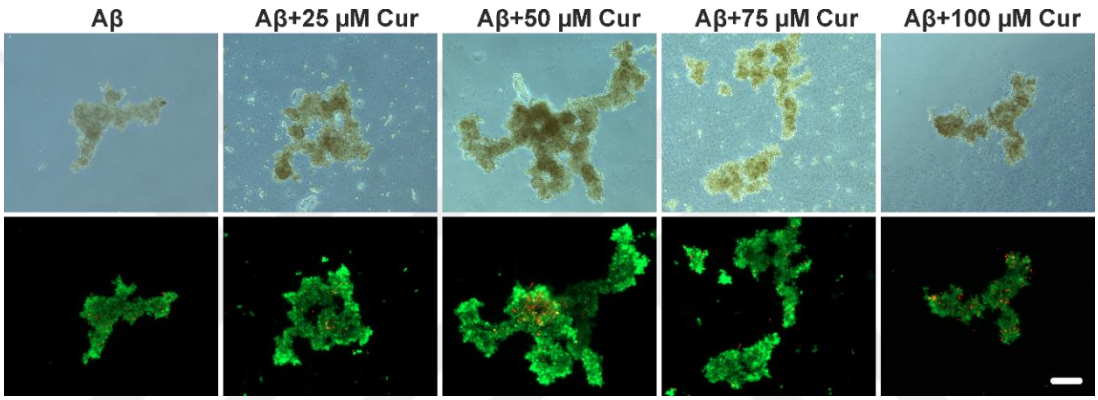

Figure 74. Bright-field and fluorescence images of 3D cultured PC-12 before and after 0-100 µM Curcumin treatment for 72h in Aβ–induced 3D Alzheimer's disease model (Scale bar: 200 µm, Green: Live, Red: Dead).

It was observed that Curcumin increased cell viability within a given range, and Curcumin prevented Aβ-induced neurotoxicity, evidenced by the increase in cell viability from 87 to 98% (Figure 75). The result showed the potential neuroprotective effect of Curcumin despite a lack of significant improvement in cell viability. Therefore, further studies were carried out of 25 µM Curcumin on 3D Alzheimer's disease model.

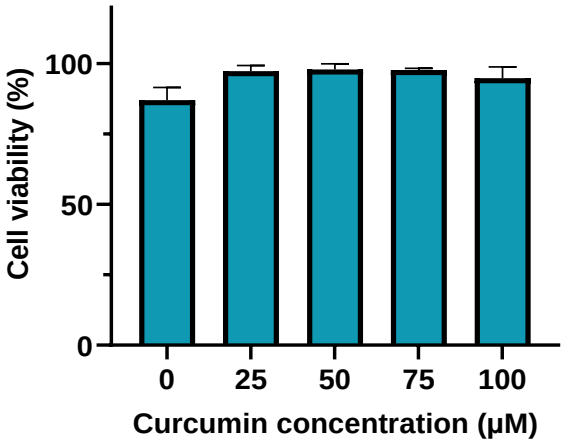

Figure 75. Cell viability measurement after 0-100 µM Curcumin treatment for 72h in Aβ–induced 3D Alzheimer's disease model of PC-12 (n=6, there is no significant difference between groups).

Furthermore, the neuroprotective effect of Curcumin was investigated for 21 days (Figure 76). The result showed that high cell viability was observed at all time intervals, showing that Curcumin protects cells from Aβ-induced neurotoxicity even in the long term. The results demonstrated that high cell viability was maintained throughout all time intervals, suggesting that Curcumin provided consistent neuroprotection for 21 days.

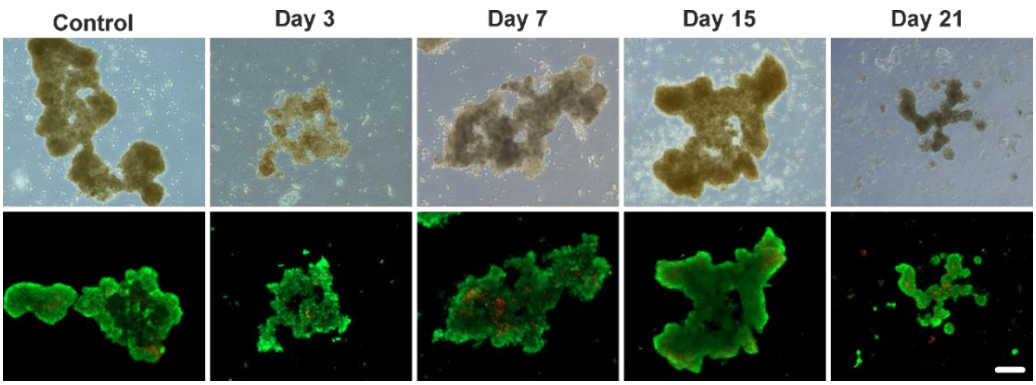

Figure 76. Bright-field and fluorescence images of 3D culture of PC-12 before and after Curcumin treatment at 25 µM for 21 days in Aβ–induced 3D Alzheimer's disease model (Scale bar: 200 µm, Green: Live, Red: Dead).

Cell viability results showed that Curcumin increased cell viability from 70 to 92, 63 to 86, and 64 to 76% on days 7, 15, and 21, respectively (Figure 77). This showed 22%, 23%, and 13% increases in cell viability when Curcumin was treated on days 7, 15, and 21, respectively. Curcumin's neuroprotection was maintained until day 15, after which cytotoxicity of the Curcumin was observed, even though it continued to protect the cells compared to the Aβ-induced group.

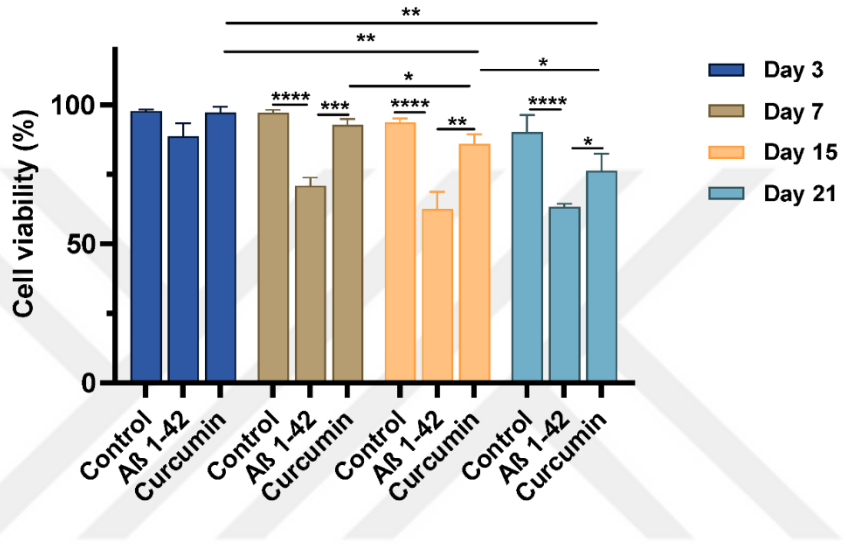

Figure 77. Cell viability after Curcumin treatment at 25 µM for 21 days in Aβ–induced 3D Alzheimer's disease model of PC-12 (n=6, *p <0 .05, **p <0 .01, ***p <0 .001, ****p<0.0001 compared to the control of each group, two-way ANOVA followed by Tukey's test).

This neuroprotective effect of Curcumin on PC-12 cells was explained by several mechanisms. It was reported that the protective effect of Curcumin on PC-12 cells against cytotoxicity induced by Aβ 1-42 is associated with the presence of a β-diketone moiety, which plays a vital role in its activity (Park and Kim, 2002). Another study reported that Curcumin derivatives increase the Bcl-2/Bax ratio and reduce Cyt-c release, thereby preventing cell apoptosis through the activation of Keap1/Nrf2/HO-1 pathways (Xu et al., 2019). Also, it was reported that Curcumin reduced fibril formation and decreased ROS activity, resulting in increasing cell viability from 58% to 90% nearly on PC-12 cells (Mazaheri et al., 2015). Curcumin increased cell viability by 19-32% on the hydrogen

peroxide (H_2O_2)-induced model of PC-12 cells in another report (Siddiqui et al., 2011). This study highlighted that Curcumin has a neuroprotective effect, but its therapeutic effect might be limited.

Furthermore, the disassociation of Aβ 1-42 aggregates by Curcumin on 3D cultured PC-12 cells was examined through immunostaining of Aβ 1-42 pre- and post-Curcumin treatment (Figure 78). The fluorescence microscopy images revealed that Curcumin effectively disassociated Aβ 1-42 into smaller fragments. These results suggest that Curcumin exhibits a neuroprotective effect against Aβ aggregates by disassociating them in 3D Alzheimer's disease model, as supported by the literature. These findings showed that Curcumin may play a role in delaying disease progression, particularly considering that the symptoms of Alzheimer's disease typically develop following the formation of pathological hallmarks, a process that can take up to 20 years in the preclinical stage (Finder and Glockshuber, 2007; Jack Jr et al., 2018; Porsteinsson et al., 2021).

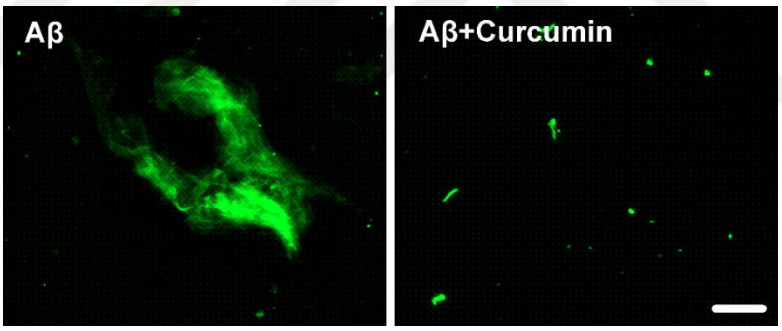

Figure 78. Fluorescence microscopy images of Aβ 1-42 aggregates in 3D Alzheimer's disease model before and after Curcumin treatment at 25 μM (Scale bar: 100 μm).

Overall, these findings suggest that Curcumin exerts a neuroprotective effect by disrupting Aβ 1-42 aggregates and engaging in multiple mechanisms beyond the scope of this thesis. Through these actions, Curcumin may help slow the progression of Alzheimer's disease, particularly during its preclinical stages. Despite its promising neuroprotective properties, additional research is necessary to understand Curcumin's pharmacokinetics, bioavailability, and long-term effects (Bourang et al., 2024; Peng and

Qian, 2014; Ratnatilaka Na Bhuket et al., 2017). In addition, there are some debates on Curcumin in terms of its unstable, reactive characteristics and poor bioavailability. The authors state that no double-blind, placebo-controlled clinical trials have successfully demonstrated curcumin's therapeutic benefits. Based on this assessment, they suggest that curcumin is unlikely to be a viable direct drug candidate (Nelson et al., 2017). Comprehensive clinical studies are essential to optimize its formulation, dosage, and delivery methods, ensuring its efficacy and safety for therapeutic use. On the other hand, the authors respond to previous claims that curcumin lacks therapeutic efficacy despite thousands of research papers and over 120 clinical trials by highlighting that a PubMed search for double-blind, placebo-controlled clinical trials on curcumin yields 49 studies, with 17 reporting significant efficacy. Additionally, 27 other clinical trials and at least five animal studies suggest curcumin has therapeutic benefits. Therefore, Curcumin should not be disregarded simply because it does not fit the conventional single-target drug model, and more research is needed to understand its potential therapeutic applications, particularly in multi-pathway diseases like Alzheimer's disease (Heger, 2017).

CHAPTER 5

CONCLUSION

This thesis introduces a 3D *in-vitro* model for Alzheimer's disease using MagLev technology, offering a significant advancement in the field of neurodegenerative disease research. For this purpose, Gx concentration and cell number for 3D cell culture formation were optimized. Cell viability ranged between 98-96% for SH-SY5Y cells and 93-92% for PC-12 cells at 10-100 mM Gx. Cell number optimization demonstrated its significant impact on the size, morphology, and viability of the 3D cultures. Additionally, spheroids were smaller and less compact at lower cell numbers (5x 10^3 cells), while excessively high cell numbers (100x 10^3 cells) resulted in irregular and oversized aggregates. Optimized Gx concentration and cell number were determined as 25x10^3, 10 mM Gx for SHS-Y5Y cells, while they were 25x10^3, 30 mM Gx for PC-12 cells. 3D cellular aggregates from differentiated SH-SY5Y and PC-12 cells were successfully developed using MagLev, effectively. Then, SH-SY5Y cells were differentiated *via* RA-BDNF sequentially during 3D cell culture. Differentiated spheroids exhibited high cell viability with notable neuronal characteristics as indicated by increased β-III tubulin and NeuN expressions. In addition, PC-12 aggregates exhibited remarkable cell viability with a compact and stable structure. Then, Aβ1-42 aggregates were obtained from monomers at 37 ºC for 72h. Aβ1-42 aggregation was confirmed by bright-field microscopy imaging, Congo red assay, and SEM analysis, successfully. Further, differentiated SH-SY5Y spheroids and PC-12 aggregates were used to model Alzheimer's disease by incorporating Aβ1-42 aggregates, which are known to induce neurotoxicity. Differentiated spheroids and PC-12 aggregates resulted in 51% cell viability for 7 days and 63% for 15 days, respectively after exposure of 50 μM Aβ1-42 aggregates. These findings showed that while SH-SY5Y spheroids were more sensitive to Aβ-induced neurotoxicity, PC-12 aggregates exhibited higher tolerance to Aβ1-42 toxicity, suggesting their potential utility in long term toxicity studies. The characterization of the 3D Alzheimer's disease models was conducted through immunostaining of ChAT, demonstrating a decrease in

fluorescence intensity of ChAT in both 3D Alzheimer's disease models compared to the control group.

Another significant contribution of this research is the evaluation of Curcumin as a therapeutic agent, which can disassociate Aβ1-42 aggregates. Before testing Curcumin on 3D Alzheimer's disease models, the disassociation of Aβ1-42 aggregates by Curcumin was tested by Congo red and Thioflavin T assays, spectrophotometrically. Both absorbance and fluorescence intensity values were decreased after Curcumin treatment. In addition, bright-field images showed that Curcumin disassociated Aβ1-42 aggregates into smaller fragments. Next, various concentrations of Curcumin were tested on 3D Alzheimer's disease models, and optimal doses were identified for maximum neuroprotection without compromising cell viability. Curcumin showed promising results in reducing Aβ-induced neurotoxicity. It suppressed Aβ1-42 neurotoxicity and increased cell viability from 51 to 94% in 3D SH-SY5Y Alzheimer's disease model, while also increasing cell viability from 63 to 86% in 3D PC-12 Alzheimer's disease model. These results were supported by immunostaining of Aβ aggregates in 3D cell culture environment, resulting in smaller Aβ aggregate formation after Curcumin treatment.

In conclusion, this thesis demonstrates the potential of MagLev technology in advancing 3D cell culture methodologies, especially for Alzheimer's disease modeling. The proposed platform not only enriches the understanding of neurodegenerative mechanisms but also provides a valuable tool for exploring novel therapeutic interventions, marking a significant contribution to the field of neurodegenerative disease modeling in 3D.

REFERENCES

Abdul Manap, Aimi Syamima, Priya Madhavan, Shantini Vijayabalan, Adeline Chia, and Koji Fukui. 2020. "Explicating Anti-Amyloidogenic Role of Curcumin and Piperine via Amyloid Beta (Aβ) Explicit Pathway: Recovery and Reversal Paradigm Effects." *PeerJ* 8:e10003.

Abdul Manap, Aimi Syamima, Amelia Cheng Wei Tan, Weng Hhin Leong, Adeline Yoke Yin Chia, Shantini Vijayabalan, Aditya Arya, Eng Hwa Wong, et al. 2019. "Synergistic Effects of Curcumin and Piperine as Potent Acetylcholine and Amyloidogenic Inhibitors With Significant Neuroprotective Activity in SH-SY5Y Cells via Computational Molecular Modeling and in Vitro Assay." *Frontiers in Aging Neuroscience* 11.

Abdulraheem, Rasheed A, Ralph N Martins, Prashant Bharadwaj, Zhaoyu Li, Ranil Coorey, Stuart Johnson, and WMAD Binosha Fernando. 2024. "Nutrients and Polyphenols-Rich Sorghum Bicolor Genotypes as Complementary Therapy for Alzheimer's Disease." *Phytochemistry Reviews*, 1–24.

Adem, Abdu, Maria E K Mattsson, Agneta Nordberg, and Sven Påhlman. 1987. "Muscarinic Receptors in Human SH-SY5Y Neuroblastoma Cell Line: Regulation by Phorbol Ester and Retinoic Acid-Induced Differentiation." *Developmental Brain Research* 33 (2): 235–42.

Ak, Tuba, and Ilhami Gülçin. 2008. "Antioxidant and Radical Scavenging Properties of Curcumin." *Chemico-Biological Interactions* 174 (1): 27–37.

Armstrong, Richard A. 2007. "Size Frequency Distributions of Abnormal Protein Deposits in Alzheimer's Disease and Variant Creutzfeldt-Jakob Disease." *Folia Neuropathologica* 45 (3): 108–14.

Ashkarran, Ali Akbar, Tina Olfatbakhsh, Milad Ramezankhani, Richard C Crist, Wade H Berrettini, Abbas S Milani, Sepideh Pakpour, and Morteza Mahmoudi. 2020. "Evolving Magnetically Levitated Plasma Proteins Detects Opioid Use Disorder as a Model Disease." *Advanced Healthcare Materials* 9 (5): 1901608.

Azevedo, Frederico A C, Ludmila R B Carvalho, Lea T Grinberg, José Marcelo Farfel, Renata E L Ferretti, Renata E P Leite, Wilson Jacob Filho, Roberto Lent, and Suzana Herculano-Houzel. 2009. “Equal Numbers of Neuronal and Nonneuronal Cells Make the Human Brain an Isometrically Scaled-up Primate Brain.” *Journal of Comparative Neurology* 513 (5): 532–41.

Balestri, Wendy, Ruchi Sharma, Victor A da Silva, Bianca C Bobotis, Annabel J Curle, Vandana Kothakota, Farnoosh Kalantarnia, Maria V Hangad, Mina Hoorfar, and Joanne L Jones. 2024. “Modeling the Neuroimmune System in Alzheimer’s and Parkinson’s Diseases.” *Journal of Neuroinflammation* 21 (1): 32.

Banerjee, Arnab, Amit Kunwar, Beena Mishra, and Kavirayani I Priyadarsini. 2008. “Concentration Dependent Antioxidant/pro-Oxidant Activity of Curcumin: Studies from AAPH Induced Hemolysis of RBCs.” *Chemico-Biological Interactions* 174 (2): 134–39.

Bao, Brian, Jean Jiang, Toshihiko Yanase, Yoshihiro Nishi, and Jeffrey R Morgan. 2011. “Connexon-Mediated Cell Adhesion Drives Microtissue Self-Assembly.” *The FASEB Journal* 25 (1): 255.

Barber, Robert C. 2012. “The Genetics of Alzheimer’s Disease.” *Scientifica* 2012 (1): 246210.

Bateman, Randall J, Chengjie Xiong, Tammie L S Benzinger, Anne M Fagan, Alison Goate, Nick C Fox, Daniel S Marcus, Nigel J Cairns, Xianyun Xie, and Tyler M Blazey. 2012. “Clinical and Biomarker Changes in Dominantly Inherited Alzheimer’s Disease.” *New England Journal of Medicine* 367 (9): 795–804.

Battisti, Antonella, Antonio Palumbo Piccionello, Antonella Sgarbossa, Silvia Vilasi, Caterina Ricci, Francesco Ghetti, Francesco Spinozzi, Antonella Marino Gammazza, Valentina Giacalone, and Annamaria Martorana. 2017. “Curcumin-like Compounds Designed to Modify Amyloid Beta Peptide Aggregation Patterns.” *RSC Advances* 7 (50): 31714–24.

Benwood, Claire, Jonathan Walters-Shumka, Kali Scheck, and Stephanie M. Willerth. 2023. “3D Bioprinting Patient-Derived Induced Pluripotent Stem Cell Models of Alzheimer’s Disease Using a Smart Bioink.” *Bioelectronic Medicine* 9 (1): 10.

Berry, Michael V, and Andre K Geim. 1997. “Of Flying Frogs and Levitrons.” *European Journal of Physics* 18 (4): 307.

Berthiaume, François, and Jeffrey Robert Morgan. 2010. *Methods in Bioengineering: 3D Tissue Engineering*. Artech House.

Bhattarai, Prabesh, Kerstin Brandt, Heike Hollak, Xin Chen, Shuijin He, Christopher L Antos, Weilin Lin, Alvin Kuriakose Thomas, Andreas Dahl, and Thomas Kurth. 2018. "3D Culture Method for Alzheimer's Disease Modeling Reveals Interleukin-4 Rescues Ab42-Induced Loss of Human Neural Stem Cell Plasticity." *Developmental Cell* 46:85–101.

Bilginer Kartal, Rumeysa, and Ahu Arslan Yildiz. 2024. "Exploring Neuronal Differentiation Profiles in SH-SY5Y Cells through Magnetic Levitation Analysis." *ACS Omega* 9 (13): 14955–62. https://doi.org/10.1021/acsomega.3c08962.

Blennow, Kaj, Bruno Dubois, Anne M Fagan, Piotr Lewczuk, Mony J De Leon, and Harald Hampel. 2015. "Clinical Utility of Cerebrospinal Fluid Biomarkers in the Diagnosis of Early Alzheimer's Disease." *Alzheimer's & Dementia* 11 (1): 58–69.

Blennow, Kaj, and Henrik Zetterberg. 2018. "Biomarkers for Alzheimer's Disease: Current Status and Prospects for the Future." *Journal of Internal Medicine* 284 (6): 643–63.

Bourang, Shima, Sina Asadian, Mehran Noruzpour, Atefeh Mansuryar, Solmaz Azizi, Hossein Ali Ebrahimi, and Vahid Amani Hooshyar. 2024. "PLA-HA/Fe3O4 Magnetic Nanoparticles Loaded with Curcumin: Physicochemical Characterization and Toxicity Evaluation in HCT116 Colorectal Cancer Cells." *Discover Applied Sciences* 6 (4): 186.

Bowen, David M, Carolyn B Smith, Pamela White, and Alan N Davison. 1976. "Neurotransmitter-Related Enzymes and Indices of Hypoxia in Senile Dementia and Other Abiotrophies." *Brain : A Journal of Neurology* 99 (3): 459–96. https://doi.org/10.1093/brain/99.3.459.

Braak, Heiko, and Eva Braak. 1991. "Neuropathological Stageing of Alzheimer-Related Changes." *Acta Neuropathologica* 82 (4): 239–59.

Browning, Alexander P, Jesse A Sharp, Ryan J Murphy, Gency Gunasingh, Brodie Lawson, Kevin Burrage, Nikolas K Haass, and Matthew Simpson. 2021. "Quantitative Analysis of Tumour Spheroid Structure." *Elife* 10:e73020.

Cai, Hongwei, Zheng Ao, Liya Hu, Younghye Moon, Zhuhao Wu, Hui Chen Lu, Jungsu Kim, and Feng Guo. 2020. “Acoustofluidic Assembly of 3D Neurospheroids to Model Alzheimer’s Disease.” *Analyst* 145 (19): 6243–53. https://doi.org/10.1039/d0an01373k.

Calan, Ozlem Gursoy, Pinar Akan, Aysenur Cataler, Cumhur Dogan, and Semra Kocturk. 2016. “Amyloid Beta Peptides Affect Pregnenolone and Pregnenolone Sulfate Levels in PC-12 and SH-SY5Y Cells Depending on Cholesterol.” *Neurochemical Research* 41 (7): 1700–1712. https://doi.org/10.1007/s11064-016-1886-0.

Cavanaugh, Sarah E, John J Pippin, and Neal D Barnard. 2014. “Animal Models of Alzheimer Disease: Historical Pitfalls and a Path Forward.” *ALTEX-Alternatives to Animal Experimentation* 31 (3): 279–302.

Cenini, Giovanna, Mathias Hebisch, Vira Iefremova, Lea J Flitsch, Yannig Breitkreuz, Rudolf E Tanzi, Deoo Y Kim, Michael Peitz, and Oliver Brüstle. 2021. “Dissecting Alzheimer’s Disease Pathogenesis in Human 2D and 3D Models.” *Molecular and Cellular Neuroscience* 110:103568. https://doi.org/10.1016/j.mcn.2020.103568.

Centeno, Eduarda G Z, Helena Cimarosti, and Angela Bithell. 2018. “2D versus 3D Human Induced Pluripotent Stem Cell-Derived Cultures for Neurodegenerative Disease Modelling.” *Molecular Neurodegeneration* 13:1–15.

Cetin, Sandra, Damijan Knez, Stanislav Gobec, Janko Kos, and Anja Pišlar. 2022. “Cell Models for Alzheimer’s and Parkinson’s Disease: At the Interface of Biology and Drug Discovery.” *Biomedicine & Pharmacotherapy* 149:112924.

Chen, Guo-fang, Ting-hai Xu, Yan Yan, Yu-ren Zhou, Yi Jiang, Karsten Melcher, and H Eric Xu. 2017. “Amyloid Beta: Structure, Biology and Structure-Based Therapeutic Development.” *Acta Pharmacologica Sinica* 38 (9): 1205–35.

Chen, Ming-Kai, Adam P Mecca, Mika Naganawa, Sjoerd J Finnema, Takuya Toyonaga, Shu-fei Lin, Soheila Najafzadeh, Jim Ropchan, Yihuan Lu, and Julia W McDonald. 2018. “Assessing Synaptic Density in Alzheimer Disease with Synaptic Vesicle Glycoprotein 2A Positron Emission Tomographic Imaging.” *JAMA Neurology* 75 (10): 1215–24.

Chen, Xianwei, Guoqiang Sun, E. Tian, Mingzi Zhang, Hayk Davtyan, Thomas G. Beach, Eric M. Reiman, Mathew Blurton-Jones, David M. Holtzman, and Yanhong Shi. 2021. "Modeling Sporadic Alzheimer's Disease in Human Brain Organoids under Serum Exposure." *Advanced Science* 8 (18). https://doi.org/10.1002/advs.202101462.

Cheung, Yuen Ting, Way Kwok Wai Lau, Man Shan Yu, Cora Sau Wan Lai, Sze Chun Yeung, Kwok Fai So, and Raymond Chuen Chung Chang. 2009. "Effects of All-Trans-Retinoic Acid on Human SH-SY5Y Neuroblastoma as in Vitro Model in Neurotoxicity Research." *NeuroToxicology* 30 (1): 127–35. https://doi.org/10.1016/j.neuro.2008.11.001.

Choi, Se Hoon, Young Hye Kim, Matthias Hebisch, Christopher Sliwinski, Seungkyu Lee, Carla D'Avanzo, Hechao Chen, Basavaraj Hooli, Caroline Asselin, and Julien Muffat. 2014. "A Three-Dimensional Human Neural Cell Culture Model of Alzheimer's Disease." *Nature* 515 (7526): 274–78.

Choi, Se Hoon, Young Hye Kim, Luisa Quinti, Rudolph E Tanzi, and Doo Yeon Kim. 2016. "3D Culture Models of Alzheimer's Disease: A Road Map to a 'Cure-in-a-Dish.'" *Molecular Neurodegeneration* 11 (1): 75. https://doi.org/10.1186/s13024-016-0139-7.

Choi, Yoon J, JiSoo Park, and Sang.-Hoon. Lee. 2013. "Size-Controllable Networked Neurospheres as a 3D Neuronal Tissue Model for Alzheimer's Disease Studies." *Biomaterials* 34 (12): 2938–46. https://doi.org/10.1016/j.biomaterials.2013.01.038.

Clark, Christopher M, Michael J Pontecorvo, Thomas G Beach, Barry J Bedell, R Edward Coleman, P Murali Doraiswamy, Adam S Fleisher, Eric M Reiman, Marwan N Sabbagh, and Carl H Sadowsky. 2012. "Cerebral PET with Florbetapir Compared with Neuropathology at Autopsy for Detection of Neuritic Amyloid-β Plaques: A Prospective Cohort Study." *The Lancet Neurology* 11 (8): 669–78.

Conto, Véronique De, Vaihere Cheung, Grégory Maubon, Zied Souguir, Nathalie Maubon, Elodie Vandenhaute, and Vincent Bérézowski. 2021. "In Vitro Differentiation Modifies the Neurotoxic Response of SH-SY5Y Cells." *Toxicology in Vitro* 77:105235.

Costa, Elisabete C, André F Moreira, Duarte de Melo-Diogo, Vítor M Gaspar, Marco P Carvalho, and Ilídio J Correia. 2016. "3D Tumor Spheroids: An Overview on the Tools and Techniques Used for Their Analysis." *Biotechnology Advances* 34 (8): 1427–41.

Costa, Renata T da, Marcella B Dos Santos, Izabel C S Silva, Raquel P de Almeida, Marcela S Teruel, Daniel C Carrettiero, and Cesar A J Ribeiro. 2021. "Methylmalonic Acid Compromises Respiration and Reduces the Expression of Differentiation Markers of SH-SY5Y Human Neuroblastoma Cells." *ACS Chemical Neuroscience* 12 (14): 2608–18.

Costas-Rodríguez, Marta, Legna Colina-Vegas, Nikolay Solovyev, Olivier De Wever, and Frank Vanhaecke. 2019. "Cellular and Sub-Cellular Cu Isotope Fractionation in the Human Neuroblastoma SH-SY5Y Cell Line: Proliferating versus Neuron-like Cells." *Analytical and Bioanalytical Chemistry* 411:4963–71.

Cui, Xiun, Yuli Hartanto, and Hua Zhang. 2017. "Advances in Multicellular Spheroids Formation." *Journal of the Royal Society Interface* 14 (127): 20160877.

Cui, Yi, Weiyuan Liu, Shuaijing Zhao, Yannan Zhao, and Jianwu Dai. 2023. "Advances in Microgravity Directed Tissue Engineering." *Advanced Healthcare Materials* 12 (23): 2202768.

Cummings, Jeffrey, Garam Lee, Aaron Ritter, Marwan Sabbagh, and Kate Zhong. 2019. "Alzheimer's Disease Drug Development Pipeline: 2019." *Alzheimer's & Dementia: Translational Research & Clinical Interventions* 5:272–93.

Cuní-López, Carla, Romal Stewart, Lotta E. Oikari, Tam Hong Nguyen, Tara L. Roberts, Yifan Sun, Christine C. Guo, Michelle K. Lupton, Anthony R. White, and Hazel Quek. 2024. "Advanced Patient-Specific Microglia Cell Models for Pre-Clinical Studies in Alzheimer's Disease." *Journal of Neuroinflammation* 21 (1): 50. https://doi.org/10.1186/s12974-024-03037-3.

Daquinag, Alexes C, Glauco R Souza, and Mikhail G Kolonin. 2013. "Adipose Tissue Engineering in Three-Dimensional Levitation Tissue Culture System Based on Magnetic Nanoparticles." *Tissue Engineering Part C: Methods* 19 (5): 336–44.

DaSilva, Kevin A, James E Shaw, and JoAnne McLaurin. 2010. "Amyloid-β Fibrillogenesis: Structural Insight and Therapeutic Intervention." *Experimental Neurology* 223 (2): 311–21.

D'Avanzo, Carla, Jenna Aronson, Young H Kim, Sehoon H Choi, Rudolph E Tanzi, and Doo Y Kim. 2015. "Alzheimer's in 3D Culture: Challenges and Perspectives." *BioEssays* 37 (10): 1139–48. https://doi.org/10.1002/bies.201500063.

Decourt, Boris, Keith Noorda, Kevin Noorda, Jiong Shi, and Marwan N Sabbagh. 2022. "Review of Advanced Drug Trials Focusing on the Reduction of Brain Beta-Amyloid to Prevent and Treat Dementia." *Journal of Experimental Pharmacology*, 331–52.

Dettmer, Ulf, Andrew J Newman, Frank Soldner, Eric S Luth, Nora C Kim, Victoria E Von Saucken, John B Sanderson, Rudolf Jaenisch, Tim Bartels, and Dennis Selkoe. 2015. "Parkinson-Causing α-Synuclein Missense Mutations Shift Native Tetramers to Monomers as a Mechanism for Disease Initiation." *Nature Communications* 6 (1): 7314.

Ding, Xiaoyuan, Fan Liu, Haohao Wang, Yan Wang, Guohui Li, Xingen Zhang, Cheng Song, Fucheng Zhu, and Dong Liu. 2024. "Ganoderic Acid a Decreased Aβ42-Induced Neurotoxicity in PC12 Cells by Reduced Mitochondrial Damage." *Brain Research* 1842:149102.

Dravid, Anusha, Brad Raos, Darren Svirskis, and Simon J O'Carroll. 2021. "Optimised Techniques for High-Throughput Screening of Differentiated SH-SY5Y Cells and Application for Neurite Outgrowth Assays." *Scientific Reports* 11 (1): 23935.

Drummond, Eleanor, and Thomas Wisniewski. 2017. "Alzheimer's Disease: Experimental Models and Reality." *Acta Neuropathologica* 133:155–75.

Duara, Ranjan, David A Loewenstein, Lake E Potter, Jason Appel, Maria T Greig, Raksha Urs, Qian Shen, Brent Small, and William Barker. 2008. "Medial Temporal Lobe Atrophy on MRI Scans and the Diagnosis of Alzheimer Disease." *Neurology* 71 (24): 1986–92.

Duff, Karen, and Mala V Rao. 2001. "Progress in the Modeling of Neurodegenerative Diseases in Transgenic Mice." *Current Opinion in Neurology* 14 (4): 441–47.

Durairajan, Siva Sundara Kumar, Qiuju Yuan, Lixia Xie, Wing-Sai Chan, Wan-Fung Kum, Irene Koo, Chenli Liu, Youqiang Song, Jian-Dong Huang, and William L Klein. 2008. "Salvianolic Acid B Inhibits Aβ Fibril Formation and Disaggregates Preformed Fibrils and Protects against Aβ-Induced Cytotoxicty." *Neurochemistry International* 52 (4–5): 741–50.

Duval, Kayla, Hannah Grover, Li-Hsin Han, Yongchao Mou, Adrian F Pegoraro, Jeffery Fredberg, and Zi Chen. 2017. "Modeling Physiological Events in 2D vs. 3D Cell Culture." *Physiology* 32 (4): 266–77.

Dwane, Susan, Edel Durack, and Patrick A Kiely. 2013. “Optimising Parameters for the Differentiation of SH-SY5Y Cells to Study Cell Adhesion and Cell Migration.” *BMC Research Notes* 6:1–11.

Encinas, Mario., Montse. Iglesias, Nuria. Llecha, and Joan. X. Comella. 1999. “Extracellular-Regulated Kinases and Phosphatidylinositol 3-Kinase Are Involved in Brain-Derived Neurotrophic Factor-Mediated Survival and Neuritogenesis of the Neuroblastoma Cell Line SH-SY5Y.” *Journal of Neurochemistry* 73 (4): 1409–21. https://doi.org/10.1046/j.1471-4159.1999.0731409.x.

Encinas, Mario, Montse Iglesias, Yuhui Liu, Hongyin Wang, Ashraf Muhaisen, Valentin Ceña, Carme Gallego, and Joan X. Comella. 2000. “Sequential Treatment of SH-SY5Y Cells with Retinoic Acid and Brain-Derived Neurotrophic Factor Gives Rise to Fully Differentiated, Neurotrophic Factor-Dependent, Human Neuron-like Cells.” *Journal of Neurochemistry* 75 (3): 991–1003. https://doi.org/10.1046/j.1471-4159.2000.0750991.x.

Engelhardt, Eliasz, Sonia M T Brucki, José Luiz S Cavalcanti, Orestes V Forlenza, Jerson Laks, and Francisco A C Vale. 2005. “Treatment of Alzheimer’s Disease: Recommendations and Suggestions of the Scientific Department of Cognitive Neurology and Aging of the Brazilian Academy of Neurology.” *Arquivos de Neuro-Psiquiatria* 63:1104–12.

Erö, Csaba, Marc-Oliver Gewaltig, Daniel Keller, and Henry Markram. 2018. “A Cell Atlas for the Mouse Brain.” *Frontiers in Neuroinformatics* 12:84.

Evin, Geneviève, and Andreas Weidemann. 2002. “Biogenesis and Metabolism of Alzheimer’s Disease Aβ Amyloid Peptides.” *Peptides* 23 (7): 1285–97. https://doi.org/https://doi.org/10.1016/S0196-9781(02)00063-3.

Fan, Wenjuan, Chen Xudong, Sun Yizheng, Shanshan Wu, Haili Wang, Shoma Suresh, Sasirekha Krishnan, Murugan Ramalingam, and Jinbo Deng. 2022. “Induced Pluripotent Stem Cell-Derived Neural Culture Model of Alzheimer’s Disease: A 3D Organoid Approach.” *Journal of Biomaterials and Tissue Engineering* 12 (5): 888–96.

Farhat, Syeda Mehpara, and Touqeer Ahmed. 2017. “Neuroprotective and Neurotoxic Implications of A7 Nicotinic Acetylcholine Receptor and Aβ Interaction: Therapeutic Options in Alzheimer’s Disease.” *Curr. Drug Targets* 18 (13): 1537–44.

Feng, Zili, Ying Li, and Yu Bai. 2021. “Elevated Temperatures Accelerate the Formation of Toxic Amyloid Fibrils of Hen Egg-White Lysozyme.” *Veterinary Medicine and Science* 7 (5): 1938–47. https://doi.org/10.1002/vms3.522.

Fernandez-Busquets, X, Jovita Ponce, Ramona Bravo, Muriel Arimon, Tánia Martianez, A Gella, Josep Cladera, and Nuria Durany. 2010. “Modulation of Amyloid β Peptide1-42 Cytotoxicity and Aggregation in Vitro by Glucose and Chondroitin Sulfate.” *Current Alzheimer Research* 7 (5): 428–38.

Ferreira, Joao N, Riasat Hasan, Ganokon Urkasemsin, Kiaw K Ng, Christabella Adine, Sujatha Muthumariappan, and Glauco R Souza. 2019. “A Magnetic Three-dimensional Levitated Primary Cell Culture System for the Development of Secretory Salivary Gland-like Organoids.” *Journal of Tissue Engineering and Regenerative Medicine* 13 (3): 495–508.

Finder, Verena H., and Rudi Glockshuber. 2007. “Amyloid-β Aggregation.” *Neurodegenerative Diseases*. https://doi.org/10.1159/000100355.

Fiore, Nicholas J, Jackson D Tamer-Mahoney, Afshin Beheshti, Thomas J F Nieland, and David L Kaplan. 2022. “3D Biocomposite Culture Enhances Differentiation of Dopamine-like Neurons from SH-SY5Y Cells: A Model for Studying Parkinson’s Disease Phenotypes.” *Biomaterials* 290:121858.

Forster, J Ilona., Sandra Köglsberger, Christophe Trefois, Olga Boyd, Aidos S Baumuratov, Rudi Balling, and Paul M Aloyse Antony. 2016. “Characterization of Differentiated SH-SY5Y as Neuronal Screening Model Reveals Increased Oxidative Vulnerability.” *Journal of Biomolecular Screening* 21 (5): 496–509. https://doi.org/10.1177/1087057115625190.

Fox, Chris, Monica Crugel, Ian Maidment, Bjorn Henrik Auestad, Simon Coulton, Adrian Treloar, Clive Ballard, Malaz Boustani, Cornelius Katona, and Gill Livingston. 2012. “Efficacy of Memantine for Agitation in Alzheimer’s Dementia: A Randomised Double-Blind Placebo Controlled Trial.” *PloS One* 7 (5): e35185.

Frisoni, Giovanni B, Marina Boccardi, Frederik Barkhof, Kaj Blennow, Stefano Cappa, Konstantinos Chiotis, Jean-Francois Démonet, Valentina Garibotto, Panteleimon Giannakopoulos, and Anton Gietl. 2017. “Strategic Roadmap for an Early Diagnosis of Alzheimer’s Disease Based on Biomarkers.” *The Lancet Neurology* 16 (8): 661–76.

Gao, Qiu-Hua, Baiqing Wen, Yani Kang, and Wen-Ming Zhang. 2022. “Pump-Free Microfluidic Magnetic Levitation Approach for Density-Based Cell Characterization.” *Biosensors and Bioelectronics* 204:114052.

Garcia-Alloza, Monica, Laura A Borrelli, Aneta Rozkalne, Bradley T Hyman, and Brian J Bacskai. 2007. “Curcumin Labels Amyloid Pathology in Vivo, Disrupts Existing Plaques, and Partially Restores Distorted Neurites in an Alzheimer Mouse Model.” *Journal of Neurochemistry* 102 (4): 1095–1104.

Gauthier, Serge, Pedro Rosa-Neto, José A Morais, and Claire Webster. 2021. “World Alzheimer Report 2021: Journey through the Diagnosis of Dementia.” *Alzheimer’s Disease International* 2022:30.

Ge, Shencheng, Alex Nemiroski, Katherine A Mirica, Charles R Mace, Jonathan W Hennek, Ashok A Kumar, and George M Whitesides. 2020. “Magnetic Levitation in Chemistry, Materials Science, and Biochemistry.” *Angewandte Chemie International Edition* 59 (41): 17810–55.

Gil-Bea, Francisco Javier, Mónica García-Alloza, Jon Domínguez, Beatriz Marcos, and María Javier Ramírez. 2005. “Evaluation of Cholinergic Markers in Alzheimer’s Disease and in a Model of Cholinergic Deficit.” *Neuroscience Letters* 375 (1): 37–41. https://doi.org/https://doi.org/10.1016/j.neulet.2004.10.062.

Gimenez-Cassina, Alfredo, Filip Lim, and Javier Diaz-Nido. 2006. “Differentiation of a Human Neuroblastoma into Neuron-like Cells Increases Their Susceptibility to Transduction by Herpesviral Vectors.” *Journal of Neuroscience Research* 84 (4): 755–67. https://doi.org/10.1002/jnr.20976.

Goldstein, Lawrence S B, Sol Reyna, and Grace Woodruff. 2015. “Probing the Secrets of Alzheimer’s Disease Using Human-Induced Pluripotent Stem Cell Technology.” *Neurotherapeutics* 12:121–25.

Gonzalez, Cesar, Enrique Armijo, Javiera Bravo-Alegria, Andrea Becerra-Calixto, Charles E Mays, and Claudio Soto. 2018. “Modeling Amyloid Beta and Tau Pathology in Human Cerebral Organoids.” *Molecular Psychiatry* 23 (12): 2363–74.

Granzotto, Alberto, Bryce Vissel, and Stefano L Sensi. 2024. “Lost in Translation: Inconvenient Truths on the Utility of Mouse Models in Alzheimer’s Disease Research.” *Elife* 13:e90633.

Grover, William H, Andrea K Bryan, Monica Diez-Silva, Subra Suresh, John M Higgins, and Scott R Manalis. 2011. "Measuring Single-Cell Density." *Proceedings of the National Academy of Sciences* 108(27):10992–96. https://doi.org/10.1073/pnas.1104651108/-/DCSupplemental.

Guevorkian, Karine, and James M Valles Jr. 2006. "Swimming Paramecium in Magnetically Simulated Enhanced, Reduced, and Inverted Gravity Environments." *Proceedings of the National Academy of Sciences* 103 (35): 13051–56.

Guroff, Gordon. 1985. "PC12 Cells as a Model of Neuronal Differentiation." In *Cell Culture in the Neurosciences*, 245–72. Springer.

Haan, Jurre den, Tjado H J Morrema, Annemieke J Rozemuller, Femke H Bouwman, and Jeroen J M Hoozemans. 2018. "Different Curcumin Forms Selectively Bind Fibrillar Amyloid Beta in Post Mortem Alzheimer's Disease Brains: Implications for in-Vivo Diagnostics." *Acta Neuropathologica Communications* 6:1–12.

Hansen, Richard A, Gerald Gartlehner, Aaron P Webb, Laura C Morgan, Charity G Moore, and Daniel E Jonas. 2008. "Efficacy and Safety of Donepezil, Galantamine, and Rivastigmine for the Treatment of Alzheimer's Disease: A Systematic Review and Meta-Analysis." *Clinical Interventions in Aging* 3 (2): 211–25.

Hansson, Oskar, John Seibyl, Erik Stomrud, Henrik Zetterberg, John Q Trojanowski, Tobias Bittner, Valeria Lifke, Veronika Corradini, Udo Eichenlaub, and Richard Batrla. 2018. "CSF Biomarkers of Alzheimer's Disease Concord with Amyloid-β PET and Predict Clinical Progression: A Study of Fully Automated Immunoassays in BioFINDER and ADNI Cohorts." *Alzheimer's & Dementia* 14 (11): 1470–81.

Hara, Yuko, Nicholas McKeehan, and Howard M Fillit. 2019. "Translating the Biology of Aging into Novel Therapeutics for Alzheimer Disease." *Neurology* 92 (2): 84–93.

Harper, James D, Stanislaus S Wong, Charles M Lieber, and Peter T Lansbury. 1997. "Observation of Metastable Aβ Amyloid Protofibrils by Atomic Force Microscopy." *Chemistry & Biology* 4 (2): 119–25.

Hasan, Md Fayad, and Eugenia Trushina. 2022. "Advances in Recapitulating Alzheimer's Disease Phenotypes Using Human Induced Pluripotent Stem Cell-Based in Vitro Models." *Brain Sciences* 12 (5): 552.

Hazel, Thomas, and Thomas Müller. 1997. “Culture of Neuroepithelial Stem Cells.” *Current Protocols in Neuroscience*, no. 1, 1–3.

Hebisch, Matthias, Stefanie Klostermeier, Katharina Wolf, Aldo R Boccaccini, Stephan E Wolf, Rudolph E Tanzi, and Doo Yeon Kim. 2023. “The Impact of the Cellular Environment and Aging on Modeling Alzheimer’s Disease in 3D Cell Culture Models.” *Advanced Science* 10 (8): 2205037.

Heemels, Marie-Thérèse. 2016. “Neurodegenerative Diseases.” *Nature* 539 (7628): 179–80.

Heger, Michal. 2017. “Don’t Discount All Curcumin Trial Data.” *Nature* 543 (7643): 40.

Hernández-Sapiéns, Mercedes A., Edwin E. Reza-Zaldívar, Ricardo R. Cevallos, Ana L. Márquez-Aguirre, Karlen Gazarian, and Alejandro A. Canales-Aguirre. 2020. “A Three-Dimensional Alzheimer’s Disease Cell Culture Model Using IPSC-Derived Neurons Carrying A246E Mutation in PSEN1.” *Frontiers in Cellular Neuroscience* 14 (June):151. https://doi.org/10.3389/fncel.2020.00151.

Irizarry, Michael C, Ferdie Soriano, Megan McNamara, Keith J Page, Dale Schenk, Dora Games, and Bradley T Hyman. 1997. “Aβ Deposition Is Associated with Neuropil Changes, but Not with Overt Neuronal Loss in the Human Amyloid Precursor Protein V717F (PDAPP) Transgenic Mouse.” *Journal of Neuroscience* 17 (18): 7053–59.

Jack Jr, Clifford R, David A Bennett, Kaj Blennow, Maria C Carrillo, Billy Dunn, Samantha Budd Haeberlein, David M Holtzman, William Jagust, Frank Jessen, and Jason Karlawish. 2018. “NIA-AA Research Framework: Toward a Biological Definition of Alzheimer’s Disease.” *Alzheimer’s & Dementia* 14 (4): 535–62.

Jao, Yu-Ning, Yu-Jen Chao, Jui-Fen Chan, and Yuan-Hao Howard Hsu. 2024. “Mass Spectrometry Analysis of Neurotransmitter Shifting during Neurogenesis and Neurodegeneration of PC12 Cells.” *International Journal of Molecular Sciences* 25 (19): 10399.

Javkhlan, Zolzaya, Sheng-Hao Hsu, Rung-Shu Chen, and Min-Huey Chen. 2024. “Interactions of Neural-like Cells with 3D-Printed Polycaprolactone with Different Inner Diameters for Neural Regeneration.” *Journal of Dental Sciences* 19 (2): 1096–1104.

Jayaprakasam, Bolleddula, Kaillathe Padmanabhan, and Muraleedharan G Nair. 2010. "Withanamides in Withania Somnifera Fruit Protect PC-12 Cells from B-amyloid Responsible for Alzheimer's Disease." *Phytotherapy Research* 24 (6): 859–63.

Jeon, Iksoo, Nayeon Lee, Jia-Yi Li, In-Hyun Park, Kyoung Sun Park, Jisook Moon, Sung Han Shim, Chunggab Choi, Da-Jeong Chang, and Jihye Kwon. 2012. "Neuronal Properties, in Vivo Effects, and Pathology of a Huntington's Disease Patient-Derived Induced Pluripotent Stem Cells." *Stem Cells* 30 (9): 2054–62.

Jiang, Xu, Mukesh Kumar, and Yonglin Zhu. 2018. "Protective Effect of Hyperforin on β Amyloid Protein Induced Apoptosis in PC12 Cells and Colchicine Induced Alzheimer's Disease: An Anti-Oxidant and Anti-Inflammatory Therapy." *Journal of Oleo Science* 67 (11): 1443–53.

Johnson, Keith A, Nick C Fox, Reisa A Sperling, and William E Klunk. 2012. "Brain Imaging in Alzheimer Disease." *Cold Spring Harbor Perspectives in Medicine* 2 (4): a006213.

Jokar, Safura, Saeedeh Khazaei, Xaniar Esmailzadeh Gameshgoli, Mona Khafaji, Behnam Yarani, Mohammad Sharifzadeh, Davood Beiki, and Omid Bavi. 2020. "Amyloid β-Targeted Inhibitory Peptides for Alzheimer's Disease: Current State and Future Perspectives." *Exon Publications*, 51–68.

Jorfi, Mehdi, Carla D'Avanzo, Rudolph E. Tanzi, Doo Yeon Kim, and Daniel Irimia. 2018. "Human Neurospheroid Arrays for In Vitro Studies of Alzheimer's Disease." *Scientific Reports* 8 (1). https://doi.org/10.1038/s41598-018-20436-8.

Jung, Gwon Soo, Kyeong Min Lee, Jin Kyu Park, Seong Kyoon Choi, and Won Bae Jeon. 2013. "Morphogenetic and Neuronal Characterization of Human Neuroblastoma Multicellular Spheroids Cultured under Undifferentiated and All-Trans-Retinoic Acid-Differentiated Conditions." *BMB Reports* 46 (5): 276–81. https://doi.org/10.5483/BMBRep.2013.46.5.196.

Kalwarczyk, Ewelina, Agnieszka Lukasiak, Damian Woznica, Weronika Switlik, Julia Anchimowicz, Piotr Zielonka, and Slawomir Jakiela. 2024. "Proliferation of SH-SY5Y Neuroblastoma Cells on Confined Spaces." *Journal of Neuroscience Methods* 409:110204.

Kaplan, David R, Kazue Matsumoto, Enrico Lucarelli, and Carol J Thielet. 1993. "Induction of TrkB by Retinoic Acid Mediates Biologic Responsiveness to BDNF and Differentiation of Human Neuroblastoma Cells." *Neuron*. Vol. 11. https://doi.org/DOI:https://doi.org/10.1016/0896-6273(93)90187-V.

Klein, William L. 2002. “Aβ Toxicity in Alzheimer’s Disease: Globular Oligomers (ADDLs) as New Vaccine and Drug Targets.” *Neurochemistry International* 41 (5): 345–52.

Klingelhutz, Alosius J, Francoise A Gourronc, Anna Chaly, David A Wadkins, Anthony J Burand, Kathleen R Markan, Sharon O Idiga, Meng Wu, Mathew J Potthoff, and James A Ankrum. 2018. “Scaffold-Free Generation of Uniform Adipose Spheroids for Metabolism Research and Drug Discovery. Sci Rep 8 (1): 523.”

Klunk, William E, Robert F Jacob, and Preston R Mason. 1999. “Quantifying Amyloid by Congo Red Spectral Shift Assay.” *Methods in Enzymology* 309:285–305. https://doi.org/10.1016/S0076-6879(99)09021-7.

Kocienski, Philip. 2022. “Synthesis of BACE1 Inhibitor E2609 (Elenbecestat).” *Synfacts* 18 (07): 0720.

Korecka, Joanna A, Ronald E van Kesteren, Eva Blaas, Sonia O Spitzer, Jorke H Kamstra, August B Smit, Dick F Swaab, Joost Verhaagen, and Koen Bossers. 2013. “Phenotypic Characterization of Retinoic Acid Differentiated SH-SY5Y Cells by Transcriptional Profiling.” *PloS One* 8 (5): e63862.

Kovalevich, Jane, and Dianne Langford. 2013. “Considerations for the Use of SH-SY5Y Neuroblastoma Cells in Neurobiology.” *Methods in Molecular Biology* 1078:9–21. https://doi.org/10.1007/978-1-62703-640-5_2.

Krishtal, Jekaterina, Olha Bragina, Kristel Metsla, Peep Palumaa, and Vello Tõugu. 2017. “In Situ Fibrillizing Amyloid-Beta 1-42 Induces Neurite Degeneration and Apoptosis of Differentiated SH-SY5Y Cells.” *PLoS ONE* 12 (10): e0186636. https://doi.org/10.1371/journal.pone.0186636.

Krokker, Lilla, Borbála Szabó, Kinga Németh, Rebeka Tóháti, Balázs Sarkadi, Katalin Mészáros, Attila Patócs, and Henriett Butz. 2021. “Three Dimensional Cell Culturing for Modeling Adrenal and Pituitary Tumors.” *Pathology and Oncology Research* 27.

Kruger, Terra M, Kendra J Bell, Thiranjeewa I Lansakara, Alexei V Tivanski, Jonathan A Doorn, and Lewis L Stevens. 2020. “A Soft Mechanical Phenotype of SH-SY5Y Neuroblastoma and Primary Human Neurons Is Resilient to Oligomeric Aβ (1–42) Injury.” *ACS Chemical Neuroscience* 11 (6): 840–50.

Kumar, Suresh, Edward J Okello, and Robin J Harris. 2012. “Experimental Inhibition of Fibrillogenesis and Neurotoxicity by Amyloid-Beta (Aβ) and Other Disease-Related Peptides/Proteins by Plant Extracts and Herbal Compounds.” *Protein Aggregation and Fibrillogenesis in Cerebral and Systemic Amyloid Disease*, 295–326.

Kummer, Markus P, and Michael T Heneka. 2014. “Truncated and Modified Amyloid-Beta Species.” *Alzheimer’s Research & Therapy* 6:1–9.

Kundaikar, Harish S, and Mariam S Degani. 2015. “Insights into the Interaction Mechanism of Ligands with Aβ42 Based on Molecular Dynamics Simulations and Mechanics: Implications of Role of Common Binding Site in Drug Design for Alzheimer’s Disease.” *Chemical Biology & Drug Design* 86 (4): 805–12.

Labour, Marie-Noëlle, Sylvain Vigier, Dan Lerner, Anne Marcilhac, and Emmanuel Belamie. 2016. “3D Compartmented Model to Study the Neurite-Related Toxicity of Aβ Aggregates Included in Collagen Gels of Adaptable Porosity.” *Acta Biomaterialia* 37:38–49. https://doi.org/https://doi.org/10.1016/j.actbio.2016.04.001.

Lambert, Marry P, Gerin Stevens, Shasta Sabo, Kathryn Barber, Geoffrey Krafft, Seth Snyder, Thomas F Holzman, and William L Klein. 1994. “β/A4-evoked Degeneration of Differentiated SH-SY5Y Human Neuroblastoma Cells.” *Journal of Neuroscience Research* 39 (4): 377–85.

Lee, Donghee, Sung Min Kim, Hye Yun Kim, and YoungSoo Kim. 2019. “Fluorescence Chemicals to Detect Insoluble and Soluble Amyloid-β Aggregates.” *ACS Chemical Neuroscience* 10 (6): 2647–57.

Lee, Han-Kyu, Clara Velazquez Sanchez, Mei Chen, Peter J Morin, John M Wells, Eugene B Hanlon, and Weiming Xia. 2016. “Three Dimensional Human Neuro-Spheroid Model of Alzheimer’s Disease Based on Differentiated Induced Pluripotent Stem Cells.” *PloS One* 11 (9): e0163072.

Lee, Yun Suk, Hye Yun Kim, YoungSoo Kim, Jae Hong Seo, Eun Joo Roh, Hogyu Han, and Kye Jung Shin. 2012. “Small Molecules That Protect against β-Amyloid-Induced Cytotoxicity by Inhibiting Aggregation of β-Amyloid.” *Bioorganic & Medicinal Chemistry* 20 (16): 4921–35.

Leung, Brendan M, Sasha Cai Lesher-Perez, Toshiki Matsuoka, Christopher Moraes, and Shuichi Takayama. 2015. “Media Additives to Promote Spheroid Circularity and Compactness in Hanging Drop Platform.” *Biomaterials Science* 3 (2): 336–44.

Li, Hang, Asanka Wijekoon, and Nic D Leipzig. 2012. “3D Differentiation of Neural Stem Cells in Macroporous Photopolymerizable Hydrogel Scaffolds.” *PLoS One* 7 (11): e48824.

Li, Xinyu D, and Jerry J Buccafusco. 2003. “Effect of β-Amyloid Peptide 1-42 on the Cytoprotective Action Mediated by A7 Nicotinic Acetylcholine Receptors in Growth Factor-Deprived Differentiated PC-12 Cells.” *Journal of Pharmacology and Experimental Therapeutics* 307 (2): 670–75.

Li, Zhao-Feng, Lei Cui, Mi-Mi Jin, Dong-Yan Hu, Xiao-Gang Hou, Shu-Shu Liu, Xiong Zhang, and Jian-Hong Zhu. 2022. “A Matrigel-Based 3D Construct of SH-SY5Y Cells Models the α-Synuclein Pathologies of Parkinson’s Disease.” *Disease Models & Mechanisms* 15 (3): dmm049125.

Liang, Chu-Chun, Po-Yen Chen, Nien-Che Liu, and I-Chi Lee. 2024. “Comparison between Dynamic versus Static Models and Real-Time Monitoring of Neuronal Dysfunction in an Amyloid-β Induced Neuronal Toxic Model on a Chip Platform.” *Lab on a Chip* 24 (7): 1887–1902.

Liedmann, Andrea, Arndt Rolfs, and Moritz J Frech. 2012. “Cultivation of Human Neural Progenitor Cells in a 3-Dimensional Self-Assembling Peptide Hydrogel.” *Journal of Visualized Experiments: JoVE*, no. 59.

Lin, Ruei-Zhen, and Hwan-You Chang. 2008. “Recent Advances in Three-dimensional Multicellular Spheroid Culture for Biomedical Research.” *Biotechnology Journal: Healthcare Nutrition Technology* 3 (9-10): 1172–84.

Lin, Yuan-Ta, Jinsoo Seo, Fan Gao, Heather M Feldman, Hsin-Lan Wen, Jay Penney, Hugh P Cam, Elizabeta Gjoneska, Waseem K Raja, and Jemmie Cheng. 2018. “APOE4 Causes Widespread Molecular and Cellular Alterations Associated with Alzheimer’s Disease Phenotypes in Human IPSC-Derived Brain Cell Types.” *Neuron* 98 (6): 1141–54.

Lone, Ali Mohd, Nawab John Dar, Abid Hamid, Wajaht Amin Shah, Muzamil Ahmad, and Bilal A Bhat. 2016. “Promise of Retinoic Acid-Triazolyl Derivatives in Promoting Differentiation of Neuroblastoma Cells.” *ACS Chemical Neuroscience* 7 (1): 82–89. https://doi.org/10.1021/acschemneuro.5b00267.

Long, Justin M, and David M Holtzman. 2019. “Alzheimer Disease: An Update on Pathobiology and Treatment Strategies.” *Cell* 179 (2): 312–39.

Louit, Aurélie, Todd Galbraith, and François Berthod. 2023. “In Vitro 3D Modeling of Neurodegenerative Diseases.” *Bioengineering*. MDPI.

Lozupone, Madia, Giuseppe Berardino, Anita Mollica, Rodolfo Sardone, Vittorio Dibello, Roberta Zupo, Luisa Lampignano, Fabio Castellana, Ilaria Bortone, and Roberta Stallone. 2022. “ALZT-OP1: An Experimental Combination Regimen for the Treatment of Alzheimer’s Disease.” *Expert Opinion on Investigational Drugs* 31 (8): 759–71.

Lv, Donglai, Zongtao Hu, Lin Lu, Husheng Lu, and Xiuli Xu. 2017. “Three-dimensional Cell Culture: A Powerful Tool in Tumor Research and Drug Discovery.” *Oncology Letters* 14 (6): 6999–7010.

Ma, Qiu-Lan, Xiaohong Zuo, Fusheng Yang, Oliver J Ubeda, Dana J Gant, Mher Alaverdyan, Edmond Teng, Shuxin Hu, Ping-Ping Chen, and Panchanan Maiti. 2013. “Curcumin Suppresses Soluble Tau Dimers and Corrects Molecular Chaperone, Synaptic, and Behavioral Deficits in Aged Human Tau Transgenic Mice.” *Journal of Biological Chemistry* 288 (6): 4056–65.

Maclean, Calum J, Harry F Baker, Rosalind M Ridley, and Harry Mori. 2000. “Naturally Occurring and Experimentally Induced β-Amyloid Deposits in the Brains of Marmosets (Callithrix Jacchus).” *Journal of Neural Transmission* 107:799–814.

Mahmoudi, Salah, and Anne Brunet. 2012. “Aging and Reprogramming: A Two-Way Street.” *Current Opinion in Cell Biology* 24 (6): 744–56.

Maiti, Panchanan, Tia C Hall, Leela Paladugu, Nivya Kolli, Cameron Learman, Julien Rossignol, and Gary L Dunbar. 2016. “A Comparative Study of Dietary Curcumin, Nanocurcumin, and Other Classical Amyloid-Binding Dyes for Labeling and Imaging of Amyloid Plaques in Brain Tissue of 5×-Familial Alzheimer’s Disease Mice.” *Histochemistry and Cell Biology* 146 (5): 609–25.

Manap, Aimi Syamima Abdul, Amelia Cheng Wei Tan, Weng Hhin Leong, Adeline Yoke Yin Chia, Shantini Vijayabalan, Aditya Arya, Eng Hwa Wong. 2019. “Synergistic Effects of Curcumin and Piperine as Potent Acetylcholine and Amyloidogenic Inhibitors with Significant Neuroprotective Activity in Sh-Sy5y Cells via Computational Molecular Modeling and in Vitro Assay.” *Frontiers in Aging Neuroscience* 10 (JUL): 206. https://doi.org/10.3389/fnagi.2019.00206.

Mann, Daena M A and Snowden S Julie. 1991. “The Topographic Distribution of Brain Atrophy in Alzheimer’s Disease.” *Acta Neuropathologica* 83:81–86.

Marques, Inês Alexandra, Carolina Fernandes, Nuno Tiago Tavares, Ana Salomé Pires, Ana Margarida Abrantes, and Maria Filomena Botelho. 2022. "Magnetic-Based Human Tissue 3D Cell Culture: A Systematic Review." *International Journal of Molecular Sciences* 23 (20): 12681.

Masters, Colin L, Randall Bateman, Kaj Blennow, Christopher C Rowe, Reisa A Sperling, and Jeffrey L Cummings. 2015. "Alzheimer's Disease." *Nature Reviews Disease Primers* 1 (1): 1–18.

Mazaheri, Mansooreh, Ali Akbar Moosavi-Movahedi, Ali Akbar Saboury, Fariba Khodagholi, Fatemeh Shaerzadeh, and Nader Sheibani. 2015. "Curcumin Protects β-Lactoglobulin Fibril Formation and Fibril-Induced Neurotoxicity in PC12cells." *PLoS One* 10 (7): e0133206.

McDonald, Carrie R, Linda K McEvoy, Lusineh Gharapetian, Christine Fennema-Notestine, Donald J Hagler Jr, Dominic Holland, Akihide Koyama, James B Brewer, and Anders M Dale. 2009. "Regional Rates of Neocortical Atrophy from Normal Aging to Early Alzheimer Disease." *Neurology* 73 (6): 457–65.

McEvoy, Eoin, Yu Long Han, Ming Guo, and Vivek B Shenoy. 2020. "Gap Junctions Amplify Spatial Variations in Cell Volume in Proliferating Tumor Spheroids." *Nature Communications* 11 (1): 6148.

Medeiros, Liana M de, Marco A De Bastiani, Eduardo P Rico, Patrícia Schonhofen, Bianca Pfaffenseller, Bianca Wollenhaupt-Aguiar, Lucas Grun, et al. 2019a. "Cholinergic Differentiation of Human Neuroblastoma SH-SY5Y Cell Line and Its Potential Use as an In Vitro Model for Alzheimer's Disease Studies." *Molecular Neurobiology* 56 (11): 7355–67. https://doi.org/10.1007/s12035-019-1605-3.

Melino, Gerry, Carol J Thiele, Richard A Knight, and Mauro Piacentini. 1997. "Retinoids and the Control of Growth/Death Decisions in Human Neuroblastoma Cell Lines." *Journal of Neuro-Oncology*. Vol. 31.

Mendonca, Leonardo Meneghin, Graciela Cristina Dos Santos, Gilmara Ausech Antonucci, Antonio Cardozo Dos Santos, Maria de Lourdes Pires Bianchi, and Lusânia Maria Greggi Antunes. 2009. "Evaluation of the Cytotoxicity and Genotoxicity of Curcumin in PC12 Cells." *Mutation Research/Genetic Toxicology and Environmental Mutagenesis* 675 (1–2): 29–34.

Menon, Venugopal P, and Adluri Ram Sudheer. 2007. “Antioxidant and Anti-Inflammatory Properties of Curcumin.” *The Molecular Targets and Therapeutic Uses of Curcumin in Health and Disease*, 105–25.

Mirica, Katherine A, Scott T Phillips, Charles R Mace, and George M Whitesides. 2010. “Magnetic Levitation in the Analysis of Foods and Water.” *Journal of Agricultural and Food Chemistry* 58 (11): 6565–69.

Mirica, Katherine A, Sergey S Shevkoplyas, Scott T Phillips, Malancha Gupta, and George M Whitesides. 2009. “Measuring Densities of Solids and Liquids Using Magnetic Levitation: Fundamentals.” *Journal of the American Chemical Society* 131 (29): 10049–58.

Moncal, Kazim Kerim, Sena Yaman, and Naside Gozde Durmus. 2022. “Levitational 3D Bioassembly and Density-Based Spatial Coding of Levitoids.” *Advanced Functional Materials* 32 (50): 2204092.

Muñoz-Llancao, Pablo, Cristian de Gregorio, Macarena Las Heras, Christopher Meinohl, Kevin Noorman, Erik Boddeke, Xiaodong Cheng, Frank Lezoualc’h, Martina Schmidt, and Christian Gonzalez-Billault. 2017. “Microtubule-Regulating Proteins and CAMP-Dependent Signaling in Neuroblastoma Differentiation.” *Cytoskeleton* 74 (3): 143–58. https://doi.org/10.1002/cm.21355.

Murillo, Jimmy Rodriguez, Livia Goto-Silva, Aniel Sánchez, Fábio C.S. Nogueira, Gilberto B. Domont, and Magno Junqueira. 2017. “Quantitative Proteomic Analysis Identifies Proteins and Pathways Related to Neuronal Development in Differentiated SH-SY5Y Neuroblastoma Cells.” *EuPA Open Proteomics* 16 (September):1–11. https://doi.org/10.1016/j.euprot.2017.06.001.

Nelson, Kathryn M, Jayme L Dahlin, Jonathan Bisson, James Graham, Guido F Pauli, and Michael A Walters. 2017. “The Essential Medicinal Chemistry of Curcumin: Miniperspective.” *Journal of Medicinal Chemistry* 60 (5): 1620–37.

Newman, David J, and Gordon M Cragg. 2007. “Natural Products as Sources of New Drugs over the Last 25 Years.” *Journal of Natural Products* 70 (3): 461–77.

Ngo, Son Tung, and Mai Suan Li. 2012. “Curcumin Binds to Aβ1–40 Peptides and Fibrils Stronger than Ibuprofen and Naproxen.” *The Journal of Physical Chemistry B* 116 (34): 10165–75.

Nishida, Hiroshi, Megumi Kushida, Yuki Nakajima, Yoshihiro Ogawa, Naoto Tatewaki, Shinji Sato, and Tetsuya Konishi. 2007. "Amyloid-β-Induced Cytotoxicity of PC-12 Cell Was Attenuated by Shengmai-San through Redox Regulation and Outgrowth Induction." *Journal of Pharmacological Sciences* 104 (1): 73–81.

Onbas, Rabia, and Ahu Arslan Yildiz. 2021. "Fabrication of Tunable 3D Cellular Structures in High Volume Using Magnetic Levitation Guided Assembly." *ACS Applied Bio Materials* 4 (2): 1794–1802. https://doi.org/10.1021/acsabm.0c01523.

Ortinau, Stefanie, Jürgen Schmich, Stephan Block, Andrea Liedmann, Ludwig Jonas, Dieter G Weiss, Christiane A Helm, Arndt Rolfs, and Moritz J Frech. 2010. "Effect of 3D-Scaffold Formation on Differentiation and Survival in Human Neural Progenitor Cells." *Biomedical Engineering Online* 9:1–18.

Parfenov, Vladislav A, Vladimir A Mironov, Kenny A van Kampen, Pavel A Karalkin, Elizaveta V Koudan, Frederico D A S Pereira, Stanislav V Petrov, Elizaveta K Nezhurina, Oleg F Petrov, and Maxim I Myasnikov. 2020. "Scaffold-Free and Label-Free Biofabrication Technology Using Levitational Assembly in a High Magnetic Field." *Biofabrication* 12 (4): 045022.

Park, Dong Hyeok, Mei Tong He, Eun Ju Cho, Karl Morten, and Jeung Sang Go. 2023. "Development of a Novel Microfluidic Perfusion 3D Cell Culture System for Improved Neuronal Cell Differentiation." *Biomedical Microdevices* 25 (3): 22. https://doi.org/10.1007/s10544-023-00660-4.

Park, HyunJung, Jaehyeon Kim, and Chongsuk Ryou. 2023. "A Three-Dimensional Spheroid Co-Culture System of Neurons and Astrocytes Derived from Alzheimer's Disease Patients for Drug Efficacy Testing." *Cell Proliferation* 56 (6): e13399. https://doi.org/https://doi.org/10.1111/cpr.13399.

Park, JiSoo, Beo K Lee, Gi S Jeong, Jung K Hyun, Justin C Lee, and Sang-Hoon Lee. 2015. "Three-Dimensional Brain-on-a-Chip with an Interstitial Level of Flow and Its Application as an in Vitro Model of Alzheimer's Disease." *Lab on a Chip* 15 (1): 141–50. https://doi.org/10.1039/c4lc00962b.

Park, Joseph, Isaac Wetzel, Ian Marriott, Didier Dréau, Carla D'Avanzo, Doo Yeon Kim, Rudolph E. Tanzi, and Hansang Cho. 2018. "A 3D Human Triculture System Modeling Neurodegeneration and Neuroinflammation in Alzheimer's Disease." *Nature Neuroscience* 21 (7): 941–51. https://doi.org/10.1038/s41593-018-0175-4.

Park, So-Young. 2010. “Potential Therapeutic Agents against Alzheimer’s Disease from Natural Sources.” *Archives of Pharmacal Research* 33:1589–1609.

Park, So-Young, and Darrick S H L Kim. 2002. “Discovery of Natural Products from Curcuma l Onga That Protect Cells from Beta-Amyloid Insult: A Drug Discovery Effort against Alzheimer’s Disease.” *Journal of Natural Products* 65 (9): 1227–31.

Park, So-Young, Hyo-Shin Kim, Eun-Kyung Cho, Bo-Youn Kwon, Sohee Phark, Kwang-Woo Hwang, and Donggeun Sul. 2008. “Curcumin Protected PC12 Cells against Beta-Amyloid-Induced Toxicity through the Inhibition of Oxidative Damage and Tau Hyperphosphorylation.” *Food and Chemical Toxicology* 46 (8): 2881–87.

Pavoni, Serena, Rafika Jarray, Ferid Nassor, Anne-Cécile Guyot, Steve Cottin, Jessica Rontard, Jacqueline Mikol, Aloïse Mabondzo, Jean-Philippe Deslys, and Frank Yates. 2018. “Small-Molecule Induction of Aβ-42 Peptide Production in Human Cerebral Organoids to Model Alzheimer’s Disease Associated Phenotypes.” *PloS One* 13 (12): e0209150.

Peng, Jin-Rong, and Zhi-Yong Qian. 2014. “Drug Delivery Systems for Overcoming the Bioavailability of Curcumin: Not Only the Nanoparticle Matters.” *Nanomedicine* 9 (6): 747–50.

Perl, Daniel P. 2010. “Neuropathology of Alzheimer’s Disease.” *Mount Sinai Journal of Medicine: A Journal of Translational and Personalized Medicine: A Journal of Translational and Personalized Medicine* 77 (1): 32–42.

Petkova, Aneta T, Yoshitaka Ishii, John J Balbach, Oleg N Antzutkin, Richard D Leapman, Frank Delaglio, and Robert Tycko. 2002. “A Structural Model for Alzheimer’s β-Amyloid Fibrils Based on Experimental Constraints from Solid State NMR.” *Proceedings of the National Academy of Sciences* 99 (26): 16742–47.

Pieri, Andrea De, Yury Rochev, and Dimitrios I Zeugolis. 2021. “Scaffold-Free Cell-Based Tissue Engineering Therapies: Advances, Shortfalls and Forecast.” *NPJ Regenerative Medicine* 6 (1): 18.

Pokharel, Smritee, Chang Hun Lee, Nailya Gilyazova, and Gordon C Ibeanu. 2018. “Analysis of Gene Expression and Neuronal Phenotype in Neuroscreen-1 (NS-1) Cells.” *International Journal of Biomedical Investigation* 1 (3).

Porsteinsson, Anton P, Richard S Isaacson, Sean Knox, Marwan N Sabbagh, and Ivana Rubino. 2021. “Diagnosis of Early Alzheimer’s Disease: Clinical Practice in 2021.” *The Journal of Prevention of Alzheimer’s Disease* 8:371–86.

Portelius, Erik, Nenad Bogdanovic, Mikael K Gustavsson, Inga Volkmann, Gunnar Brinkmalm, Henrik Zetterberg, Bengt Winblad, and Kaj Blennow. 2010. “Mass Spectrometric Characterization of Brain Amyloid Beta Isoform Signatures in Familial and Sporadic Alzheimer’s Disease.” *Acta Neuropathologica* 120 (2): 185–93. https://doi.org/10.1007/s00401-010-0690-1.

Qiao, Jingbo, Pritha Paul, Sora Lee, Lan Qiao, Erlena Josifi, Joshua R Tiao, and Dai H Chung. 2012. “PI3K/AKT and ERK Regulate Retinoic Acid-Induced Neuroblastoma Cellular Differentiation.” *Biochemical and Biophysical Research Communications* 424 (3): 421–26.

Quagliarini, Erica, Luca Digiacomo, Damiano Caputo, Alessandro Coppola, Heinz Amenitsch, Giulio Caracciolo, and Daniela Pozzi. 2022. “Magnetic Levitation of Personalized Nanoparticle–Protein Corona as an Effective Tool for Cancer Detection.” *Nanomaterials* 12 (9): 1397.

Raja, Waseem K., Alison E. Mungenast, Yuan Ta Lin, Tak Ko, Fatema Abdurrob, Jinsoo Seo, and Li Huei Tsai. 2016. “Self-Organizing 3D Human Neural Tissue Derived from Induced Pluripotent Stem Cells Recapitulate Alzheimer’s Disease Phenotypes.” *PLoS ONE* 11 (9). https://doi.org/10.1371/journal.pone.0161969.

Ranjan, Vivek Damodar, Lifeng Qiu, Jolene Wei Ling Lee, Xuelong Chen, Se Eun Jang, Chou Chai, Kah Leong Lim, et al. 2020. “A Microfiber Scaffold-Based 3D: In Vitro Human Neuronal Culture Model of Alzheimer’s Disease.” *Biomaterials Science* 8 (17): 4861–74. https://doi.org/10.1039/d0bm00833h.

Ranjan, Vivek Damodar, Lifeng Qiu, Eng King Tan, Li Zeng, and Yilei Zhang. 2018. “Modelling Alzheimer’s Disease: Insights from in Vivo to in Vitro Three-dimensional Culture Platforms.” *Journal of Tissue Engineering and Regenerative Medicine* 12 (9): 1944–58.

Rao, Praveen P N, Tarek Mohamed, Karan Teckwani, and Gary Tin. 2015. “Curcumin Binding to Beta Amyloid: A Computational Study.” *Chemical Biology & Drug Design* 86 (4): 813–20.

Ratnatilaka Na Bhuket, Pahweenvaj, Asma El-Magboub, Ian S Haworth, and Pornchai Rojsitthisak. 2017. “Enhancement of Curcumin Bioavailability via the Prodrug Approach: Challenges and Prospects.” *European Journal of Drug Metabolism and Pharmacokinetics* 42:341–53.

Riegerova, Petra, Jindřich Brejcha, Dagmar Bezděková, Tomáš Chum, Eva Mašínová, Nikola Čermáková, Saak V Ovsepian, Marek Cebecauer, and Martin Štefl. 2021. “Expression and Localization of AβPP in SH-SY5Y Cells Depends on Differentiation State.” *Journal of Alzheimer’s Disease* 82 (2): 485–91.

Riviere, Marie-Emmanuelle, Jessica B Langbaum, R Scott Turner, Juha O Rinne, Yihan Sui, Pilar Cazorla, Javier Ricart, Kathleen Meneses, Angelika Caputo, and Pierre N Tariot. 2024. “Effects of the Active Amyloid Beta Immunotherapy CAD106 on PET Measurements of Amyloid Plaque Deposition in Cognitively Unimpaired APOE E4 Homozygotes.” *Alzheimer’s & Dementia* 20 (3): 1839–50.

Rösler, Michael, Tony Bayer, Ravi Anand, Ana Cicin-Sain, Serge Gauthier, Yves Agid, Peter Dal-Bianco, Hannes B Stähelin, Richard Hartman, and Marguirguis Gharabawi. 1999. “Efficacy and Safety of Rivastigmine in Patients with Alzheimer’s Disease: International Randomised Controlled TrialCommentary: Another Piece of the Alzheimer’s Jigsaw.” *Bmj* 318 (7184): 633–40.

Rossi, Luisa, Stefania Mazzitelli, Mario Arciello, Concetta R Capo, and Giuseppe Rotilio. 2008. “Benefits from Dietary Polyphenols for Brain Aging and Alzheimer’s Disease.” *Neurochemical Research* 33:2390–2400.

Rouleau, Nicolas, William L. Cantley, Volha Liaudanskaya, Alexander Berk, Chuang Du, William Rusk, Emily Peirent, Cole Koester, Thomas J.F. Nieland, and David L. Kaplan. 2020. “A Long-Living Bioengineered Neural Tissue Platform to Study Neurodegeneration.” *Macromolecular Bioscience* 20 (3). https://doi.org/10.1002/mabi.202000004.

Rubenstein, Richard, Hui Deng, Carol L Scalici, and Michael C Papini. 1991. “Alterations in Neurotransmitter-Related Enzyme Activity in Scrapie-Infected PC12 Cells.” *Journal of General Virology* 72 (6): 1279–85.

Ruiz-León, Yolanda, and Angel Pascual. 2003. “Induction of Tyrosine Kinase Receptor B by Retinoic Acid Allows Brain-Derived Neurotrophic Factor-Induced Amyloid Precursor Protein Gene Expression in Human SH-SY5Y Neuroblastoma Cells.” *Neuroscience* 120 (4): 1019–26. https://doi.org/10.1016/S0306-4522(03)00391-9.

Şahin, Meryem, Gül Öncü, Mustafa Alper Yılmaz, Doğuş Özkan, and Hale Saybaşılı. 2021. "Transformation of SH-SY5Y Cell Line into Neuron-like Cells: Investigation of Electrophysiological and Biomechanical Changes." *Neuroscience Letters* 745:135628.

Sakagami, Hiroshi, Ryuichiro Suzuki, Yoshiaki Shirataki, Soichi Iwama, Mika Nakagawa, Hayato Suzuki, Kenta Tanaka, Nobuaki Tamura, and Hiroshi Takeshima. 2017. "Re-Evaluation of Culture Condition of PC12 and SH-SY5Y Cells Based on Growth Rate and Amino Acid Consumption." *In Vivo* 31 (6): 1089–95.

Santillo, Silvia. 2022. "Changes in Biophysical Properties of Undifferentiated SH-SY5Y Cells during Long-Term Cultures." *Neuroscience* 482:143–58.

Santos Picanco, Leide C Dos, and Priscilla F Ozela. 2018. "Alzheimer's Disease: A Review from the Pathophysiology to Diagnosis." *New Perspectives for Pharmacological Treatment. Current Medicinal Chemistry* 25 (26): 3141–59.

Sarkar, Bibekananda, Monisha Dhiman, Sunil Mittal, and Anil K Mantha. 2017. "Curcumin Revitalizes Amyloid Beta (25–35)-Induced and Organophosphate Pesticides Pestered Neurotoxicity in SH-SY5Y and IMR-32 Cells via Activation of APE1 and Nrf2." *Metabolic Brain Disease* 32:2045–61.

Sarvestani, Zeinab Rohani, Majid Hashemi, and Zahra Solati. 2023. "π-Stacking Interactions between Curcumin and Aromatic Ring of Amino Acids in Amyloid Fibrils: A Theoretical Study." *Computational and Theoretical Chemistry* 1225:114175.

Schneider, Lonnie, Samantha Giordano, Blake R Zelickson, Michelle S Johnson, Gloria A Benavides, Xiaosen Ouyang, Naomi Fineberg, Victor M Darley-Usmar, and Jianhua Zhang. 2011. "Differentiation of SH-SY5Y Cells to a Neuronal Phenotype Changes Cellular Bioenergetics and the Response to Oxidative Stress." *Free Radical Biology and Medicine* 51 (11): 2007–17.

Sehar, Ujala, Priyanka Rawat, Arubala P Reddy, Jonathan Kopel, and Hemachandra P Reddy. 2022. "Amyloid Beta in Aging and Alzheimer's Disease." *International Journal of Molecular Sciences* 23 (21): 12924.

Seidel, Diana, Dana Krinke, Heinz-Georg Jahnke, Anika Hirche, Daniel Kloß, Till G A Mack, Frank Striggow, and Andrea Robitzki. 2012. "Induced Tauopathy in a Novel 3D-Culture Model Mediates Neurodegenerative Processes: A Real-Time Study on Biochips." *PLoS One* 7 (11): e49150.

Sen, Payel, Parisha P Shah, Raffaella Nativio, and Shelley L Berger. 2016. “Epigenetic Mechanisms of Longevity and Aging.” *Cell* 166 (4): 822–39.

Seo, Ju Yeon, Song Bin Park, Seo Yeon Kim, Gyeong Jin Seo, Hyeon-Ki Jang, and Tae-Jin Lee. 2023. “Acoustic and Magnetic Stimuli-Based Three-Dimensional Cell Culture Platform for Tissue Engineering.” *Tissue Engineering and Regenerative Medicine* 20 (4): 563–80.

Serdar, Belgin Sert, Tuğba Erkmen, Bekir Uğur Ergür, Pınar Akan, and Semra Koçtürk. 2020. “Comparison of Medium Supplements in Terms of the Effects on the Differentiation of SH-SY5Y Human Neuroblastoma Cell Line.” *Neurological Sciences and Neurophysiology* 37 (2): 82–88. https://doi.org/10.4103/NSN.NSN_15_20.

Serio, Tricia R, Anil G Cashikar, Anthony S Kowal, George J Sawicki, Jahan J Moslehi, Louise Serpell, Morton F Arnsdorf, and Susan L Lindquist. 2000. “Nucleated Conformational Conversion and the Replication of Conformational Information by a Prion Determinant.” *Science* 289 (5483): 1317–21.

Sharow, Kyle A, Boris Temkin, and Mary Ann Asson-Batres. 2012. “Retinoic Acid Stability in Stem Cell Cultures.” *International Journal of Developmental Biology* 56 (4): 273–78.

Sheng, Morgan, Bernardo L Sabatini, and Thomas C Südhof. 2012. “Synapses and Alzheimer’s Disease.” *Cold Spring Harbor Perspectives in Biology* 4 (5): a005777.

Sheppard, Olivia, and Michael Coleman. 2020. “Alzheimer’s Disease: Etiology, Neuropathology and Pathogenesis.” *Exon Publications*, 1–21.

Shi, Wei, Sukanta Dolai, Samar Rizk, Afshan Hussain, Hussnain Tariq, Saadyah Averick, William L’Amoreaux, Abdeslem El Idrissi, Probal Banerjee, and Krishnaswami Raja. 2007. “Synthesis of Monofunctional Curcumin Derivatives, Clicked Curcumin Dimer, and a PAMAM Dendrimer Curcumin Conjugate for Therapeutic Applications.” *Organic Letters* 9 (26): 5461–64.

Siddiqui, Maqsood A, Mahendra P Kashyap, Vinay K Tripathi, Vinay K Khanna, Sandjay Yadav, and Aditya B Pant. 2011. “Differential Protection of Pre-, Co-and Post-Treatment of Curcumin against Hydrogen Peroxide in PC12 Cells.” *Human & Experimental Toxicology* 30 (3): 192–98.

Sidell, Neil, Marzia Pasquali, Srividya Malkapuram, Arun B Barua, and Randal K Wada. 2003. “In Vitro and in Vivo Effects of Easily Administered, Low-Toxic Retinoid and Phenylacetate Compounds on Human Neuroblastoma Cells.” *British Journal of Cancer* 89 (2): 412–19. https://doi.org/10.1038/sj.bjc.6601108.

Silveira, Isabella A, Adam S Mullis, Dana M Cairns, Anna Shevzov-Zebrun, Jordyn Whalen, Alexa Galuppo, Katherine G Walsh, and David L Kaplan. 2022. “Screening Neuroprotective Compounds in Herpes-Induced Alzheimer’s Disease Cell and 3D Tissue Models.” *Free Radical Biology and Medicine* 186:76–92.

Simões, Rui F., Rafaela Ferrão, Margarida R. Silva, Sonia L.C. Pinho, Lino Ferreira, Paulo J. Oliveira, and Teresa Cunha-Oliveira. 2021. “Refinement of a Differentiation Protocol Using Neuroblastoma SH-SY5Y Cells for Use in Neurotoxicology Research.” *Food and Chemical Toxicology* 149 (March):111967. https://doi.org/https://doi.org/10.1016/j.fct.2021.111967.

Singh, Anurag Kumar, Sachchida Nand Rai, Anand Maurya, Gaurav Mishra, Rajendra Awasthi, Anshul Shakya, Dinesh Kumar Chellappan, Kamal Dua, Emanuel Vamanu, and Sushil Kumar Chaudhary. 2021. “Therapeutic Potential of Phytoconstituents in Management of Alzheimer’s Disease.” *Evidence-Based Complementary and Alternative Medicine* 2021 (1): 5578574.

Slanzi, Anna, Giulia Iannoto, Barbara Rossi, Elena Zenaro, and Gabriela Constantin. 2020. “In Vitro Models of Neurodegenerative Diseases.” *Frontiers in Cell and Developmental Biology* 8:328.

Souza, Glauco R, Jennifer R Molina, Robert M Raphael, Michael G Ozawa, Daniel J Stark, Carly S Levin, Lawrence F Bronk, Jeyarama S Ananta, Jami Mandelin, and Maria-Magdalena Georgescu. 2010. “Three-Dimensional Tissue Culture Based on Magnetic Cell Levitation.” *Nature Nanotechnology* 5 (4): 291–96.

Sreenivasamurthy, Sai, Mahek Laul, Nan Zhao, Tiffany Kim, and Donghui Zhu. 2023. “Current Progress of Cerebral Organoids for Modeling Alzheimer’s Disease Origins and Mechanisms.” *Bioengineering & Translational Medicine* 8 (2): e10378.

Srinivasan, Padma Pradeepa, Vaishali N Patel, Shuang Liu, Daniel A Harrington, Matthew P Hoffman, Xinqiao Jia, Robert L Witt, Mary C Farach-Carson, and Swati Pradhan-Bhatt. 2017. “Primary Salivary Human Stem/Progenitor Cells Undergo Microenvironment-Driven Acinar-like Differentiation in Hyaluronate Hydrogel Culture.” *Stem Cells Translational Medicine* 6 (1): 110–20.

Srivastava, Akriti, Shripriya Singh, Anushka Pandey, Chetan S Rajpurohit, Vinay K Khanna, and Aditya B Pant. 2018. “Secretome of Differentiated PC12 Cells Enhances Neuronal Differentiation in Human Mesenchymal Stem Cells via NGF-like Mechanism.” *Molecular Neurobiology* 55:8293–8305.

Strother, Lisa, Gareth B Miles, Alison R Holiday, Ying Cheng, and Gayle H Doherty. 2021. “Long-Term Culture of SH-SY5Y Neuroblastoma Cells in the Absence of Neurotrophins: A Novel Model of Neuronal Ageing.” *Journal of Neuroscience Methods* 362:109301.

Subramaniam, Anand Bala, Dian Yang, Hai-Dong Yu, Alex Nemiroski, Simon Tricard, Audrey K Ellerbee, Siowling Soh, and George M Whitesides. 2014. “Noncontact Orientation of Objects in Three-Dimensional Space Using Magnetic Levitation.” *Proceedings of the National Academy of Sciences* 111 (36): 12980–85.

Szobota, Stephanie, Pranav D. Mathur, Sairey Siegel, Kristen Ann Black, Uri H Saragovi, and Alan C Foster. 2019. “BDNF, NT-3 and Trk Receptor Agonist Monoclonal Antibodies Promote Neuron Survival, Neurite Extension, and Synapse Restoration in Rat Cochlea Ex Vivo Models Relevant for Hidden Hearing Loss.” *PLoS ONE* 14 (10): e0224022.

Tackenberg, Christian, and Roger M Nitsch. 2019. “The Secreted APP Ectodomain SAPPα, but Not SAPPβ, Protects Neurons against Aβ Oligomer-Induced Dendritic Spine Loss and Increased Tau Phosphorylation.” *Molecular Brain* 12:1–4.

Tang-Schomer, Min D, James D White, Lee W Tien, Ian L Schmitt, Thomas M Valentin, Daniel J Graziano, Amy M Hopkins, Fiorenzo G Omenetto, Philip G Haydon, and David L Kaplan. 2014. “Bioengineered Functional Brain-like Cortical Tissue.” *Proceedings of the National Academy of Sciences* 111 (38): 13811–16.

Tanzi, Rudolph E, James F Gusella, Paul C Watkins, Gail A P Bruns, Peter St George-Hyslop, Margaret L Van Keuren, David Patterson, Susan Pagan, David M Kurnit, and Rachael L Neve. 1987. “Amyloid β Protein Gene: CDNA, MRNA Distribution, and Genetic Linkage near the Alzheimer Locus.” *Science* 235 (4791): 880–84.

Temova Rakuša, Žane, Petja Škufca, Albin Kristl, and Robert Roškar. 2021. “Retinoid Stability and Degradation Kinetics in Commercial Cosmetic Products.” *Journal of Cosmetic Dermatology* 20 (7): 2350–58.

Tepe, Ugur, Bahar Aslanbay Guler, and Esra Imamoglu. 2023. “Applications and Sensory Utilizations of Magnetic Levitation in 3D Cell Culture for Tissue Engineering.” *Molecular Biology Reports* 50 (8): 7017–25.

Terrasso, Ana Paula, Catarina Pinto, Margarida Serra, Augusto Filipe, Susana Almeida, Ana Lúcia Ferreira, Pedro Pedroso, Catarina Brito, and Paula Marques Alves. 2015. “Novel Scalable 3D Cell Based Model for in Vitro Neurotoxicity Testing: Combining Human Differentiated Neurospheres with Gene Expression and Functional Endpoints.” *Journal of Biotechnology* 205:82–92.

Thapa, Arjun, Stephen D Jett, and Eva Y Chi. 2016. “Curcumin Attenuates Amyloid-β Aggregate Toxicity and Modulates Amyloid-β Aggregation Pathway.” *ACS Chemical Neuroscience* 7 (1): 56–68.

Tomitaka, Asahi, Tomohiro Koshi, Shinsuke Hatsugai, Tsutomu Yamada, and Yasushi Takemura. 2011. “Magnetic Characterization of Surface-Coated Magnetic Nanoparticles for Biomedical Application.” *Journal of Magnetism and Magnetic Materials* 323 (10): 1398–1403.

Tseng, Hubert, Liezl R Balaoing, Bagrat Grigoryan, Robert M Raphael, Thomas C Killian, Glauco R Souza, and Jane K Grande-Allen. 2014. “A Three-Dimensional Co-Culture Model of the Aortic Valve Using Magnetic Levitation.” *Acta Biomaterialia* 10 (1): 173–82.

Tseng, Hubert, Jacob A Gage, Robert M Raphael, Robert H Moore, Thomas C Killian, Jane K Grande-Allen, and Glauco R Souza. 2013. “Assembly of a Three-Dimensional Multitype Bronchiole Coculture Model Using Magnetic Levitation.” *Tissue Engineering Part C: Methods* 19 (9): 665–75.

Türker, Esra, Nida Demirçak, and Ahu Arslan-Yildiz. 2018. “Scaffold-Free Three-Dimensional Cell Culturing Using Magnetic Levitation.” *Biomaterials Science* 6 (7): 1745–53. https://doi.org/10.1039/c8bm00122g.

Velander, Paul, Ling Wu, Frances Henderson, Shijun Zhang, David R Bevan, and Bin Xu. 2017. “Natural Product-Based Amyloid Inhibitors.” *Biochemical Pharmacology* 139:40–55.

Velankanni, Priyanka, Satheeswaran Balasubramanian, Azhwar Raghunath, Frank Arfuso, Gautam Sethi, and Ekambaram Perumal. 2019. “Curcumin as a Potential Therapeutic for Alzheimer’s Disease: A Multi-Targeted Approach.” In *Medicinal Plants*, 79–102. CRC Press.

Villemagne, Victor L, Vincent Doré, Samantha C Burnham, Colin L Masters, and Christopher C Rowe. 2018. “Imaging Tau and Amyloid-β Proteinopathies in Alzheimer Disease and Other Conditions.” *Nature Reviews Neurology* 14 (4): 225–36.

Walsh, Dominic M, Aleksey Lomakin, George B Benedek, Margaret M Condron, and David B Teplow. 1997. “Amyloid β-Protein Fibrillogenesis: Detection of a Protofibrillar Intermediate.” *Journal of Biological Chemistry* 272 (35): 22364–72.

Wang, Shao-wei, Yu-Jiong Wang, Ya-jing Su, Wei-wei Zhou, Shi-gao Yang, Ran Zhang, Min Zhao, Ya-nan Li, Zi-ping Zhang, and Da-wei Zhan. 2012. “Rutin Inhibits β-Amyloid Aggregation and Cytotoxicity, Attenuates Oxidative Stress, and Decreases the Production of Nitric Oxide and Proinflammatory Cytokines.” *Neurotoxicology* 33 (3): 482–90.

Webberley, Thomas S, Ryan J Bevan, Joshua Kerry-Smith, Jordanna Dally, Daryn R Michael, Sophie Thomas, Meg Rees, James E Morgan, Julian R Marchesi, and Mark A Good. 2023. “Assessment of Lab4P Probiotic Effects on Cognition in 3xTg-AD Alzheimer’s Disease Model Mice and the SH-SY5Y Neuronal Cell Line.” *International Journal of Molecular Sciences* 24 (5): 4683.

Wilcock, Gordon K, Margaret M Esiri, David M Bowen, and Currien C Smith. 1982. “Alzheimer’s Disease: Correlation of Cortical Choline Acetyltransferase Activity with the Severity of Dementia and Histological Abnormalities.” *Journal of the Neurological Sciences* 57 (2): 407–17. https://doi.org/https://doi.org/10.1016/0022-510X(82)90045-4.

Wilson, David M, Mark Cookson, Ludo Van Den Bosch, Henrik Zetterberg, David Holtzman, and Ilse Dewachter. 2023. “Hallmarks of Neurodegenerative Diseases.” *Cell* 186 (4): 693–714.

Wong, Dean F, Paul B Rosenberg, Yun Zhou, Anil Kumar, Vanessa Raymont, Hayden T Ravert, Robert F Dannals, Ayon Nandi, James R Brašić, and Weiguo Ye. 2010. “In Vivo Imaging of Amyloid Deposition in Alzheimer Disease Using the Radioligand 18F-AV-45 (Flobetapir F 18).” *Journal of Nuclear Medicine* 51 (6): 913–20.

Wray, Selina. 2021. “Modelling Neurodegenerative Disease Using Brain Organoids.” In *Seminars in Cell & Developmental Biology*, 111:60–66. Elsevier.

Wu, Chun, Justin Scott, and Joan Emma Shea. 2012. “Binding of Congo Red to Amyloid Protofibrils of the Alzheimer Aβ9-40 Peptide Probed by Molecular Dynamics Simulations.” *Biophysical Journal* 103 (3): 550–57. https://doi.org/10.1016/j.bpj.2012.07.008.

Xie, Danni, Ting Deng, Zhenwei Zhai, Tao Sun, and Ying Xu. 2023. “The Cellular Model for Alzheimer’s Disease Research: PC12 Cells.” *Frontiers in Molecular Neuroscience* 15:1016559.

Xie, Guanghong, Wulin Tian, Teng Wei, and Fangning Liu. 2015. “The Neuroprotective Effects of β-Hydroxybutyrate on Aβ-Injected Rat Hippocampus in Vivo and in Aβ-Treated PC-12 Cells in Vitro.” *Free Radical Research* 49 (2): 139–50.

Xu, Jialin, Leilei Zhou, Qi Weng, Linxia Xiao, and Qingyong Li. 2019. “Curcumin Analogues Attenuate Aβ25-35-Induced Oxidative Stress in PC12 Cells via Keap1/Nrf2/HO-1 Signaling Pathways.” *Chemico-Biological Interactions* 305:171–79.

Yakupova, Elmira I, Liya G Bobyleva, Ivan M Vikhlyantsev, and Alexander G Bobylev. 2019. “Congo Red and Amyloids: History and Relationship.” *Bioscience Reports* 39 (1): BSR20181415.

Yan, Jun, Jinhui Hu, Anqiu Liu, Lin He, Xingshu Li, and Hui Wei. 2017. “Design, Synthesis, and Evaluation of Multitarget-Directed Ligands against Alzheimer’s Disease Based on the Fusion of Donepezil and Curcumin.” *Bioorganic and Medicinal Chemistry* 25 (12): 2946–55. https://doi.org/10.1016/j.bmc.2017.02.048.

Yanagisawa, Daijiro, Nor Faeizah Ibrahim, Hiroyasu Taguchi, Shigehiro Morikawa, Koichi Hirao, Nobuaki Shirai, Takayuki Sogabe, and Ikuo Tooyama. 2015. “Curcumin Derivative with the Substitution at C-4 Position, but Not Curcumin, Is Effective against Amyloid Pathology in APP/PS1 Mice.” *Neurobiology of Aging* 36 (1): 201–10.

Yanakiev, Mario, Olivia Soper, Daniel A Berg, and Eunchai Kang. 2023. “Modelling Alzheimer’s Disease Using Human Brain Organoids: Current Progress and Challenges.” *Expert Reviews in Molecular Medicine* 25:e3.

Yang, Fusheng, Giselle P Lim, Aynın N Begum, Oliver J Ubeda, Mychica R Simmons, Surendra S Ambegaokar, Pingping Chen. 2005. "Curcumin Inhibits Formation of Amyloid β Oligomers and Fibrils, Binds Plaques, and Reduces Amyloid in Vivo." *Journal of Biological Chemistry* 280 (7): 5892–5901. https://doi.org/10.1074/jbc.M404751200.

Yang, Hong Na, Jing Wang, Jin Hua Sun, Xiao Dun Liu, Wei Ming Duan, and Ting Yu Qu. 2016. "A New Method to Effectively and Rapidly Generate Neurons from SH-SY5Y Cells." *Neuroscience Letters* 610 (January):43–47. https://doi.org/10.1016/j.neulet.2015.10.047.

Yin, Wenke, Xiong Zhang, and Yu Li. 2012. "Protective Effects of Curcumin in APPswe Transfected SH-SY5Y Cells." *Neural Regeneration Research* 7 (6).

Yoshida, Kenta, Anita Moein, Tobias Bittner, Susanne Ostrowitzki, Helen Lin, Lee Honigberg, Jin Y Jin, and Angelica Quartino. 2020. "Pharmacokinetics and Pharmacodynamic Effect of Crenezumab on Plasma and Cerebrospinal Fluid Beta-Amyloid in Patients with Mild-to-Moderate Alzheimer's Disease." *Alzheimer's Research & Therapy* 12:1–12.

Zeng, Zhiwen, Jinying Xu, and Wenhua Zheng. 2017. "Artemisinin Protects PC12 Cells against β-Amyloid-Induced Apoptosis through Activation of the ERK1/2 Signaling Pathway." *Redox Biology* 12:625–33.

Zhai, Kevin, Aranka Brockmüller, Peter Kubatka, Mehdi Shakibaei, and Dietrich Büsselberg. 2020. "Curcumin's Beneficial Effects on Neuroblastoma: Mechanisms, Challenges, and Potential Solutions." *Biomolecules* 10 (11): 1469.

Zhang, Dawei, Mari Pekkanen-Mattila, Mansoureh Shahsavani, Anna Falk, Ana I Teixeira, and Anna Herland. 2014. "A 3D Alzheimer's Disease Culture Model and the Induction of P21-Activated Kinase Mediated Sensing in IPSC Derived Neurons." *Biomaterials* 35 (5): 1420–28.

Zhang, Dongdong, Zhe Wang, Chenxia Sheng, Weijun Peng, Shan Hui, Wei Gong, and Shuai Chen. 2015. "Icariin Prevents Amyloid Beta-induced Apoptosis via the PI3K/Akt Pathway in PC-12 Cells." *Evidence-Based Complementary and Alternative Medicine* 2015 (1): 235265.

Zhang, Lu, Yu Fang, Xuan Cheng, Yajun Lian, Zhaoshu Zeng, Chuanjie Wu, Hongcan Zhu, and Hongliang Xu. 2018. "The Potential Protective Effect of Curcumin on Amyloid-*β*-42 Induced Cytotoxicity in HT-22 Cells." Edited by Mai S Li. *BioMed Research International* 2018:8134902. https://doi.org/10.1155/2018/8134902.

Zhang, Ming, Hong-xia Zheng, Yang-yang Gao, Bo Zheng, Jing-ping Liu, He Wang, Zhan-jun Yang, and Zhi-ying Zhao. 2017. “The Influence of Schisandrin B on a Model of Alzheimer’s Disease Using β-Amyloid Protein Aβ1-42-Mediated Damage in SH-SY5Y Neuronal Cell Line and Underlying Mechanisms.” *Journal of Toxicology and Environmental Health, Part A* 80 (22): 1199–1205. https://doi.org/10.1080/15287394.2017.1367133.

Zhang, Yi, Haiyan Chen, Xiaoyan Long, and Tao Xu. 2022. “Three-Dimensional-Engineered Bioprinted in Vitro Human Neural Stem Cell Self-Assembling Culture Model Constructs of Alzheimer’s Disease.” *Bioactive Materials* 11 (May):192–205. https://doi.org/10.1016/j.bioactmat.2021.09.023.

Zhao, Lin. 2020. “Alzheimer’s Disease Facts and Figures.” *Alzheimers Dement* 16 (3): 391–460.

Zhong, Michael Z, Thomas Peng, Mariana Lemos Duarte, Minghui Wang, and Dongming Cai. 2024. “Updates on Mouse Models of Alzheimer’s Disease.” *Molecular Neurodegeneration* 19 (1): 23.

Zhou, Yongqiang, Weize Li, Lei Xu, and Lvyi Chen. 2011. “In Salvia Miltiorrhiza, Phenolic Acids Possess Protective Properties against Amyloid β-Induced Cytotoxicity, and Tanshinones Act as Acetylcholinesterase Inhibitors.” *Environmental Toxicology and Pharmacology* 31 (3): 443–52.

Zhou, Yufeng. 2016. “The Application of Ultrasound in 3D Bio-Printing.” *Molecules* 21 (5): 590.

Zhou, Zeng, Wei Feng, Kamyab B Moghadas, Nazanin Baneshi, Bahareh Noshadi, Sh Baghaei, and Abasi Dehkordi. 2024. “Review of Recent Advances in Bone Scaffold Fabrication Methods for Tissue Engineering for Treating Bone Diseases and Sport Injuries.” *Tissue and Cell* 88:102390. https://doi.org/https://doi.org/10.1016/j.tice.2024.102390.

Zhu, Judy T T, Roy C Y Choi, Glanice K Y Chu, Anna W H Cheung, Qiu T Gao, Jun Li, Zhi Y Jiang, Tina T X Dong, and Karl W K Tsim. 2007. “Flavonoids Possess Neuroprotective Effects on Cultured Pheochromocytoma PC12 Cells: A Comparison of Different Flavonoids in Activating Estrogenic Effect and in Preventing β-Amyloid-Induced Cell Death.” *Journal of Agricultural and Food Chemistry* 55 (6): 2438–45.

VITA

Rümeysa Bilginer Kartal

Education:

PhD in Bioengineering 2017-2025, İzmir Institute of Technology, İzmir, Turkey

B.S. in Genetic and Bioengineering 2011-2016, Istanbul University, İstanbul, Turkey

Project Experience:

-The Scientific and Technological Research Council of Turkey (TUBITAK), 223M335, Development of a 3D Alzheimer's Model using PC-12 Cells with Magnetic Levitation Method, 2024-2025

-Scientific Research Project (Izmir Institute of Technology), 2022IYTE-1-0058, Identification of cell differentiation using magnetic levitation technique, 2022-2023

List of Selected Publications:

-R. Bilginer-Kartal & A.Arslan-Yildiz, Exploring Neuronal Differentiation Profiles in SH-SY5Y Cells through Magnetic Levitation Analysis, ACS omega, 2024,

- O. Yildirim-Semerci, **R. Bilginer-Kartal** & A.Arslan Yildiz, Exploring the Use of Water-Extracted Flaxseed Hydrocolloids in 3D Cell Culture, Tissue engineering part C: Methods,2024

- O.Yildirim-Semerci, **R.bilginer-kartal** & A.Arslan-yildiz, Arabinoxylan based psyllium seed hydrocolloid: Single-step aqueous extraction and use in tissue engineering, International journal of biological macromolecules, 2024

-R. Bilginer Kartal, D. Ozkendir-Inanc, U.H. Yildiz, A.Arslan-Yildiz, Biocomposite scaffolds for 3D cell culture: Propolis enriched polyvinyl alcohol nanofibers favoring cell adhesion. Journal of Applied Polymer Science, 2020

-R. Bilginer-Kartal & A.Arslan-Yildiz, A facile method to fabricate propolis enriched biomimetic PVA architectures by co-electrospinning. Materials Letters, 2020